Investigating the gating mechanism of the large conductance mechanosensitive channel by SDLS and EPR spectroscopy [Redacted version]

Charalampos Kapsalis

A thesis submitted for the degree of PhD
at the
University of St Andrews

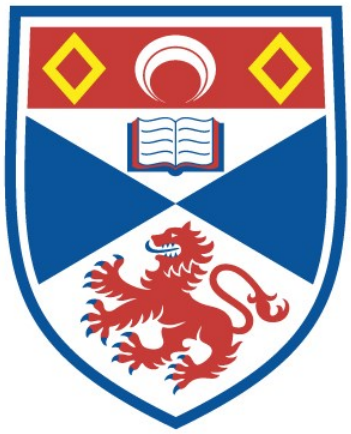

2020

ABSTRACT

Mechanosensation is the ability of cells to sense and respond to mechanical stimuli deriving from their environment. Despite being a fundamental cellular response though, the molecular basis of mechanotransduction is still largely unknown. The mechanosensitive (MS) channel of large conductance, MscL, is expressed by all prokaryotes, it is the MS channel with the highest pressure activation threshold and acts as a last resort safety valve. It responds to the lateral tension of the membrane and, by opening its pore of ≈35Å, it rapidly allows solutes to exit the cell in order to rescue it from lysis during severe hypoosmotic shock. Despite its importance and abundance, the gating and activation mechanism of MscL has not been elucidated. Thus, in the main project presented, MscL's gating mechanism is investigated as a means to gain insight on the mode of mechanosensation itself. Activation of the channel through site-directed spin labelling (SDSL) reveals that the nano-pockets, transmembrane hydrophobic crevices of the protein, are crucial for the activation of MscL. SDSL at the nano-pockets' entrance hinders lipid acyl chains from penetrating them and this causes the channel to adopt a more expanded state, as demonstrated by EPR spectroscopy, which is more prone to opening, as revealed by single-molecule electrophysiology. Since MscL is only found in prokaryotes, manipulation of its gating mechanism could lead to the channel being used as a novel form of antibiotic target. Moreover, due to its large pore, it could also be utilized in nanotechnological applications for targeted drug delivery.

Candidate's declaration

I, Charalampos Kapsalis, do hereby certify that this thesis, submitted for the degree of PhD, which is approximately 60,000 words in length, has been written by me, and that it is the record of work carried out by me, or principally by myself in collaboration with others as acknowledged, and that it has not been submitted in any previous application for any degree.

I was admitted as a research student at the University of St Andrews in February 2016.

I received funding from an organisation or institution and have acknowledged the funder(s) in the full text of my thesis.

Date 09/10/2020 Signature of candidate

Supervisor's declaration

I hereby certify that the candidate has fulfilled the conditions of the Resolution and Regulations appropriate for the degree of PhD in the University of St Andrews and that the candidate is qualified to submit this thesis in application for that degree.

Date 09/10/2020 Signature of supervisor(s)

Christos Pliotas

Date 9/10/2020

Carlos Penedo

Permission for publication

In submitting this thesis to the University of St Andrews we understand that we are giving permission for it to be made available for use in accordance with the regulations of the University Library for the time being in force, subject to any copyright vested in the work not being affected thereby. We also understand, unless exempt by an award of an

embargo as requested below, that the title and the abstract will be published, and that a copy of the work may be made and supplied to any bona fide library or research worker, that this thesis will be electronically accessible for personal or research use and that the library has the right to migrate this thesis into new electronic forms as required to ensure continued access to the thesis.

I, Charalampos Kapsalis, confirm that my thesis does not contain any third-party material that requires copyright clearance.

The following is an agreed request by candidate and supervisor regarding the publication of this thesis:

Printed copy

No embargo on print copy.

Electronic copy

Embargo on part (Chapter 4 (all), Chapter 6 (all), Chapter 3 (Section 3.2.7) and Chapter 7(Sections 7.2.2 and 7.2.4)) of electronic copy for a period of 2 years on the following ground(s):

- Publication would be commercially damaging to the researcher, or to the supervisor, or the University
- Publication would preclude future publication

Supporting statement for electronic embargo request

Chapter 4: Findings are very novel and can lead to an important publication within the next 2 years Chapter 6: Findings are under review for publication at the moment Chapter 3: Included data can lead to a publication within the next 1-1.5 years Chapter 7: Included parts are conclusions and discussion associated with Chapters 4 and 6

Title and Abstract

- I agree to the title and abstract being published.

Date 09/10/2020 Signature of candidate

Date 09/10/2020 Signature of supervisor(s)

Christos Pliotas

Date 9/10/2020

Carlos Penedo

Underpinning Research Data or Digital Outputs

Candidate's declaration

I, Charalampos Kapsalis, hereby certify that no requirements to deposit original research data or digital outputs apply to this thesis and that, where appropriate, secondary data used have been referenced in the full text of my thesis.

Date 09/10/2020 Signature of candidate

Table of Contents

List of abbreviations

ALPS, amphipathic lipid packing sensor ; **ASIC**, acid – sensing ion channels ; **AUC**, area under the curve ; **BR2**, bradykinine receptor 2 ; **BSA**, bovine serum albumin ; **CL**, cardiolipin ; **CW-EPR**, continuous wave electron paramagnetic resonance ; **D2O**, deuterium oxide ; **DDM**, n – dodecyl β – D – maltoside ; **DEER**, double electron-electron resonance ; **DjlA**, DnaJ – like protein ; **DLPC**, dilauroyl phosphatidyl choline ; **DMPC**, dimyristoyl phosphatidyl choline ; **DPPC**, dipalmitoyl phosphatidyl choline ; **DSPC**, distearoyl phosphatidyl choline ; **DTT**, dithiothreitol ; **EcMscL**, *Escherichia coli* MscL ; **EcMscS**, *Escherichia coli* MscS ; **EDTA**, ethylenediaminetetraacetic acid ; **ENaC / DEG**, amiloride – sensitive sodium channel / degenerins ; **EPR**, electron paramagnetic resonance ; **ESEEM**, electron spin echo envelope modulation ; **ES-MS**, electrospray mass spectrometry ; **GUV**, giant unilamellar vesicles ; **IMAC**, immobilized metal affinity chromatography ; **IPTG**, Isopropyl β- d-1-thiogalactopyranoside ; **K2P**, potassium dependent channels ; **LB**, Luria Bertani broth ; **LDS**, lithium dodecyl sulfate ; **MaMscL**, *Methanosarcina acetivorans* MscL ; **MS**, mechanosensitive ; **MscK**, potassium – dependent mechanosensitive ion channel ; **MscL**, mechanosensitive channel of large conductance ; **MscM**, mechanosensitive ion channel of mini conductance ; **MscS**, mechanosensitive channel of small conductance ; **MSP1D1**, membrane scaffold protein 1 D1 ; **MTSSL**, S-(1–oxyl-2, 2, 5, 5–tetramethyl-2, 5–dihydro-1H–pyrrol–3-yl)methyl methanethiosulfonate ; **Ni^{2+} – NTA**, Ni^{2+}-nitrilotriacetic acid ; **NMR**, nuclear magnetic resonance ; **NOMPC**, no mechanoreceptor potential C channel ; **OD**, optical density ; **PA**, phosphatidic acid ; **PBS**, phosphate-buffered saline ; **PC**, phosphatidyl choline ; **PCR**, polymerase chain reaction ; **PDB**, protein data bank ; **PE**, phosphatidyl ethanolamine ; **PELDOR**, pulsed electron-electron double resonance ; **PG**, phosphatidyl glycerol ; **PI**, phosphatidyl inositol ; **PLB**, planar lipid bilayer ; **PS**, phosphatidyl serine ; **PTEN**, phosphatase and tensin homologue ; **RraA**, regulator of ribonuclease activity A protein ; **SaMscL**, *Staphylococcus aureus* MscL ; **SDS**, sodium dodecyl sulfate ; **SDSL**, site directed spin labelling ; **SDS-PAGE**, sodium dodecyl sulfate polyacrylamide gel electrophoresis ; **SEC**, size exclusion chromatography ; **TbMscL**, *Mycobacterium tuberculosis* MscL ; **TCEP**, tris - (2-carboxyethyl) phosphine hydrochloride ; **TEMPOL**, 4-hydroxy-2,2,6,6-tetramethyl-piperidine-1-oxyl ; **TM**, transmembrane ; **TRP**, transient receptor potential ; **TRPA**, TRP – ankyrin ; **TRPC**, TRP – canonical ; **TRPM**, TRP - melastatin ; **TRPML**, TRP - mucolipin ; **TRPN**, TRP – NOMPC – like ; **TRPP**, TRP – polycystin ; **TRPV**, TRP – vanilloid ; **WT**, wild type

CHAPTER 1: INTRODUCTION

1. 1. Lipids and Biological Membranes

1. 1. 1. Lipids and lipid bilayers

Lipids constitute one of the four major types of biological molecules, the other three being carbohydrates, proteins and nucleic acids. They play some very important roles in single – cell and higher organisms, as they act as cell – signaling molecules[1, 2], they are the most efficient energy storage and provision type of biomolecules[3, 4], they are the starting molecules for the biosynthesis of signaling molecules (e. g. prostaglandins from arachidonic acid[5, 6]) and hormones (e.g. testosterone, estrogens and cortisol from cholesterol[7]) etc. Their most fundamental, and possibly most important, role is that they are the building blocks of biological membranes, which are the universal means of compartmentalization and protection in all living cells. All lipids that are present in biological membranes are amphipathic (or amphiphilic), which means that they consist of a hydrophobic and a hydrophilic (or polar) part. The polar part can be neutral, negatively charged, positively charged or zwitterionic (containing both a negatively and a positively charged moiety in their structure). It is exactly this characteristic of theirs that renders them ideal for the formation of biological membranes. When exposed to an aqueous environment, lipids spontaneously orient themselves so that their polar parts remain hydrated, i. e. in contact with the water molecules, while the hydrophobic parts do not come into direct contact with the polar environment. In order to achieve this, they adopt a two – sheet formation, the lipid bilayer, in which the polar parts act as a two – sided wall that contains the hydrophobic parts and secludes them from direct contact with the aqueous surroundings[4]. All biological membranes, including the cell membrane, are such lipid bilayer formations. Those bilayers are highly dynamic structures, characterized by fast diffusion and migration of individual lipids along each leaflet, as well as slower movement of lipids from one bilayer leaflet to the opposite (flip – flop move)[8, 9]. Due to the chemical characteristics of the lipids that comprise them and their own structural and physical properties, lipid bilayers are optimal for the compartmentalization of the cell and the containment of the cytoplasm, since they are not readily permeable by the polar contents of the cell (e. g. proteins and nucleic acids) or the environment (e. g. harmful toxins or metals).

Lipids are a highly diverse class of biological molecules, as different combinations of polar head groups and hydrophobic parts yield a vast variety of molecules[4]. Furthermore, lipids that seemingly differ very little in their structures (e. g. by one or two methyl groups in one of their hydrocarbon chains or just by a double bond) may

display quite different physical and chemical properties. Due to this variety, there are many different ways to classify them, depending on their polar head groups, their hydrophobic parts or the nature of their backbone's structure. A relatively recent and comprehensive classification system, based mainly on lipidomic analyses, identifies the following main lipid categories, each further sub – divided into individual categories: fatty acids, glycerolipids, glycerophospholipids, sphingolipids, polyketides, saccharolipids (or glycolipids), prenol lipids and sterol lipids[10] (Fig. 1.1, a – h).

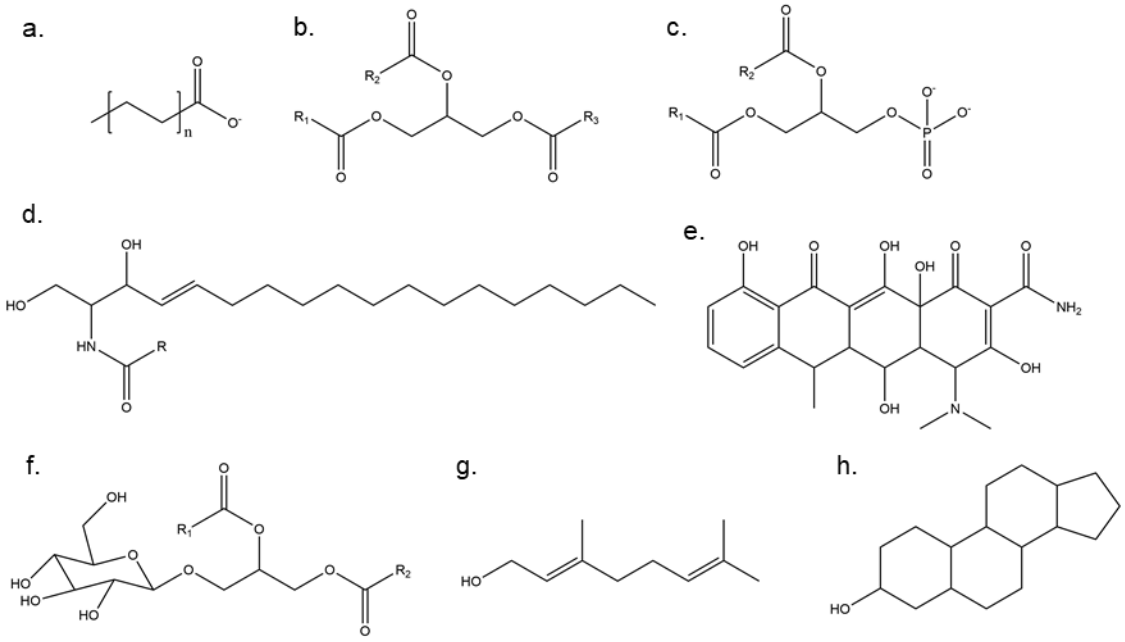

Fig. 1. 1: Chemical structures of different lipids. **a.** Fatty acid **b.** Triacylglycerol (glycerolipid), **c.** Diacylglycerol phosphate (glycerophospholipid), **d.** Ceramide (sphingolipid), **e.** Doxycycline (polyketide), **f.** Saccharolipid, **g.** Geraniol (prenol lipid), **h.** Sterol.

The simplest common type of those amphipathic lids are the fatty acids, which consist of an aliphatic hydrocarbon chain (the hydrophobic part) and a carboxyl head – group which is negatively charged at physiological pH values. Simple as they may be, they are highly important since they play the pivotal role of the hydrophobic part in many other types of more complex lipids, such as in all phospholipids. A major way through which those lipids may differ is the number of carbon atoms that comprise their aliphatic chain, which is typically even and varies from 14 to 24. Despite that fact, some organisms (including several species of bacteria[11]) are able to synthesize and utilize odd – chain saturated fatty acids, especially C 15:0 and C 17:0 (in this nomenclature, the first number denotes the number of carbon atoms of the acyl chain and the second the number of double bonds present)[12]. Another

structural element that increases the diversity of simple fatty acids is the degree of the saturation of their aliphatic chains. Mono – and poly -unsaturated fatty acids containing cis double bonds are most usually found in dietary fats derived from plants, e. g. olive oil contains very high amounts of the mono – unsaturated oleic acid (C 18:1 or cis – 9 – octadecaenoic acid), as well as the poly – unsaturated linoleic (C 18:2 or cis, cis - 9, 12 – octadecadienoic) and α – linolenic (C 18:3 or cis, cis, cis - 9, 12, 15 – octadecatrienoic) acids. Fatty acids with trans – double bonds are usually associated with margarines and other types of processed oils (in which cases they are the result of the hydrogenation process), but they are also naturally found in dairy products, as well as in prokaryotic cells[13].

The large diversity of lipids in general is reflected on the lipid species that can be found on membranes too. However, the vast majority of lipids found in biological membranes are phospholipids, glycolipids and cholesterol[14]. Cholesterol plays a very important role in cell membranes of higher organisms, as it is an integral and distinctive part (along with sphingolipids) of the membrane rafts[15], while at the same time it also acts as a regulator of the bilayer's curvature, water penetration, thickness, compressibility and fluidity[16]. However, despite its high importance in most eukaryotic cells, bacteria are not able to synthesize it. Instead of that, they biosynthesize hopanoids, which are pentacyclic tri – terpenoid derivatives that act as functional cholesterol analogues[18].

Nevertheless, by far the most abundant species of lipid found in biological membranes are the phospholipids[14, 19]. The backbone of phospholipids is an alcohol, either glycerol (in the case of glycerophospholipids) or the more complex sphingosine (in the case of sphingolipids). In the case of the more common glycerophospholipids, which are of the highest interest for this thesis and are found in abundance in both eukaryotic and bacterial cells, the hydroxyl groups of the C – 1 and C – 2 carbon atoms of glycerol are esterified with the carboxyl groups of fatty acids. After esterification of the C – 1 and C – 2 hydroxyl groups, the remaining C – 3 carbon hydroxyl group is esterified with a phosphoric acid, so glycerophospholipids are in essence diacylglycerols. Interestingly, the glycerophospholipids found in archaea display some differences (others subtle and others more pronounced, but fundamental nevertheless) compared to those found in eukaryotes and bacteria. Firstly, the hydrophobic part of the molecule is not comprised of fatty acid acyl chains, but rather from isoprenoid alkyl hydrocarbon chains. Secondly, the ester bond between the glycerol backbone and the phosphoric acid is on the C – 1, rather than the C – 3, hydroxyl group. But most importantly, no further ester bonds are found in the archaeal glycerophospholipids, since the aforementioned isoprenoid hydrocarbon chains are connected to the glycerol through ether, rather than ester, bonds. The benefit of ether bonds is that they are much harder to get hydrolyzed compared to ester bonds, which is advantageous in the case of archaeal cells which

are often found in extreme environments[20]. Glycerophospholipids containing ether bonds (called plasmalogens) are also found in eukaryotic and bacterial cells, but they only have one ether bond directly on the main glycerol backbone. Furthermore, they are not as abundant and, although they do play important physiological roles, they are not as important in biological membrane formation as they are in archaeal cells[21, 22].

Back to the common case of diacylglycerol lipids, if no further modifications take place, this molecule is the negatively charged phosphatidic acid (diacylglycerol 3 – phosphate), the simplest of the glycerophospholipids. Although small quantities of phosphatidic acid do exist in cell membranes, the vast majority of those molecules are used for the further synthesis of other, more complex lipids. In the case of the most common glycerophospholipids, the phosphate group of the phosphatidic acid forms an ester bond with a hydroxyl group of a serine, an ethanolamine, a choline, another glycerol or an inositol (non – modified or phosphorylated). This way, the major glycerophospholipid sub – categories of phosphatidyl serine (PS, zwitterionic), phosphatidyl ethanolamine (PE, zwitterionic), phosphatidyl choline (PC, zwitterionic), phosphatidyl glycerol (PG, anionic) and phosphatidyl inositol (PI, anionic, even more so when the inositol moiety is phosphorylated) are formed.

1. 1. 2. The effect of different glycerophospholipids on lipid bilayers and their biological significance

The great variety of lipids and, in particular, glycerophospholipids, that can be found in biological membranes is a direct result of the number of possible combinations between (a) the modifications of the phosphate group (polar part) and (b) all the different fatty acids (and their combinations) that can be used to esterify the glycerol backbone (hydrophobic part). Furthermore, both the head groups and the acyl chains can individually affect the physical and chemical properties of a biological membrane, mostly due to the influence each one of them has on the lipid packing, which in turn influences the curvature of the bilayer (although without being the only contributing factor[23]).

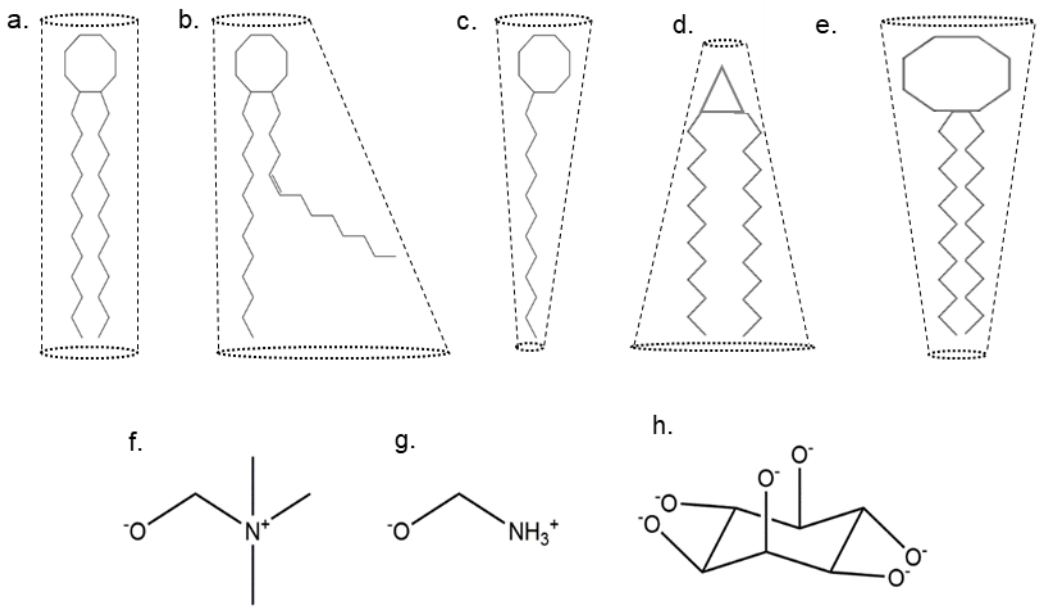

Fig. 1. 2: a. Cylindrical shape, **b.** Conical shape due to the acyl chains' structure, **c.** Reverse conical shape due to the acyl chains' structure / number, **d.** Conical shape due to the head group's size, **e.** Reverse conical shape due to the head group's size, **f.** Choline head group, **g.** Ethanolamine head group, **h.** Inositol head group

The glycerophospholipid's polar head group is mainly characterized by its size, its polarity and by whether it is (positively) charged or neutral (zwitterionic). Each of these qualities plays its part on how the head group affects the packing of lipids packing inside the bilayer. The size and volume of the head group affect the overall shape of the lipid molecule (Fig. 1.2 a – e), which, in turn, affects the packing of the individual lipids inside the bilayer and, therefore, its shape and curvature[24]. The most typical symmetrical glycerophospholipid is phosphatidyl choline. For a given pair of esterified saturated fatty acids, the choline head group (Fig. 1.2.f) of this lipid category is of appropriate size so that overall the lipid molecule approximates a cylindrical shape (Fig. 1. 2.a), which is ideal for tight lipid packing in the bilayer, without the introduction of any geometrical defects.

In contrast, a lipid with exactly the same pair of esterified fatty acids (as those in the previously mentioned phosphatidyl choline molecule) but a smaller head group, for example a phosphatidyl ethanolamine (Fig. 1.2.g) or a phosphatidic acid moiety, will have a roughly conical shape (Fig. 1. 2 d), with the cone's largest base at the hydrophobic side, since the polar head group takes up much less volume compared to the two saturated fatty acids that are esterified to the glycerol backbone. Other common lipids with conical shapes are the diacyl glycerols. On the other hand, if the lipid is a phosphatidyl inositol (Fig. 1.2.h) molecule with the same fatty acids, its

shape will be roughly that of a reverse cone (Fig. 1.2.e) with its base at the polar head group side, since the inositol moiety has a larger volume than that of the two saturated fatty acids. Another common kind of lipids that has a reverse cylindrical shape are most lyso – lipids (Fig. 1.2 c), which only contain one fatty acid esterified to the glycerol backbone, while the other one is hydrolyzed leaving a (usually the C – 2) hydroxyl group free[25]. Lipids with a cylindrical shape (Fig. 1.2 a) form largely "flat" bilayers, without any extreme curvature. Lipids with a reverse conical shape (Fig. 1.2 c & e) cause the bilayer to gain a positive (i. e. outwards) curvature, while those with a conical shape (Fig. 1.2 b & d) promote negative (i. e. inwards) curvature of the bilayer[24, 26]. Thus, the spontaneous curvature for cylindrical lipids is zero, that of reverse conical lipids is positive and the one of conical lipids is negative.

When lipids with different spontaneous curvatures are situated in proximity inside a lipid bilayer a geometrical mismatch occurs, leading to a defect or imperfection, a "gap" on the bilayer or biological membrane[24]. Both the curvature induction and the geometrical defects are important features that the lipid shape mismatches introduce to the bilayer. It is widely accepted that there are membrane proteins that localize in parts of the membrane with high curvature, either positive or negative[27-30]. Interestingly, geometrical lipid packing perturbations and membrane curvature are so interwoven, that some bilayer curvature sensor domains that exist in membrane proteins, such as the amphipathic lipid packing sensor (ALPS) domain, actually sense lipid packing defects rather than the bilayer curvature itself[28]. Furthermore, the charge of the lipid head groups seems to have an effect on the physical and chemical properties of the bilayer as well. For example, some negatively charged glycerophospholipids, such as phosphatidyl serine and phosphatidyl inositol – phosphate have been shown to increase the interfacial tension and stiffen phosphatidyl choline bilayers when they are added to them[31]. Also, anionic lipids seem to be associated with, or even promote recruitment and anchoring of, some specific membrane proteins and / or protein domains (such as the phosphatase and tensin homologue (PTEN) Proteins, the auxilin-1 PTEN-like domain, as well as the mechanosensitive ion channel of large conductance from *Mycobacterium tuberculosis*, TbMscL, too)[32-34].

Regarding the hydrophobic part of the lipids, the nature of the fatty acids that are esterified to the glycerol backbone also plays an important role on the physical properties of the lipid bilayer. Saturated fatty acids (as well as unsaturated fatty acids with trans double bonds) are straight (Fig. 1.2.a, c, d, e). This means that they occupy less volume per molecule, while at the same time maximizing the useful surface available for the development of hydrophobic interactions with other fatty acid chains of nearby lipids. The magnitude of the latter effect is proportional to the length of the hydrocarbon acyl chain; the longer the saturated fatty acid, the more useful surface is available for the creation of hydrophobic interactions with adjacent lipid acyl

chains. Consequently, bilayers with a high percentage of glycerophospholipids with saturated esterified fatty acids are more tightly packed, more rigid and stiff, and with reduced permeability. On the other hand, cis double bonds introduce a kink to the fatty acid that contains them (Fig. 1.2.b). This means that lipids containing fatty acids with cis double bonds take up more volume, leading to higher surface area per lipid molecule. Simultaneously, the surface available for hydrophobic interactions is reduced. Thus, bilayers containing high amounts of lipids with cis double bonds are more fluid, have lower transition temperatures, and they are more permeable. Moreover, since cis-unsaturated fatty acids take up more space, a lipid that contains one (or even more so, two) such acyl chains is more likely to have a conical shape (Fig. 1.2.b), and the effect is even more pronounced when this kind of fatty acids are paired with a head group of smaller size, such as ethanolamine or a plain phosphate

This is probably a reason why different biological membranes from different organelles may have very diverse lipid compositions[4]. For example, the cytosolic membrane of animal cells normally contains very high levels of lipids with saturated fatty acids, as well as a relatively high percentage of cholesterol of up to 30 % molar ratio[30]. This combination of straight saturated acyl chains paired with high amounts of cholesterol leads to a very rigid membrane which is ideal in the case of the cell membrane, whose role is to act as a cell – protecting barrier with low permeability from and to the inside of the cell. On the other hand, organelles that need a flexible membrane, fluid and relatively permeable, utilize higher amounts of unsaturated lipids. For example, the endoplasmic reticulum typically contains an abundance of lipids with unsaturated fatty acid side chains, while it only contains very low amounts of cholesterol, at an approximate 5 % molar ratio[30].

1. 2. Membrane proteins and Mechanosensitive ion channels

1. 2. 1. Membrane proteins

Membrane proteins is a vast and very diverse family of proteins which are integrated in or strongly interact with biological membranes. According to their function inside the living cells, they can be divided into the following generalized categories[35]: membrane receptor proteins, transport proteins, membrane enzymes and cell adhesion proteins. Each category is then subdivided into further sub – categories. Similarly, membrane proteins can be divided into two broader categories, depending on their exact localization regarding the lipid bilayer. The two main categories are the integral membrane proteins, which are permanently and strongly associated with the membrane, and the peripheral membrane proteins, whose association with membranes is only ephemeral[36,37]. The domains of these proteins that span the membrane can adopt one of two distinctive secondary structure motifs: the more

extensively found α – helix, and the β – sheet (which is more broadly, but not solely, found in porins)[38]. On the other hand, peripheral membrane proteins do not actually penetrate the membrane and do not come in direct contact with the hydrophobic core of the lipid bilayer. The interaction of these proteins with the membrane is often indirect, as they may interact with other, integral membrane proteins and remain anchored on them. When their interaction with the membrane is direct, this is through the polar head groups of the lipids found in one of the bilayer's leaflets, typically the inner leaflet of the cytosolic membrane[39].

Integral membrane proteins are found in large quantities in all living cells and serve a variety of purposes. They are so abundant that, according to predictions based on genomic sequencing data, about 30 % of the total number of proteins produced in human (*Homo sapiens)*, *Escherichia coli* and *Saccharomyces cerevisiae* cells are integral membrane proteins[40], and the percentage seems to be in the range of 20 – 30 % for the genomes of most organisms[41]. For instance, in the case of the most widely used microorganism for experimental purposes, *E. coli*, out of the ≈ 4200 total proteins expressed, approximately 1000 are *in silico* predicted to be membrane proteins, while this has been shown experimentally for about 600 of them[42].

Due to the crucial position they occupy on the cell's topology, they act as gatekeepers of the cell membrane and, taking into account the very large variety of their functions, membrane proteins are very common pharmacological targets. In turn, this makes them very attractive and also very important research targets. Unfortunately, due to their nature, membrane proteins are fairly hard to study for a number of reasons. Firstly, despite 20 – 30 % of most organisms' genes encoding integral membrane proteins, their expression levels are typically low and they are not actually found in large quantities in biological membranes. This means that they most usually have to be overexpressed through heterologous expression, with the most common expression system being *E. coli* cells by far[43]. The major problem with this approach is that membrane proteins that are overexpressed from recombinant plasmids frequently aggregate in the host organism's cytoplasm, which means that it is often very hard to obtain high enough amounts of the target protein in a stable, correctly folded and properly functional state[44]. This issue is so multifactorial and the implications are so many, that even the use of different specific strains of the same overexpression organism (e. g. *E. coli*) can affect not only the yield, but the functionality of the overexpressed membrane protein as well[45]. In order to overcome this cytoplasmic aggregation problem and the high cell toxicity it is accompanied by, cell – free expression systems have been devised[46, 47]. This method has been successfully used to overexpress membrane proteins like the mechanosensitive ion channel of large conductance (MscL) in the presence of detergent micelles[48] or subunit complexes of the multi – subunit F(0) – F(1) – ATP synthase in the presence of unilamellar liposomes[49]. The main drawback of this approach is that the simplest

cell – free expression systems which are the most widely used, like *E. coli* or archaeal extracts for instance, are not sufficient to help overcome some of the major problems that arise during conventional heterologous protein overexpression in *E. coli* (e. g. post – translational modifications of mammalian proteins are still impossible, while the produced protein yields are not always necessarily that high). At the same time, methods utilizing more complex cell – free expression systems are either not efficient enough or not very well – established yet, while they can also be very costly and complicated[50].

Furthermore, the natural environment of membrane proteins is biological membranes, but most experimental techniques used to study them cannot be used while the protein is still situated inside its native lipid bilayer. As a consequence of that, membrane proteins need to be first extracted from the native membrane before being properly studied. This is usually done with detergents, which have a lipid – like structure, in the sense that their molecular structure is comprised of a polar part (that may or may not be ionic) and a hydrophobic part. This means that detergents naturally and spontaneously form micelles in order to not allow any direct contact between the surrounding aqueous environment and their hydrophobic parts, in a manner similar to how lipids spontaneously form bilayers and micelles. Membrane proteins can then get reconstituted inside those micelles and satisfy the need of their hydrophobic transmembrane parts to not come in contact with water molecules. The problem with this approach is that detergents, just like natural lipids, make up a large family of compounds whose chemical and physical properties can differ drastically, even if the dissimilarities in their molecular structures are only subtle. The main consequence of this is that the membrane protein – extraction capacity and properties vary significantly between different detergents. In addition, individual membrane proteins seem to have a preference for specific detergents with specific properties[51], in the sense that the structural stability of the extracted protein may vary depending on the detergent used during the extraction procedure[52]. Lastly, even in cases where the appropriate detergent (or detergent combination) for the efficient extraction of a seemingly structurally stable membrane protein from the membrane is found, the extracted and detergent – solubilized protein might end up being only partly functional (or even not functional at all). The functionality of most membrane proteins can potentially be altered, reduced or completely abolished in the presence of some kinds of detergents[53].

1. 2. 2. Mechanosensitive ion channels and their roles in eukaryotes and prokaryotes

Transmembrane integral membrane proteins can be further divided into sub – categories depending on their physiological function inside the living cell. One of these categories contains all the transmembrane transporter proteins, which is a vast

and very diverse collection of proteins that are not necessarily closely related. A large sub – family of transmembrane transporters is that of ion channels[35]. These channels allow the passage of ions (e. g. Cl^-, K^+, Na^+, Ca^{2+} etc) or small molecules through their pores and across the membrane, after the application of some kind of stimulus that is specific for each channel (e. g. build – up of voltage, binding of a ligand or an ion, lateral tension applied across the plane of the membrane etc), a process that could not be possible otherwise, since it is very energetically unfavourable for the charged and hydrated ions to pass through the hydrophobic core of a lipid bilayer[36]. Many ion channels are selective, meaning that they only allow one type of ion or molecule to pass through (e. g. K^+ channels, Ca^{2+} channels etc), while others are non – selective. The main feature that distinguishes ion channels from other transporters is that the transport of ions and molecules through them is passive, which means that the energy needed for the transport is provided by some kind of gradient that has been built up between the two sides of the membrane, be it a chemical, an electrical or an osmotic one[36].

There is a variety of stimuli that trigger the gating of ion channels and the passage of ions and molecules through their pores. One of those stimuli is lateral tension which is spread and propagated across the plane of the lipid bilayer inside of which they are embedded. Those ion channels are called mechanosensitive ion channels and their intrinsic ability to sense and respond to the bilayer's tension is called mechanosensitivity[54, 55]. In a more broad sense, mechanosensation is the ability of living cells to sense mechanical stimuli that come from their surrounding environment and respond to them, and the mechanosensitive ion channels that are found in their cell membranes are the main means through which they achieve that. It would make sense if mechanosensation was one of the first and oldest sensory transmission procedures to evolve in living cells, as such mechanical stimuli can be constantly found throughout a cell's environment[56]. How important mechanosensation is can be easily concluded by the ubiquity of mechanosensitive ion channels, which spans all kingdoms of life, since it has been demonstrated that such channels exist in mammalian cells[57-59], plants[60], fungi[61, 62], as well as in prokaryotic cells (both in bacteria[63-65] and archaea[66-68]). Despite its obvious high importance though, the exact way and the molecular means through which those channels are able to closely interact with their surrounding membranes and sense the bilayer's lateral tension have still not been identified and elucidated.

In higher organisms, such as mammals and other vertebrates, mechanosensitive ion channels serve a large variety of very important purposes. For example, they are involved in some of the most fundamental and complex processes taking place in living organisms, such as the sensations of touch[57, 69] and hearing[70, 71], the ability to sense temperature fluctuations[59, 72] and pain[58], as well as cardiovascular function and physiology[73, 74]. Mechanosensitive ion channels also seem to be implicated in

some serious and potentially life – threatening pathophysiological conditions, such as cardiac arrhythmias[75] and obesity – related insulin resistance that can lead to hepatic steatosis, especially in mice fed with a diet high in fat[76].

Interestingly, mechanosensitive channels (mainly those found in eukaryotic cells) usually respond to other kinds of stimuli, and not solely to mechanical stretching of the biological membrane. In eukaryotes, mechanosensitive ion channels can be divided into 3 broad super – families: the epithelial Na^+ channel (also known as amiloride – sensitive sodium channel / degenerins (ENaC / DEG)[77] super – family, the transient receptor potential (TRP) super – family and the K1 – selective (or two – pore – domain potassium channels, K2P) super – family. An important sub – family of the ENaC / DEG super – family consists of the acid – sensing ion channels (ASIC). This is a family of voltage – independent sodium channels that are abundantly found in neurons and respond to elevated extracellular proton concentrations by gating[78]. Other members of the ENaC / DEG super – family have been associated with the ability of the nematode to mechanosense[79] and move around in its environment[80]. The sub – family of TRP ion channels is possibly the most diverse of the three, as it consists of a further 7 sub – families with multiple different proteins in each one: TRP – canonical (TRPC), TRP - vanilloid (TRPV), TRP - melastatin (TRPM), TRP – polycystin (TRPP), TRP - mucolipin (TRPML), TRP - ankyrin (TRPA), and TRP – NOMPC – like (TRPN, with NOMPC standing for the No mechanoreceptor potential C channel)[81]. An important and heavily studied part of this family is the TRPV – 1 channel, which is non – selective and responds to a large number of diverse stimuli, which include lateral bilayer tension[82] and capsaicin[83], a small lipid – like molecule. The K2P channel super – family, also known as potassium leak channels, is possibly the least diverse, consisting of just 15 members, all of them identified in mammals, and grouped into 6 distinct sub – families: TREK, TALK, TASK, TWIK, THIK, and TRESK[84, 85]. The members of this mechanosensitive ion channel family are abundantly found in neural cells[86] as well as in retinal cells from mice[87]. Two of the most extensively studied K2P channels, TRAAK and TREK – 1, both belonging to the TREK K2P sub – family, seem to play important roles in neural function[59, 88]. Finally, there are a further two important mechanosensitive ion channels found in mammals, called Piezo 1 and Piezo 2. Those channels were discovered relatively recently[57] and they seem to comprise their own separate and evolutionary conserved family[89], since they do not seem to have any significant similarities with proteins belonging to other mechanosensitive ion channel super – families. Nevertheless, they play very important roles, both physiological and pathological. Namely, they are involved in cardiovascular architecture[90] and there is convincing evidence that they are strongly involved in baroreception[91] by mediating blood pressure sensing by neurons[92]. In addition, Piezo 1 seems to be implicated in neoplastic diseases, as a contributing factor to metastatic cancers[93].

Prokaryotic mechanosensitive ion channels act as osmoregulators, responding to changes in the osmotic pressure between the cell's cytoplasm and its environment. So, in essence, they allow the prokaryotic cell to adjust and regulate its cytoplasmic volume and, thus, its turgor pressure, in response to changes in the osmolarity of its environment. When the prokaryotic cell finds itself in a hypo – osmotic environment, water molecules enter the cytoplasm in order to reduce the concentration of the cytoplasmic solute compounds (e. g. ions, proteins and free sugar molecules) and equilibrate the osmotic pressure which, in this case, is higher inside the cell. This influx of water causes the cytoplasm to increase in volume and, as the cell swells, its cell membrane gets stretched. The mechanosensitive ion channels of the cell membrane can then sense the lateral tension produced by this stretching and they open their pores as a direct result of this, allowing solutes to exit the cytoplasm, rapidly reducing their concentration inside the cell. This way the osmotic pressure is equilibrated and the cell remains intact and unharmed.

There are two distinct mechanosensitive ion channel families identified in prokaryotic cells[94]. The first one is the MscS – like family, named after one of the most abundant such proteins, the mechanosensitive ion channel of small conductance (MscS). This is a heavily studied and very well – characterized mechanosensitive channel to date. It was identified through electrophysiology experiments on giant spheroplasts of *E. coli*[95], which essentially are enlarged *E. coli* cells that are devoid of their outer membrane. MscS purified from *E. coli* cells (EcMscS) is a symmetric homo – heptamer, with each one of the identical subunits comprising 286 amino acid residues. All MscS orthologues from other microorganisms that have been studied have also been shown (or predicted) to be heptamers as well[96]. A characteristic feature of MscS is that it has three amphipathic transmembrane α – helices in its structure and, interestingly, the most conserved part of its amino acid sequence between different orthologues is the pore – forming TM3a helix, as well as the parts of the protein immediately after it, the TM3b helix and the subsequent β domain[96]. Apart from MscS itself, the MscS – like family of mechanosensitive ion channels is comprised from a number of other such proteins, the most prominent of which are MscK (potassium – dependent mechanosensitive ion channel) and MscM (mechanosensitive ion channel of mini conductance). MscK, also known as KefA due to the name of the gene that encodes this protein, was first identified as a cation – specific mechanosensitive channel with increased sensitivity to K^+ ions[97, 98]. The case of MscM is somewhat more complicated since it seems to be a family of similar and / or related mechanosensitive ion channels rather than one distinct protein per se, as it has been shown with patch – clamp electrophysiology experiments that even in the case of mutants with the gene encoding for MscM deleted (strains lacking the gene ybdG), a MscM – like conductance can still be detected on occasion[99]. In any case, multiple members of the MscS – like family of mechanosensitive channels are usually present in the same cell. For example, each *E. coli* cell contains multiple

molecules of each of the following mechanosensitive channels: MscS, MscK, YnaI (another low – conductance mechanosensitive ion channel), YbiO (a mechanosensitive channel of moderate conductance), YbdG and YjeP (another MscM or MscM – like protein)[63, 100]. Furthermore, MscS – like proteins have also been identified in plants[60] as well as in fungi[61] and yeast[62].

The other family of mechanosensitive ion channels in prokaryotic cells is the MscL family[94, 96]. The MscL family is dramatically less diverse compared to the MscS – like family, since it only contains bacterial and archaeal orthologues of the mechanosensitive ion channel of large conductance. MscL proteins have so far never been identified in any kind of non – prokaryotic cell and each bacterial or archaeal cell only expresses and contains one member of the MscL family. Despite this very low diversity, MscL proteins play a very important role in the prokaryotic cell.

1. 3. The mechanosensitive ion channel of large conductance, MscL

1. 3. 1. The historical background and a general overview of MscL's function

The mechanosensitive ion channel of large conductance, MscL, is possibly the most heavily – studied mechanosensitive ion channel and one of the very first to be identified ever[64]. It was initially detected through patch – clamp electrophysiology experiments conducted on giant *E. coli* spheroplasts, during which a previously unidentified single – channel conductance of ≈ 970 pS was measured. This conductance was at first attributed, largely due to its high value, to a non – selective porin of the outer membrane, with a potential preference of anions over cations[95]. Today, it is known that this protein is MscL, a non – selective mechanosensitive ion channel that is situated on the inner membrane of prokaryotic cells.

Mechanosensitive ion channels in prokaryotic cells play the role of osmoregulators, facilitating the equilibration of the osmotic pressure between the cytoplasm of the cell and its surrounding environment. In this scope, the role that MscL plays in the cell is of the utmost importance among the mechanosensitive channels, as it acts as a last – resort safety valve for the prokaryotic cell. During a hypo – osmotic shock water from the aqueous environment enters the cytoplasm, which causes the cell to swell up and, in turn, the cell membrane to stretch. If the membrane keeps getting stretched beyond a certain point, called the lytic limit, it will naturally rupture, resulting in the lysis of the cell. MscL sense this membrane stretch through the bilayer's lateral tension and, just as the lytic limit of the bilayer is approached, it gates by opening its non – selective pore to a very big diameter of up to an estimated 30 – 40 Å[101-103], allowing high concentrations of solutes to exit the cell in relatively small time, and

thus rapidly facilitating osmotic pressure equilibration and rescuing the cell from lysis. This large pore opening results to a total conductance of ≈ 3 nS which is a very high value[64], especially when compared to the total conductance value of other prokaryotic mechanosensitive ion channels, such as with that of MscS (≈ 1.25 nS, the second largest value measured for such channels, but still less than half of MscL's conductance)[63], MscK (≈ 0.875 nS, less than a third compared to that of MscL)[98] and MscM (≈ 0.375 nS, just one eighth of MscL's conductance)[99, 104].

Moreover, this unusually wide (for an ion channel) pore opening does not only increase and affect the channel's conductance, but also the species of solutes that are expelled through the channel's pore. It is not only ions, but even larger molecules, such as small proteins, that are allowed to exit the cell through the gating of MscL as well. In order to assess the opening of the channel's pore experimentally, a number of compounds of different size have been used, with their estimated diameters ranging from as low as ≈ 15 Å, up to ≈ 78 Å[101]. The compound diameter estimation was approximate, taking into account the assumption that the compounds used were spherical. In this particular study it was observed that all molecules with an estimated diameter of ≤ 30 Å were able to freely pass through the channel's pore. The compound with the lowest molecular weight that was not able to permeate MscL's pore was found to have an estimated diameter of ≈ 37 Å. It was thus concluded that the fully open channel has a pore diameter that lies in the range between ≈ 30 Å and ≈ 36 Å, with a minimum estimated pore opening of 30 Å. Even if this is an overestimation that arises from the assumption that all compounds used were spherical, which might not necessarily be the case, it is still a good indication that the channel's pore diameter at full opening mode will probably exceed 20 – 25 Å.

The fact that its purpose is to act as a last – resort safety valve for the cell, as well as its very high conductance and its quite large pore, might explain why MscL is naturally so hard to open and needs such high negative pressures to get activated experimentally using patch – clamp electrophysiology. To be precise, among all mechanosensitive channels that are known and tested with this method, MscL has been shown to have by far the highest pressure – activation threshold, with pressure values of ≈ 22 mN/m (milli Neutons per metre) of negative applied pressure for TbMscL and ≈ 12 mN/m for EcMscL, which is significantly higher when compared to the corresponding values for the *E. coli* orthologue of MscS (≈ 7 mN/m) or the eukaryotic channel Piezo 1 (4 mN/m), and even an order of magnitude higher compared to the activation pressure threshold of the potassium – dependent TRAAK channel[105-108].

1. 3. 2. The structure of TbMscL

As stated earlier, MscL orthologues can be found in all bacteria and archaea. Despite the differences between the cells in which this protein can be found, all MscL orthologues have some very big similarities. For example, all MscL orthologues identified are relatively small integral inner membrane proteins that are homo – oligomeric, with each of the monomers between orthologues ranging in molecular weight between 16 – 17 KDa. Probably the two most widely studied MscL orthologues are the ones from *Mycobacterium tuberculosis*, TbMscL, and *Escherichia coli,* EcMscL. The former, TbMscL, was also the first of the orthologues whose crystal structure in its closed state was obtained and solved at a resolution of 3.5 Å (Fig. 1.3 a & b), revealing beyond any doubt the structure of the protein's monomers in space and their different domains[109]. The full – length, wild type TbMscL was shown to be a symmetric homo – pentamer. Each monomer was found to consist of the following domains, going from the N – terminus to its C – terminus: a) a short and amphipathic N – terminal α – helix at the cytosolic side of the membrane, which is sometimes called the S1 helix, that is connected through a relatively short intracellular loop to b) the first, pore lining transmembrane α – helix, TM1, which penetrates the membrane and is connected through its C – terminal side to c) a fairly long and flexible periplasmic loop, whose role is to connect the aforementioned TM1 with d) the second transmembrane α – helix, TM2, that is the part of the channel that comes mostly in contact with the hydrophobic core of the surrounding bilayer, and which is further connected, through another small cytoplasmic loop region to e) the last, C – terminal α – helix, which protrudes inside the cytoplasm.

As easily seen in the crystal structure of TbMscL (Fig. 1.3 a & b), the TM1 helix of each monomer comes into contact with a total of 4 other transmembrane α – helices: the two TM1 helices of the two adjacent monomers, the TM2 helix of the same monomer and the TM2 helix of one of a neighbouring subunit. The TM1 helices are tilted with respect to the plane of the bilayer, and this gives MscL's pore roughly a reverse conical shape. At the periplasmic (top) edge of the pore, the distance between the TM1 helices is the longest, allowing the pore to reach a diameter of ≈ 18 Å (Fig. 1.3 b). Moving downwards along the pore, those helices start converging, until they meet close to the cytosolic edge of the surrounding lipid bilayer (which lies roughly at their N – terminus) and form the restriction site of the pore (at residue 21), which has a diameter of approximately 4 Å (Fig. 1.3 b). At this part of the TM1 helices, hydrophobic residues (such as valine and isoleucine residues) are quite abundant and, importantly, the amino acid sequence at this part of the protein is highly conserved between orthologues from different prokaryotic organisms[109]. This way, the TM1 helices form a hydrophobic barrier at the constriction site of the

channel's pore, which does not allow solutes to cross the membrane as long as this remains closed.

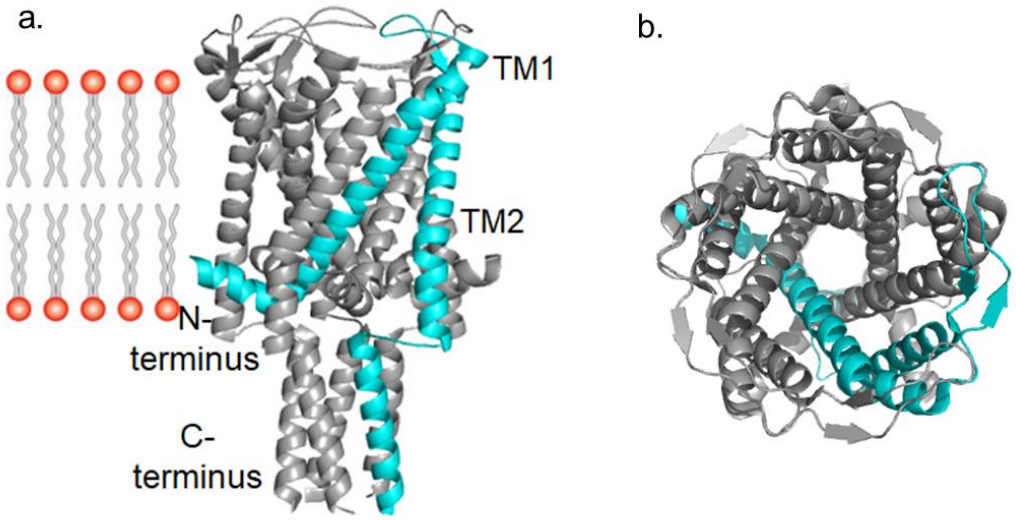

Fig. 1.3: The pentamer of TbMscL as shown by the crystal structure. One of the monomers is coloured cyan for clarity. **a)** Side view of the channel with the transmembrane part designated by a lipid bilayer cartoon, and the monomer's domains are named on the structure. **b)** Top view of the channel's pore.

In addition, due to the tight packing of the transmembrane helices, the contact surface between individual subunits in the transmembrane part of the protein is quite extended, allowing for a high number of hydrophobic or other types of interactions to develop in a single monomer as well as between adjacent subunits. This could possibly play a role in the high pressure threshold of activation that is needed for the opening of TbMscL. Furthermore, it can be observed that the two kinds of transmembrane helices have distinct roles in the channel's structure: the TM1 helices are the ones that mostly make up the lining of the pore, and the ones that form the constriction site, while the TM2 helices mostly line the "external" surface of the channel, so they are the ones that come into most contact with the lipid bilayer that surrounds the channel. This could also potentially mean that the mediation of interactions between the protein and its surrounding annular lipids mainly occurs through the TM2 helices. Finally, the C – terminal helices from all the monomers form a tight bundle inside the cysoplasm, which brings the individual subunits of MscL further into close contact.

1. 3. 3. The structure of MscL orthologues and dispute over its oligomeric state

Until the crystal structure of the first MscL orthologue, TbMscL, was published[109], researchers could not agree on the oligomeric state of the protein. The dispute was about whether MscL is a homo – pentamer or a homo – hexamer, since there were some early cross linking experiments and some studies that used two – dimensional electron microscopy that pointed towards the latter[110, 111]. Nevertheless, TbMscL's crystal structure demonstrated that the protein is a symmetric homo – pentamer. Despite that, a few years later a new crystal structure was published, this time that of the *Staphylococcus aureus* orthologues of MscL, SaMscL[112]. In this case, the protein was crystallized in an expanded and possibly intermediate, but non – conducting state. Interestingly, the crystal structure revealed SaMscL to be a homo – tetramer, against what was theorized before (a homo – hexamer) or what was shown for TbMscL (a homo – pentamer). However, this finding was almost immediately greeted with skepticism[113] and, since then, it has often been considered an artefact that was introduced because of the experimental and methodological approach of the study, and there are two main reasons used to support this point of view.

The first argument arises due to the specific MscL construct that was used for the purposes of this study. There was a C – terminal truncation in the SaMscL construct used, namely Δ (95 – 120), which means that the protein was missing 26 amino acid residues at the C-terminus (SaMscL C - Δ26). This was initially deemed important and relevant to the oligomeric state of the SaMscL construct because it was shown that this is the case regarding another MscL orthologue, EcMscL[114]. When various mutants of EcMscL with deletions and / or truncations at the C – terminal end of the monomer were generated and the oligomeric state of those mutant channels was assessed, it was shown that the number of monomers that assembled in order to form a functional channel could differ. In detail, the conclusion of the study was that there is no preference for the adoption of a pentameric state, unless residue L129 and the C – terminal amino acid residues following it in the sequence were present. Interestingly, the experiments showed that, once the apparently important residues L129 and K130 were present, the presence of more C – terminal residues progressively facilitated the assembly of EcMscL monomers towards a pentameric protein. Important as these findings may be, they are not adequate as evidence against the existence of the tetrameric SaMscL. That is because, through *in vitro* cross linking experiments, it was demonstrated that both the previously used truncated SaMscL CΔ26 construct and the wild type protein adopted a preferentially tetrameric oligomeric state in detergent solution[112].

Despite that, there is another, more well – founded argument that could be used to support the view that the tetrameric SaMscL crystal structure was a methodological artefact, which has to do with the detergent used for the extraction of the channel

from the membrane and for its solubilization. In a study where native protein mass spectrometry was employed, it was clearly demonstrated that there is a large number of factors that influence and affect the oligomeric state that different MscL orthologues could adopt, and one of the main effectors was found to be the detergent used for the protein's solubilization and extraction[115]. Furthermore, even when the same detergent (i. e. LDAO, lauryl dimethyl amine oxide) was used for one specific construct, the effect on the oligomeric state was shown to be temperature – dependent. Moreover, the effects mentioned seemed to be further exaggerated in cases where the SaMscL construct used was a C – terminal truncation variant. The SaMscL C – Δ26 construct was typically detected in a tetrameric state in varying conditions, while the C – GFP – tagged wild type protein was always and only detected as a pentamer under the same experimental conditions. In addition, another study using the same truncated SaMscL construct showed that, both *in vivo* and in a native lipid environment, the channel adopts solely the pentameric oligomeric state[116]. These lines of evidence combined point towards the view that the tetrameric crystal structure observed for the C – Δ26 SaMscL construct was very possibly indeed a methodologically derived artefact, that arose from the experimental conditions used (namely, the C – terminal truncation, the detergent used and potentially the temperature at which the experiments were performed). All those pieces of evidence presented so far strongly support the view that TbMscL and its prokaryotic orthologues are assembled as symmetric homo – pentamers in nature.

In addition, there are some more recent MscL orthologue crystal structures that further support the argument for a pentameric MscL, this time coming from an archaeal microorganism, *Methanosarcina acetivorans* (MaMscL, which was also shown to be a pentamer on the membrane and in detergent solution)*[117].* This was the first time a non – bacterial MscL orthologue was crystallized and its structure solved. Two crystal structures of MaMscL were obtained in this study, in two distinct conformational states: one in its usual closed state and one in an expanded, intermediate state. Whether the latter expanded structure is also representative of a sub – conducting intermediate state or the protein in this conformation is still non – conducting, is still unclear. In order for this MscL orthologue, called MaMscL, to be crystallized, the full – length wild type channel had to be fused through its C – terminal end with the enzyme riboflavin synthase (MjRS, from the archaea *Methanocaldococcus jannaschii*), which is a soluble pentameric protein. Apart from the fact that, as stated earlier, these crystal structures further support the view that MscL is a pentamer, they are also very significant and important for another reason: this was the first time any of the MscL orthologues ever investigated was trapped in any state other than its closed one (in their natural pentameric assembly). The crystal structure of the expanded state is, in a way, possibly a snapshot of one of the intermediate steps that eventually lead to the channel's full pore opening. Since no

MscL orthologue has ever been crystallized in its fully open conformation and, moreover, the gating mechanism of the channel was not yet known, this expanded state crystal structure could potentially prove to be a very helpful preliminary insight of the route through which MscL's closed state gets destabilized and the channel transitions towards the fully open one. Furthermore, the fact that the closed state channel was also crystallized in the same study adds to its importance, since it means that direct comparisons could be made between the two conformations of the same orthologue (e. g. individual amino acid residue displacement, tilting and / or rotation of the transmembrane α – helices, etc) and conclusion about the course of the gating mechanism could possibly be drawn, without the need to utilize software – based simulations and structural models. Finally, an interesting fact regarding the expanded state crystal structure is that the means by which the protein was "trapped" and eventually crystallized in this conformation are still unknown[117]. The only hint provided, which could shed some light on this question is the specific condition that was used in the crystallization plate's well, which contained a very high concentration (1.6 M) of $(NH4)_2SO_4$, combined with the fact that the crystals were obtained after a quite long incubation time of five months in the crystallization plate.

1. 4. Towards unraveling the gating mechanism of MscL

1. 4. 1. The role of the interactions between MscL and the membrane, and its implications

Despite a long history of research on MscL which has led to the clarification of some aspects of the channel's features and characteristics, the exact way through which the channel is activated and gates has not been elucidated at the level of molecular detail. The crystallization of the channel in its fully open state would potentially provide us with essential details regarding its gating mechanism, but this has not been achieved yet either. The reason why the open crystal structure has not yet been obtained has to do with the physiological role that MscL plays in the prokaryotic cell: the channel's main, and most possibly only, natural trigger that initiates activation and gating is the lateral tension (stretching) of the surrounding lipid bilayer. Consequently, capturing the native, wild type channel in an open conformation while the protein is in an aqueous detergent environment (which is needed for its crystallization) and not embedded inside a bilayer, has been proven to be very challenging. This might even be impossible, if we take into consideration that no natural physiological agonist has been identified that is able to trigger or promote the channel's activation and opening, whether inside a lipid bilayer or outside of it, since MscL is a solely mechanosensitive channel that is not sensitive to other kinds of triggers (e. g. voltage, ligands, etc).

In addition, the sheer fact that MscL is an integral membrane protein poses its own challenges on any attempt to trap the channel in an open conformation and crystallize it. Firstly, an important prerequisite for the crystallization procedure is that the membrane – extracted and purified protein is very monodisperse, while at the same time it remains well – folded and structurally stable throughout the whole process, which might take weeks or months, and this is rarely the case with membrane proteins[118]. Also, the transmembrane parts of membrane proteins are designed to interact with the fatty acid core of the lipid bilayers they are embedded in, and are thus comprised mostly (if not exclusively) of hydrophobic amino acid residues, and this is well - known to make crystallization of membrane proteins quite challenging, due to the fact that after solubilization, these parts of the protein are "covered" by the micelles of the detergent used[119]. If we take into account the fact that the hydrophilic parts of MscL (namely, the periplasmic loop and the cytosolic C – terminal α – helical bundle) are a quite small percentage of its total surface when compared to its transmembrane, hydrophobic part, the difficulty to obtain the crystal structure of the native, wild type protein in its open conformation seems to increase significantly.

An important prerequisite for the crystallization of a protein is that the purified sample is highly monodispersed. Regarding this, another difficulty that arises with the crystallization of MscL is that, according to the functional and (limited) structural data available so far, the activation and gating mechanism seems to be fairly complicated, with the channel adopting a sequence of distinct intermediate expanded conformations between the fully closed and the fully open one, with some of them being putatively non – conducting while others are sub – conducting[120]. And as if things were not complicated enough, it still needs to be clarified whether all of those individual intermediate states that have been identified are indeed the consecutive and progressive steps of a unique and coherent mechanism of the channel's gating, which eventually leads to MscL's natural full opening, or if they are steps of unrelated and possibly futile pore expansion pathways that are not capable of leading to the fully conducting and open state, and which are introduced as methodological artefacts due the experimental procedure followed.

All of the above underline the challenges faced during the attempts to artificially activate the wild type MscL, trap it in its fully open state and characterize it through X – ray crystallography. This is the reason why in most studies that have had this scope, other methods and means were typically employed towards the goal of triggering the channel's activation or expansion. These studies have led to the identification of a number of features and factors that seem to contribute and play a role, less or more significant, in the channel's gating. These factors, depending on whether they are intrinsic characteristics of the protein itself or they are external triggers, can be divided into two broad categories: (a) amino acid residues that have

been suggested to play a part in the ability of MscL itself to mechanosense[34, 121, 122], and (b) lipids of the surrounding membrane that are suggested to have an effect on the sensitivity of the channel[123].

1. 4. 2. The role of individual amino acid residues on MscL's gating

Specific individual amino acid residues can have an impact on MscL's ability to mechanosense, and tampering with such amino acids has been used as a means to alter the intrinsic ability of the channel to sense and respond to the lateral tension of the lipid bilayer. In general, amino acid residues that are found to be highly conserved among the sequences of a given protein's orthologues are very likely to play an important or even crucial role in the physiological mode of function of this protein. An initial and rough estimation of the conservation of specific domains and, consequently, individual amino acid residues, that may be important for the function (or structure) of a given protein can be generated through the genomic analysis and comparison of the genes that encode the orthologues of the protein in question between different organisms.

The first genetic comparative analysis of the genes of MscL orthologues from a large number of different bacterial genomes that was published demonstrated quite clearly that there are parts and domains among those proteins, the amino acid sequences of which are highly conserved. Not surprisingly, regions that correspond to the channel's transmembrane core, on the two transmembrane helices TM1 and TM2, had the highest conservation levels, while the C – terminal α – helix of the orthologues investigated displayed high conservation rates in parts, too[124]. A subsequent and more detailed genomic analysis, in which genomes from archaea were compared alongside bacterial ones, was able to identify individually specific amino acid residues with high conservation rates among an even larger number of MscL orthologues[125]. In addition, this analysis was able to also pinpoint a large number of conservative mutations: these are cases where, despite the occurrence of an amino acid that is not conserved between two orthologues of the same protein, the chemical and / or physical properties of the protein's sequence at the position remains roughly the same, e. g. the mutation of a basic amino acid like arginine to another basic one, like lysine, which conserves the polarity and charge of the protein structure, is considered a conservative mutation.

Once individual amino acid residues of possible functional importance have been identified through the initial comparative genomic analysis, the next step is to investigate the exact role those residues play in the function and / or structure of the protein in question. An efficient way to achieve this is through generation of random mutants of those residues. The first study concerning MscL that adopted this

approach employed the introduction of random mutations in the gene of the EcMscL orthologue, and it successfully led to the identification of specific and unique mutations in the protein that exhibited a gain of function phenotype (the expression of MscL mutants that were more sensitive and gated more easily when compared to the wild type protein)[126]. Those mutations were subsequently categorized depending on the severity of the gain of function phenotype that they brought about. The importance of this study was that it managed to pinpoint residue G22 of EcMscL. This is a TM1 residue that, by comparison and analogy to the TbMscL's closed crystal structure, should lie secluded from the aqueous buffer inside the channel's pore and close to its outermost constriction site. Due to its position in a part of the protein that is in theory crucial for its mechanosensitive gating mechanism, it ended up being possibly the most extensively studied EcMscL amino acid residue[121, 127]. A final rigorous attempt towards identifying critical sites on the structure of EcMscL was undertaken, with the production of a library of 113 cysteine mutants of this orthologue[122]. The significant difference between this one and the previous studies is that it was taken a step further, with the cysteine mutants being subsequently post – translationally modified with a number of different methanethiosulfonate reagents. The utilization of different modification reagents, which were characterized by a variety of individual physical and chemical properties, allowed the assessment not only of the effect of amino acid mutations, but also that of the introduction of electrical charge and the alteration of the hydrophobicity of specific parts on the protein's structure.

Finally, gain of function mutation studies have not only been conducted on EcMscL, but on TbMscL too. At the C – terminal end of TbMscL's TM2 helix, so at the site of the lipid head group edge of the inner leaflet of the lipid bilayer, lies a cluster of positively charged amino acid residues: arginine R98, lysine K99 and the final lysine K100. Such positively charge amino acids at this part of the protein's structure could be expected to act as some kind of anchor for negatively charged polar lipid head groups of annular membrane lipids that come into direct contact with the protein. Interestingly, such clusters of positively charged amino acids can be found in all MscL orthologues. A gain of function study that used those amino acid residues as mutation targets showed that mutation of each individual one of them to glutamine (a mutation that preserves the polarity and roughly the side chain length of the residue, but eliminates the charge), and especially the R98Q individual mutation, led to gain of function phenotypes[34]. The simultaneous mutation of all three residues to glutamines, i. e. R98Q – K99Q – K100Q, produced a severe gain of function phenotype according to cell survival studies, while the same was true for an unrelated mutation of the TM1 helix and pore – lining residue V21 to lysine (V21K)[34].

1. 4. 3. The role of the surrounding bilayer and specific phospholipids

Integral membrane proteins, including mechanosensitive ion channels, are physiologically found embedded inside the membranes of cells. It is thus very reasonable to expect that their function is, at least to some extent, assisted and / or regulated by their immediate environment, which is the surrounding lipid bilayer, and this would seem even more natural in the case of mechanosensitive ion channels, since their physiological role is to sense the stretching and deformations of the membrane they find themselves in. Contrary to what described in the case of the effect of amino acid residue mutations before, where mutations have a direct effect and alter the primary, secondary and maybe even the tertiary structure of the protein, the role that lipids that lipids play is more indirect (for example, at least in the case of mechanosensitive channels, they do not tend to act as agonists or ligands[108, 128]). Thus, lipids are typically expected to exert their effect on the protein through alterations of the local physical properties (for example, the curvature and / or the thickness) of the bulk of the surrounding bilayer (so, the non – annular lipids). The extent to which a specific species of phospholipid can affect the bilayer's properties, as well as the exact nature of the change they can bring about, largely (if not solely) depends on the physical and chemical properties of the phospholipid itself. The degree of the aliphatic acyl chain's saturation, as well as the size and the charge of the polar head group, are all able to affect and change the curvature of the lipid bilayer, while the length of the esterified fatty acids and the degree of their saturation affect not only the thickness of the bilayer, but its fluidity as well[24, 129]. This means that the properties of a lipid bilayer and, consequently, the modulating effect it can have on a mechanosensitive ion channel's function, can be manipulated by doping the given bilayer with phospholipids of specific physical chemical properties[130-132].

Interestingly, the effect that a given alteration of the properties of a bilayer will have on a mechanosensitive ion channel largely depends on the individual channel as well. A very prominent example of this regarding prokaryotic mechanosensitive channels is the effect that the lipid bilayer's thickness has on the activation and gating of MscL and MscS. Thicker bilayers, consisting of longer acyl chain lipids, have been proposed to favour the closed – state conformation of MscL, while the gradual thinning of said bilayer seems to reduce the pressure activation threshold of the channel and increase the channel's sensitivity towards gating[133]. A response like this on behalf of the channel is not necessarily surprising, since the thinning of the bilayer could be acting as a simulation of some of the properties of a biological membrane as it is being stretched: large lateral tension, through which the surface of the bilayer increases, propagated throughout a finite and given number of lipid molecules would naturally result in the thinning of the lipid bilayer. In the case of MscL, the effect of the bilayer's thickness might be connected with easier opening of the channel through a proposed mechanism for gating: The channel in its

completely expanded state has an estimated full pore opening of ≈ 30 Å and, in order for this to be achieved, the transmembrane helices need to tilt enough with regard to the bilayer's plane, so that the angle reaches ≈ 45°. If indeed such a large tilting move were to happen, it would lead to a considerable "shortening" or "flattening" of the channel, of possibly more than 25 Å[134, 135]. During such a gating process, there would be a better matching and a more energetically favourable overlap between the short (or tilted due to lateral tension) hydrophobic lipid acyl chains and the shortened transmembrane and hydrophobic surface of MscL, although in this case correlation must not necessarily be taken to imply causation. In addition, thinner bilayers are usually a result of an assembly of lipids with shorter acyl chains. Between short acyl chains there are fewer hydrophobic interactions to keep the lipids close to one another and, thus, pulling them apart through lateral tension could be expected to be easier, requiring a smaller amount of energy and, consequently, a reduced amount of negative pressure. On the other hand though, MscS has not been shown to be as sensitive to changes in the thickness of the surrounding bilayer[123].

What is even more interesting is that the effect of specific lipid species has been shown to have a different effect among MscL orthologues as well. Those differences are unsurprisingly theorized to have a connection with the specific organism that each orthologue has been evolving in, and probably manifest through differentiations in the amino acid sequence of each protein. An important and prominent example of this is the drastically different effect that phosphatidyl inositol has on TbMscL and EcMscL. For experimental purposes, TbMScL is typically expressed in strains of *E. coli* cells, but as shown earlier, its sensitivity to gating is much reduced compared to that of native EcMscL. Regarding their lipid compositions, the most characteristic difference between the two bacteria, *Mycobacterium tuberculosis* and *Escherichia coli*, is that the cell membrane of the first is quite rich in phosphatidyl inositol (comprised approximately 12% of this lipid[136]), while this lipid species is completely absent in the case of the latter. The importance of the existence of phosphatidyl inositol for an increase in TbMscL's functionality was experimentally demonstrated by addition of this lipid species in lipid vesicles inside which the channel was embedded[136].On the contrary, when EcMscL was reconstituted in such phosphatidyl inositol – enriched vesicles, no effect on its ability to mechanosense could be detected.

Another lipid species that is often utilized in relevant studies is lyso phosphatidylcholine, or LPC, due to its characteristic properties: this lipid is comprised of a relatively large polar head group but only one acyl chain, which gives it a roughly reverse conical shape. This means that LPC has an intense local effect on the surrounding bilayer, strongly inducing negative curvature. From a mechanical point of view, negative curvature simulates some properties, namely the bending, of a lipid bilayer that finds itself under intense turgor pressure and, thus, lipids that

induce this kind of curvature could be expected to affect a mechanosensitive ion channel's sensitivity and activation. In the case of MscS, the strong effect of LPC on the channel's gating was clearly demonstrated through the combination of a number of different techniques, including single molecule planar lipid bilayer electrophysiology experiments, X–ray crystallography and molecular dynamics simulations, while at the same time causing partial dissociation of the channel under circumstances[128]. While MscS was reconstituted inside a planar lipid bilayer, once LPC was added to the bilayer from the channel's cytosolic face, the channel was activated for minutes to hours, reaching a maximum conductance of approximately three quarters of the channel's expected total conductance during full opening. This leads to the conclusion that, in the absence of applied negative pressure, LPC is capable of activating MscS *in vitro*, but it lacks the ability to cause the full opening of the channel's pore. In the case of MscL, it has been suggested that, via altering the interactions and coupling between the channel and its surrounding lipid bilayer[137], LPC can have an influence on the activation threshold of the protein, but the effect is significantly less pronounced compared to that on MscS[106].

1. 5. The "Lipid moves first" model: Direct interactions between mechanosensitive channels and lipids

1. 5. 1. The binding site of mechanosensation and the "Force – from – lipids" principle

Mechanosensitive ion channels can be found throughout all kingdoms of life, serving a large variety of different purposes depending on the organism there are found in, and play crucial physiological roles in each individual cell. Despite this apparent high significance of mechanosensitivity in living cells, the exact way through which lipid bilayer tension is sensed by mechanosensitive channels and converted into a biochemical response is not yet known in any molecular detail. So far, the best, though very generalized and undetailed, model of how mechanosensitive channels sense lateral tension from the bilayer is the "Force – from – lipids" principle[138], which is founded on the logical assumption that, since mechanosensitive channels gate in response to deformations of the surrounding membrane, the initiating step that sets the gating mechanism in motion must be a change in the lipid environment of the protein. This can be a global stretching of the bilayer, a local deformation such as induction of curvature, or a combination of those[139]. This model is generalized enough so that it can be applied to the large variety of mechanosensitive channels, but it lacks any kind of molecular detail that is essential for the deeper understanding of the process of mechanotransduction and, consequently, its potential manipulation.

The fact that mechanosensation is still not well understood has largely to do with the high dissimilarity observed among mechanosensitive channels. Typically, families of proteins with a common or similar physiological function tend to have a distinguishing feature, a characteristic fingerprint on some level or levels of their structure, e. g. the active site of enzymes that catalyze a similar reaction or the binding site of a ligand, and this feature can be used to categorize said proteins in families. However, no such distinguishing feature has ever been associated with the ability of ion channels to mechanosense, the "binding site" of mechanosensation is still elusive, as different mechanosensitive ion channels have not been shown to have any prominent amino acid sequence similarities. As if this did not pose a challenge hard enough, they lack any important similarities in other aspects of their structure too, e. g. their size or their oligomeric states. This means that the fingerprint of mechanosensation must be something less expected or something more subtle than a simple resemblance in the amino acid sequences of mechanosensitive channels. And since the role of MS channels in general is to sense the tension of the bilayer, it would be expected that their distinguishing feature should lie somewhere on their hydrophobic transmembrane surface, rather than in other parts of the protein like the pore.

1. 5. 2. Hydrophobic nano – pockets and the "Lipid moves first" principle

Molecular dynamics models of the lateral tension sensitivity of mechanosensitive channels embedded in lipid bilayers suggest that there are two areas on a channel's surface that display increased sensitivity: one close to the edge of the outer leaflet of the bilayer and one close to the edge of the inner one, with the latter being more sensitive than the former[139-141]. Interestingly, an unusual structural feature can be identified on this lower – leaflet region of mechanosensitive ion channels: a varying number of hydrophobic void crevices, or nano – pockets. Such nano – pockets can be seen in the crystal structures of both prokaryotic (e. g. MscL[109] and MscS[128, 142, 143]) and eukaryotic (e. g. TRPV - 1[83, 144] and TRAAK[145]) mechanosensitive ion channels (Fig. 1.4 a & b). As expected, such voids are naturally unstable and collapse in molecular dynamics simulations[146]. Thus, not to much surprise, in a high – resolution crystal structure of MscS those nano – pockets were found to be penetrated and occupied by acyl chains[128]. Similarly, resiniferatoxin[147] and capsaicin[83] bind to the transmembrane core of TRPV – 1, while another compound, norfluoxetine, which is the active metabolite of the drug Prozac, has been shown to bind to an equivalent region of the mechanosensitive potassium channel TREK – 2[148]. What all those compounds, but especially the first two, have in common, is that their structures resemble that of a lyso phospholipid, such as LPC.

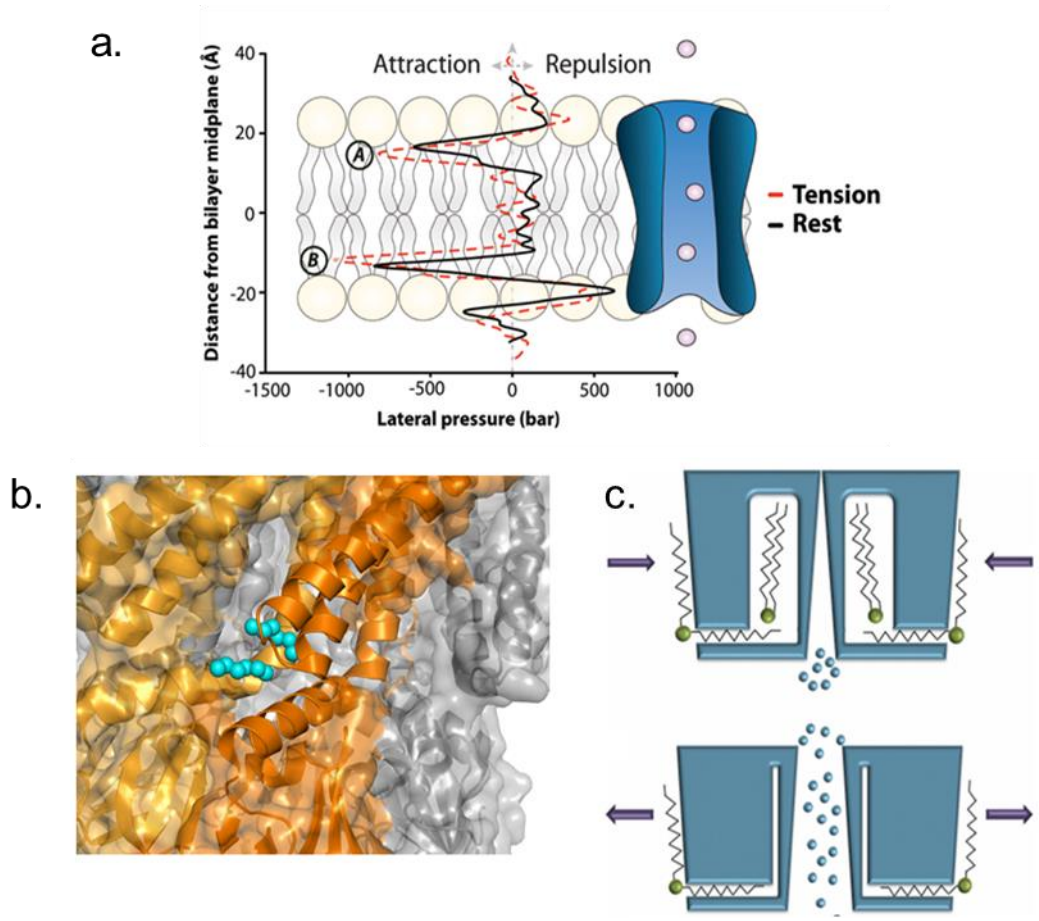

Fig. 1. 4: a. Tension – sensitivity profile of a mechanosensitive ion channel in a lipid bilayer (adapted from Martinac et al, Curr Op Membranes, 2017). **b.** The nano – pocket of MscS (orange helices) occupied by two acyl chains (cyan spheres), as revealed by its crystal structure (adapted from Pliotas et al, Nat Struc Mol Biol, 2015). **c.** An illustration of the "Lipid moves first" principle of protein – lipid interactions of mechanosensitive ion channels upon gating (adapted from Pliotas & Naismith, Curr Op Struc Biol, 2017).

Hence, since those nano – pockets seem to play a crucial role in the ability of ion channels to mechanosense, an advanced model of how mechanosensitivity works has been proposed, called the "Lipid moves first" principle, which is an evolution of the more simplistic "Force – from – lipids" model that takes into account the newly proposed "active sites" of mechanosensitivity[128, 146, 149]. According to the "Lipid moves first" principle, as long as those nano – pockets remain occupied by lipid acyl chains, the mechanosensitive channel remains closed. Once lateral tension forces the annular lipids to evacuate those nano – pockets, a void is created inside them. In order for those unnatural voids to be eliminated, the protein alters its conformation

and the resulting global structural rearrangements eventually lead to the opening of the pore (Fig. 1.4 c). This model can also explain the mode of activation and gating by LPC, which leads to a value of conductance that is smaller than what expected for the full pore opening. This lipid only has one acyl chain, so it is unable to fully occupy the nano – pockets, and thus the channel has to rearrange its structure to accommodate for the empty space. But since a part of the nano – pockets is still occupied by that one acyl chain of the LPC, the channel has to only partially rearrange its conformation, which leads to an intermediate rather than full pore opening[128, 146].The “Lipid moves first” model of the mechanosensitive ion channel’s gating mechanism is more detailed and comprehensive than the much more simplistic and superficial “Force – from – lipids” principle, so can be applied to channels that are solely mechanosensitive as well as channels that respond to other stimuli too, and is able to provide the activation mechanism with a specified molecular trigger that links the deformations of the bulk of the lipid bilayer with the mechanosensitive channels and their physiological response to it. In other words, according to this model and contrary to the usual point of view as described earlier, a number of the annular lipids that come in direct contact with the protein play the role of ligands “bound” to the nano – pockets of the channel, with the pore remaining closed for as long as those tight physical and chemical interactions between the lipids and the hydrophobic crevices are in place. Nevertheless, the validity of this model has not been experimentally verified explicitly yet.

1. 6. Electron Paramagnetic Resonance (EPR) spectroscopy

1. 6. 1. The basics of EPR and Continuous Wave EPR (CW – EPR)

EPR is the general name for a collection of different physical chemical techniques which are often used for the biophysical assessment of the structure of proteins. As the name implies, EPR is based on the ability of unpaired electrons, which are a characteristic feature of paramagnetic chemical compounds such as radicals, to absorb energy and change their spin state when they find themselves inside an externally applied magnetic field. As the unpaired electron relaxes back to its initial ground spin state, it emits energy (heat). In that sense, EPR is a family of techniques similar to NMR, which relies on the absorption of energy by nuclei with a non – zero magnetic spin number under the influence of an externally applied magnetic field.

In order for EPR experiments to be conducted, at least one unpaired electron, so in essence at least one radical, is needed on the protein molecule, but since (with the exception of some cofactors and metal ions) proteins do not typically contain any paramagnetic centers, the unpaired electron has to be introduced on the structure

of the protein in the form of a post – translational modification with a paramagnetic radical. This is achieved through subsequent steps of site – directed mutagenesis and paramagnetic spin labelling, an approach that has been used extensively on proteins since its initial development in 1989[150]. Through the first step of site – directed mutagenesis, if no native cysteine residues are present at a site of interest, an amino acid residue of interest on the protein is mutated to a cysteine and the mutant protein is subsequently expressed and purified. Afterwards, the mutated cysteine is reacted with a paramagnetic compound (the spin label) and, thus, a paramagnetic center is generated on the protein. The first such spin label used for this procedure was S - (1 – oxyl - 2, 2, 5, 5 – tetramethyl - 2, 5 – dihydro - 1H – pyrrol – 3 - yl) methyl methanethiosulfonate, or simply MTSSL, which is still the most widely used paramagnetic compound for this approach. Through its methanethiosulfonate moiety, MTSSL can react with the cysteine forming a disulfide bond, which has the advantage of being reversible and the spin label can be eliminated from the protein with the use of reducing agents.

The EPR spectrum of the nitroxyl radical of MTSSL introduced on a protein through site – directed spin labelling can then be obtained with continuous wave EPR (CW – EPR) spectroscopy, which is the simplest and most basic of the EPR techniques discussed here. The unpaired electron introduced through the nitroxyl radical is characterized by its electron spin quantum number $S = ½$, with its magnetic components being $m_s = + ½$ (dubbed parallel spin) and $m_s = - ½$ (dubbed antiparallel spin). For as long as the electron is not affected by an external magnetic field, the two spin states are degenerate, meaning that they are of equal energy. Once the unpaired electron finds itself inside a magnetic field though, the energy levels of the two magnetic spin states split due to the Zeeman effect (Fig. 1.5 a), with each state characterized by its energy $E = m_s g_e \mu_B B_0$, with g_e being the electron spin g – factor (which is ≈ 2.0023 for a free electron), μ_B being Bohr's magneton and B_0 being the externally applied magnetic field. Hence, the energy difference between the high (excited, $m_s = - ½$) and low (ground, $m_s = + ½$) energy states is $\Delta E = g_e \mu_B B_0$, which is proportional to the externally applied magnetic field. This means that, if an electron that is in the ground energy state absorbs a photon of energy $h \nu = \Delta E$, it will be excited to the high energy level. This is the condition of resonance in EPR spectroscopy. In this simple case, where the unpaired electron does not interact with any other magnetic components in its direct environment, there is only one energy difference ΔE for a given magnetic field B_0 and, hence, the EPR spectrum would only consist of a single emission peak.

In reality, the EPR spectrum of a nitroxyl radical contains three discreet emission peaks due to interactions between the unpaired electron and its surrounding nuclei. The splitting of the initial single emission peak into three is caused by the hyperfine interaction between the unpaired electron and the ^{14}N nucleus (Fig. 1.5 b). ^{14}N has

a non – zero nuclear spin quantum number I = 1, with its magnetic components being m_I = - ½, 0 and + ½ which, in the presence of the external magnetic field, are split in a way similar to the ones of the unpaired electron. This causes the two energy levels of the electron to be further split into three each, one for each of the magnetic spin states of the ^{14}N nucleus. Thus, a total of six discreet energy levels are available for the electron. This leads to three possible permitted transitions: (m_s = + ½, m_i = + 1) → (m_s = - ½, m_i = + 1), (m_s = + ½, m_i = 0) → (m_s = - ½, m_i = 0) and (m_s = + ½, m_i = - 1) → (m_s = - ½, m_i = - 1) (Fig. 1.5 b). According to the applying selection rules, an EPR transition is permitted, meaning that it is of high probability, as long as $\Delta m_s = \pm 1$ while $\Delta m_I = 0$, and forbidden transitions ($\Delta m_s \neq 0$ and $\Delta m_I \neq 0$) typically become progressively less probable as the energy gap ΔE increases (so, in higher magnetic field values). Those three permitted transitions are the ones that give the EPR spectrum of the nitroxyl radical its characteristic 3 – peak line shape. Typically, CW – EPR spectra are not presented as the emission peaks, but rather as the first derivative.

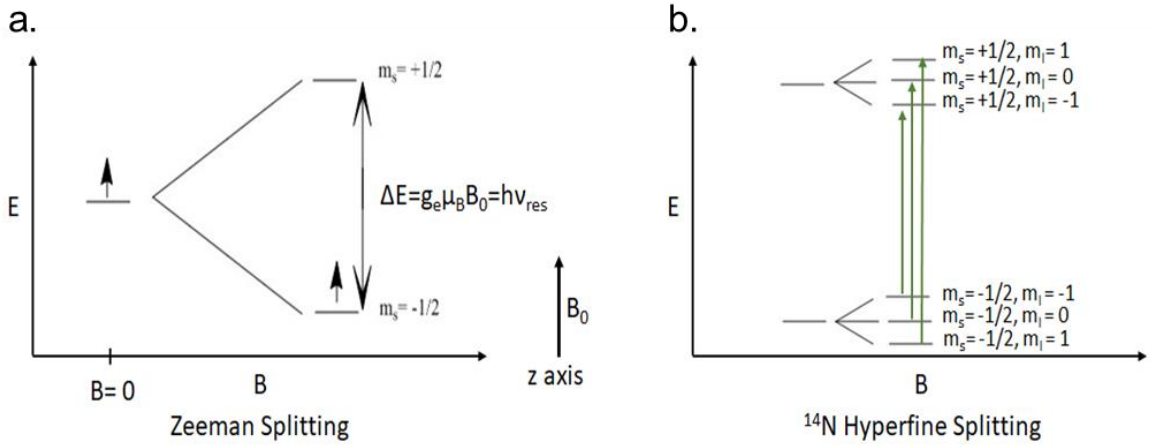

Fig. 1. 5: a. The splitting of the unpaired electron's energy levels due to the Zeeman effect upon application of an externally applied magnetic field. **b.** Further splitting of the electron's energy levels due to the hyperfine interactions with the ^{14}N nucleus. The three permitted EPR transitions are shown as arrows.

The exact ΔE values of the permitted transitions also depend on the environment of the spin label, and this is the most important piece of information provided by a CW – EPR experiment. First – derivative peaks of spin labels that are more exposed to the aqueous solution, and thus are able to move more freely in the space surrounding them, are sharp and have a smaller width, while those of more restricted spin labels are broader. This, combined with the inherently differing ΔE values between the three transitions, means that, in order for the condition of resonance to be fulfilled for the sum of the unpaired electrons of the sample, one of the two

externally applied components, the magnetic field or the microwave radiation, has to be kept constant while the other one is being changed. In practice, in a CW – EPR experiment, the frequency of the microwave radiation is kept constant at ≈ 9.8 GHz for X – band EPR experiments, while the applied magnetic field is varied. Under these conditions, nitroxide resonance typically arises at ≈ 3500 G. Through its ability to assess the mobility of the paramagnetic spin label on a protein, CW – EPR has been utilized in the case of MscL in an attempt to qualitatively measure a potential conformational change[135]. Nevertheless, this approach has been questioned as it failed to accurately describe verified conformational transitions of MscS upon activation[151]. The pulsed – EPR methods described in section 1.6.2 have been shown to be much more reliable for such an approach, providing structural information of high accuracy and detail.

1. 6. 2. Pulsed Electron – Electron Double Resonance

Pulsed Electron – Electron Double Resonance (PELDOR) or Double Electron – Electron Resonance (DEER) is, as the name implies, a pulsed EPR technique that utilizes short microwave pulses at two different, but still resonant, frequencies (Fig. 1. 6 a) and eventually allows the measurement of the distance between paramagnetic centers. This way it can provide structural information on proteins with high accuracy. The most widely – used setup for PELDOR experiments is the 4 – pulse[152] sequence (Fig. 1. 6 a). The two resonant frequencies, ν_A and ν_B, are used in order to independently excite two species of unpaired electrons in the sample, electrons A and electrons B, which are initially in different ground states (their m_s numbers are the same but their m_I numbers are different). Measurements are typically performed at Q band frequency (≈ 34GHz) and at very low temperatures (usually around 50K using liquid He).

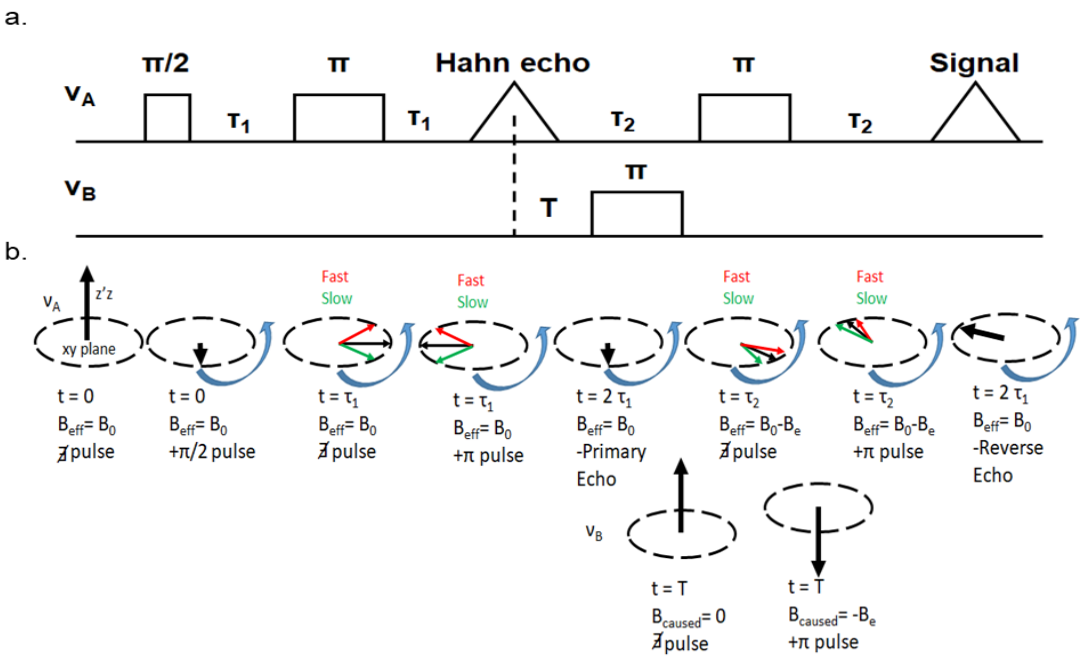

Fig. 1. 6: a. The pulse sequence applied during a PELDOR experiment at both resonant frequencies ν_A and ν_B. Microwave pulses (rectangles) are denoted by their length, echoes are shown as triangles. Time intervals between pusles and echoes are also shown. **b.** The behaviour of the A (top) and B (bottom) spins' magnetization during a PELDOR experiment, at frequencies ν_A and ν_B, respectively. Dashed circles denote the xy plane. Black arrows show the bulk (average) magnetization vector of all spins, red arrows denote the magnetization vector of individual spins that precess faster than average and green arrows denote the ones that precess faster. The blue curved arrow denotes the direction of precession.

Initially, at t = 0 and inside an externally applied static magnetic field B_0 which is parallel to the z – axis, all the electron spins, both of A and B electrons, are oriented parallel to B_0 (Fig. 1. 6 b). Then, at the resonant microwave frequency ν_A, a π/2 pulse is used, which turns the magnetization of the A electrons to the xy – plane and, thus, perpendicular to the static magnetic field. As the electron spins start to relax back to their previous, ground state (along the z – axis), they also start dephasing, meaning that the relaxation rates of individual electrons differ due to the slightly different immediate magnetic environment each one experiences. At this point, in a constant time interval t = τ_1 after the first pulse, a second pulse is used at frequency ν_A, but this time it is a π pulse, which means that the electron spin vectors are turned by 180^o while remaining on the xy – plane. As a result, the direction of relaxation is reversed and this gives the opportunity to the slowly relaxing electrons to "catch up" with the fast relaxing ones, in a process called refocusing of the spin magnetization.

At t = 2 τ_1, so at an interval τ_1 after the π pulse, the refocusing is complete and as a result the so – called Hahn echo is generated. From this point on, the A spins start dephasing again as before, just in the opposite direction. After a constant time interval t = τ_2 after the Hahn echo, a second π pulse is applied in frequency ν_A, which again turns the magnetization of the spins by 180^o which eventually causes the spins to refocus again in the way described before, leading to the generation of a second refocused echo at t = τ_2 after the second π pulse. Meanwhile though, a π pulse is applied at the resonant frequency ν_B, at variable time intervals T between the two π pulses at frequency ν_A. This ν_B π pulse turns the magnetization of the electron species B from + z to - z, meaning that it also changes the sign of the (small) local magnetic field B_B exerted by each individual B electron to its immediate local environment. This means that if an A electron is close enough for dipolar coupling to occur (typically at a distance of up to 70 – 80 Å) with one or more B electrons, the effective magnetic field B_{eff} that it experiences will change. The extent of the change of each individual B_{eff} depends on the distance between the two electrons A and B and the angle between their spin vectors, and as explained before, it affects the dephasing and refocusing rate of the A electrons. The resulting refocused echo will then, due to the variable time T that the ν_B π pulse is applied, oscillate with the frequency of the dipolar coupling between the two electron species A and B[153].

PELDOR has often been applied very successfully on both soluble[154] and membrane[151, 155-159] proteins for the determination of intra – molecular distances in the range of 15 – 70 or 80 Å, providing important information on both a structural and functional basis. By full deuteration of both the protein and the surrounding buffer, a strategy that significantly reduces the spin magnetization relaxation rates, measurements of distances up to 160 Å have been achieved[160]. More importantly, regarding mechanosensitive ion channels, PELDOR has been successfully utilized for the assessment of MscS's conformational state both in detergent solution and reconstituted in liposomes[151], something that is not possible with other biophysical techniques such as X–ray crystallography. The fact that it has been successfully used on MscS means that it could possibly be successfully used for the study of MscL too, since the difficulties posed by both channels with respect to the PELDOR methodology and the experimental procedure are roughly the same. Importantly, this means that sufficient spin – labelling of the (notoriously difficult to spin – label) transmembrane parts of MscL is probably an obstacle that can be overcome through the design of cysteine mutants at strategic parts of the protein. In addition, it means that accurate and reliable distance distributions can be obtained despite the multi – spin effects that will arise and can compromise the quality of the data acquired[161], since MscS (a heptamer) suffers from them even more than MscL (a pentamer) would.

1. 6. 3. Electron Spin Echo Envelope Modulation

Electron Spin Echo Envelope Modulation (ESEEM) is another pulsed EPR technique that is used for the assessment of the immediate local environment that surrounds a nitroxyl spin label (distances up to 10 Å). There are two main pulse sequences, the 2 – pulse and the 3 – pulse ESEEM, with both only making use of a single microwave frequency. Measurements are performed typically at low temperatures (≈ 70 – 80 K, using constant liquid N_2 flow) and at relatively low frequencies (around 9.5 GHz as compared to approximately 34GHz for PELDOR), where the forbidden transitions (both $\Delta m_S \neq 0$ for the spin label's unpaired electron and $\Delta m_I \neq 0$ for the nearby nuclei in question) targeted by the technique are more probable. In 2 – pulse ESEEM, two consecutive π/2 and π microwave pulses, separated by a time interval τ, lead to the generation of a Hahn echo. As this time interval is incremented, the generated echo oscillates with the transition frequencies of nearby nuclei, typically ^1H and ^2H, that are coupled to the protein's introduced paramagnetic center. In the case of 3 – pulse ESEEM three π/2 pulses are used, separated by time intervals τ and T, with the first one being constant and the second one variable, and incrementing the second interval T is what leads to the oscillation of the produced echo with the coupled nuclear frequencies. In cases where there are multiple species of nuclei coupled to the paramagnetic center, 3 – pulse ESEEM has an advantage compared to the 2 – pulse sequence, since choosing an appropriate first time interval τ can suppress the contribution of one of the nuclear species to the acquired spectrum, taking advantage of the technique's so – called "blind spots" at nuclear Larmor frequencies of $1/\tau$[162].

1. 7. The aims of the present thesis

It has already been underlined that mechanosensation plays a very important role in all living organisms, both physiologically and pathologically. Nevertheless, on the one hand, and despite a big number of studies conducted on the matter and the proposal of models that aim to explain its exact nature in molecular detail, mechanosensation is still not clearly understood at a basic level. On the other hand, the mechanosensitive ion channel of large conductance, MscL, has been so far very extensively studied but, despite years of research efforts, its mode of mechanical activation and its gating mechanism have not been elucidated. Importantly, as mentioned earlier, MscL is the mechanosensitive ion channel with the highest activation pressure threshold, which means that it is the hardest one to force open solely by means of lateral bilayer tension. This gives MscL a prominent place of high importance in the search for the basis of mechanosensation: if a trigger can be found that can force this channel to open by meddling with its ability to mechanosense,

chances are this trigger would bring about a similar effect on most, if not all, other mechanosensitive channels, while the other way around would not necessarily apply. Furthermore, MscL is solely mechanosensitive, with no other natural stimulus ever discovered that could activate it. This implies that, if its activation was to be provoked, this would be a result of triggering and meddling with its mechanosensitivity, without the possibility of another route of activation being involved.

Hence, MscL seems like the ideal model system for the in – depth investigation of the basis of mechanosensation among such ion channels. At the same time, if successful, this approach could shed some light on the gating mechanism of MscL itself, opening the way for the channel to be manipulated at will. A channel with a pore opening as wide as the one expected for MscL could be used in many different and important applications as long as the reversible opening of said pore could be tamed and manipulated. This potential has already been demonstrated in a case where MscL was engineered to respond and gate upon UV irradiation, leading to the development of a controlled and reversible nanovalve[163-165]. This means that the regulated manipulation of the channel's activation and gating, whose prerequisite is their elucidation, could lead to MscL being utilized, for example, as a nano – valve for the controlled release of substances, most importantly drugs, inside the body, aiming for a targeted approach in pharmacological applications[166, 167]. In addition, MscL's large pores makes it a good candidate to act not only as a nano – valve for targeted drug – delivery, but it also renders it a potential drug target itself. Knowledge of the channel's possible activation triggers could lead to the development of a new class of antibiotics that target the protein, which is omnipotent in bacteria, both pathogenic and not, which could provide pharmacological research with a great advantage in the ever - growing struggle against antibiotic – resistant strains of bacteria[168-172].

Thus, the goal of the main project of this thesis (Chapter 3) is the investigation and elucidation of the gating mechanism of MscL and its activation, which is very important in its own right and could be utilized in a variety of applications. Furthermore, and maybe even more importantly, this can be used to shed light on the subject of mechanosensation itself in a more broad sense. In order for this goal to be achieved, the "Lipid moves first" principle was tested and knowledge was derived from the identification and subsequent targeting of MscL's nano – pockets, and especially residue L89 that lies at their entrance, through site – directed mutagenesis and spin - labelling. In addition, a number of approaches (for example, the neutralization of the positively charged cluster on the bottom of MscL's TM2 helix) that had been previously proposed was also tested, but in this case the assessment of their efficacy was performed through pulsed EPR methods, most importantly PELDOR, which are more suitable at providing us with the structural

detail that is needed in order to identify whether they are successful at triggering a conformational change on the channel or not.

In addition, more aspects of MscL's structure and function were probed through EPR spectroscopy. In Chapter 4, the main goal was to investigate the way MscL responds to changes in the length of the hydrophobic core of surrounding lipid bilayers, by (subtly) adapting its conformation. In order for this to be achieved, co-expression of WT and cysteine-mutated MscL, and the assembly of mixed pentamers had to be tuned (at a molecular level) as close as possible to a 4-to-1 ratio. This would make intra-monomer PELDOR measurements of the protein's oligomer much more accurate and reliable, a goal that has been long-sought.

Furthermore, Chapter 5 is dedicated to the attempts to create (in collaboration with G. Skretas from the National Hellenic Research Foundation, Athens, Greece) *E. coli* strains that are capable of overexpressing recombinant proteins that are otherwise very hard (or impossible) to express in bacterial cells (i.e. human bradykinin receptor 2, BR2). The most important goal of this project was to prove that the overexpressed protein (TbMscL and BR2) is of high quality and at the same time it is produced at high enough quantities that would allow its biochemical / biophysical characterization.

Finally, Chapter 6 describes a structural comparison (through EPR spectroscopy) of the nanopocket region of two MscL orthologues, TbMscL and EcoMscL. A single residue, L89, at this part of the protein, but not its adjacent ones, was proven to be very important for the function and mechanosensitivity of TbMscL. This means that precision at the single aminoacid level is needed for the channel's expansion to be triggered, but this precision might not be able to be achieved through aminoacid sequence alignment. Hence, the ultimate goal was to assess whether aminoacid sequence alignment alone is able to precisely identify EcMscL's equivalent to TbMscL's L89, modifications of which could potentially trigger a conformational change of EcMscL, or whether a more sophisticated, structure-based approach is needed when high precision and detail is needed.

CHAPTER 2: MATERIALS & METHODS

2. 1. Site directed mutagenesis and cell transformation

2. 1. 1. Vectors used and primer design

Mutation primers were designed using the SnapGene Viewer software and ordered from Integrated DNA Technologies. The TbMscL mutants were generated on a pJ411:140126 vector while the EcoMscL mutants on a pET - 52b vector. In the case of the TbMscL WT – mutant co-expression experiments, TbMscL mutants were generated on a pASK75 or a pBAD33 vector, with the plasmids provided by Dr Georgios Skretas (Institute of Chemical Biology, National Hellenic Research Foundation). For the *E. coli* SuptoxD and SuptoxR[173, 174] strains experiments, the TbMscL mutant was generated on a pASK75[175] plasmid, while for the human bradykinin receptor 2 (BR2) the plasmid used was the pASKBR2[174], again provided by Dr Georgios Skretas. In all cases, the protein construct carried a C – terminal 6 x His tag.

TbMscL and EcMscL mutants were generated using a modified Stratagene QuikChange protocol[176]. In order to increase the efficiency of the mutagenesis process, the primers were designed with the following characteristics: a) Their G – C base content was between 40 and 60% of their total base length, b) If possible, 1 – 2 G or C bases at the 5' end and a maximum of 3 G and C among the last 5 bases at the 3' end of their sequence, c) The two primers (one for the sense and one for the antisense DNA strand) had similar (within 2 – 3 ^{o}C) melting temperatures for their respective template DNA strand ($T_{m,\ p\text{-}t}$) , which were normally in the range of 50 – 65 ^{o}C, and d) when possible, the melting temperature between the two primers, $T_{m,\ p\text{-}p}$, was approximately 6 – 10 ^{o}C lower than the two individual $T_{m,\ p\text{-}t}$ temperatures. The last two conditions are achieved by designing mismatching primers with relatively extended 3' ends, a strategy that ensures the minimal overlap possible between the sequences of the two primers. This way, the annealing step of the following amplification reaction can be done at an appropriate temperature (3 – 5 ^{o}C above the $T_{m,\ p\text{-}p}$ and 3 – 5 ^{o}C below the $T_{m,\ p\text{-}t}$), so that the primers bind much more readily to their respective template DNA strands compared to one another. In addition, the minimum number of base changes possible was used for each individual codon mutation, while the codon bias for *E. coli* (the organism in which the mutated protein would later be expressed) was also taken into consideration. In the case of cysteine, the two equivalent codons are roughly equally abundant in the *E.*

coli genome (approximately 45% TGT and 55% TGC), hence they were used interchangeably depending on the mutation site.

2. 1. 2. Plasmid amplification reaction

a.

Amplification Reaction Mixture						
Template DNA	For. Primer	Rev. Primer	Pfu DNA polymerase	Pfu Buffer	dNTP mix	Water
5-10 ng	10 µM	10 µM	3-5 lU	5 µL	200 µM	to 50 µL

b.

Amplification Reaction Conditions						
Cycle	#1	#2			#3	
Repeat	x 1	x 30			1	
Temperature (℃)	94	94	55 - 62	72	72	4
Time (min)	1	1	1	15	30	∞
Purpose	Initial Denaturation	Denaturation	Annealing	Extension	Final Extension	Storage

Table 2. 1: a. Plasmid amplification reaction mixture. **b.** Plasmid amplification reaction conditions

For the plasmid amplification, the reaction mixture consisted of 100 nM of each mutagenesis primer, approximately 40 ng of the template plasmid DNA to be amplified, 200 µM of each of the dNTPs, 3 – 5 U of Pfu polymerase and appropriate enzyme buffer containing 20 mM Tris – HCl at pH 8.8, 10 mM $(NH_4)_2SO_4$, 10 mM KCl, 0.1% v/v Triton X-100, 0.1 mg/mL BSA and 2 mM $MgSO_4$ in a final volume of 50 µL (Table 2. 1 a). Pfu polymerase, the enzyme buffer and the dNTP mix were all purchased from Thermo Fisher Scientific. The amplification reaction consisted of the following steps (Table 2. 1 b): 1) Initial denaturation at 94 ^oC for 1 min, 2) Further denaturation at 94 ^oC for an additional 1 min, 3) Primer – template annealing at an appropriate temperature as described earlier, typically between 55 and 62 ^oC, for 1 min, 4) Extension through Pfu polymerase action at 72 ^oC for 15 min, 5) Final

extension step at 72 ^{o}C for 30 min, and 6) Storage at 4 ^{o}C overnight. Steps 2 – 4 were repeated in cycle 30 times. Afterwards, 10 U of the restriction enzyme DpnI was added to the reaction mixture along with the appropriate enzyme buffer containing 33 mM Tris – acetate at pH 7.9, 10 mM magnesium acetate, 66 mM potassium acetate and 0.1 mg/mL BSA, and left incubating at 37 ^{o}C for 4 h, until satisfactory removal of the methylated template DNA used. DpnI enzyme and its buffer (Tango buffer) were acquired from Thermo Fisher Scientific.

2. 1. 3. Competent cells preparation

Before transformation with the amplified plasmid, *E. coli* DH5α cells (Thermo Fisher Scientific) were made competent through $CaCl_2$ / $MgSO_4$ treatment. A healthy colony of DH5α cells was used to inoculate 10 mL of sterile Luria – Bertani (LB) broth and left incubating in a shaking incubator overnight at 37 ^{o}C and 200 rpm. Next morning, 2 mL of the overnight culture was used to inoculate 100 mL LB and incubated in a shaking incubator at 37 ^{o}C and 200 rpm until they reached an OD_{600} = 0.3 – 0.4 (early logarithmic phase). At this point, the culture was split in two parts, transferred into two ice – chilled Falcon tubes and left to cool down on ice for 30 min. Afterwards, the tubes were centrifuged at 3500 rpm for 10 min at 4 ^{o}C. After centrifugation the supernatants were discarded and each pellet was resuspended carefully through gentle agitation (not pipetting) in 12.5 mL 100 mM $CaCl_2$ and 12.5 mL 100 mM $MgSO_4$. Both solutions were sufficiently chilled on ice beforehand. The tubes were left on ice again for 30 min, centrifuged at 3500 rpm for 10 min at 4 ^{o}C and the supernatants were once again discarded. The pellets were then resuspended gently in 2.5 mL $CaCl_2$ 100 mM and 2.5 mL $MgSO_4$ 100 mM (both ice – cold) and 1 mL of pre – chilled 60% glycerol was added to the cells, to a final concentration of 12% v/v. $CaCl_2$, $MgSO_4$ and glycerol were all obtained from Sigma – Aldrich. The competent cells were split into 50 µL aliquots and kept at -80 ^{o}C until used further.

2. 1. 4. Cell transformation

In the case of cell transformation for plasmid amplification before DNA sequencing, a 50 µL competent *E. coli* DH5α aliquot was thawed and 5 µL of the amplification reaction mixture was added and left to chill on ice for 30 min. Then, the cells were subjected to a heat shock in a 42 ^{o}C water bath for 1 min before immediately put on ice again for 2 min. Afterwards, 500 µL of LB was added to the cells and the culture was incubated at 37 ^{o}C for 1 – 1.5 h. Finally, 250 µL of the culture was spread on an

LB – agar plate containing the appropriate antibiotic (50 μg/mL kanamycin for TbMscL pJ411:140126 (DNA 2.0), 100 μg/mL ampicillin for TbMscL pASK75 and EcoMscL pET - 52b, and 30 μg/mL chloramphenicol for TbMscL pBAD33) and incubated overnight in a static incubator at 37 ^{o}C. Next morning the plates with successful colony growth were collected and stored at 0 – 4 ^{o}C.

In the case of transformation for the overexpression of protein, the cell line used was *E. coli* BL21 (DE3) (Thermo Fisher Scientific), and cells were made competent and transformed as described previously for the *E. coli* DH5α cells. The only exception was the case of BL21 (DE3) cells transformed with two plasmids (either WT pBAD33 and double – mutant pASK75, or WT pJ411:140126 and double – mutant pASK75) for the WT – mutant co-expression experiments. Here, competent BL21 (DE3) cells were first transformed with one of the plasmids and spread on an LB-agar plate with the appropriate antibiotic as described. Then, a single colony from the plate was used to inoculate 10 mL LB with the appropriate antibiotic and incubated at 37 ^{o}C and 200 rpm overnight. Next morning, the transformed BL21 (DE3) cells were made competent again with the method described in section 2.1.3, with the difference that all solutions used were supplemented with the appropriate antibiotic concentration for the existing plasmid. Once made competent again, the cells were re – transformed, this time with the second plasmid, as previously described, and spread on a custom – made LB-agar plate containing both selection antibiotics (either chloramphenicol and ampicillin, or ampicillin and kanamycin).

2. 1. 5 DNA sequencing preparation

Before protein expression and purification, all plasmids were sequenced to ensure that the desired mutation was introduced to the gene. To do this, plasmid was purified from transformed cells using a Qiagen plasmid mini prep kit using the standard protocol. A single colony from a fresh plate with transformed DH5α cells was used to inoculate 10 mL LB with the appropriate antibiotic concentration and incubated overnight at 37 ^{o}C and 200 rpm. Next morning the culture was centrifuged at 3500 rpm for 6 min at room temperature. The supernatant was discarded and the pellet was resuspended in 250 μL P1 buffer (resuspension buffer containing 50 mM Tris-HCl, 10 mM EDTA pH 8.0 and 50 μg/ml RNase A) and transferred into a 1.5 mL Eppendorf tube. Then 250 μL P2 buffer (lysis buffer containing 200 mM NaOH and 1% SDS) was added to the tube and mixed thoroughly, and the lysis reaction was left to proceed for 3 – 5 min. Afterwards, 350 μL N3 buffer (neutralization buffer containing 4.2 M guanidine hydrochloride and 0.9 M potassium acetate, pH 4.8) was added and the solution was mixed thoroughly. The tube was centrifuged in a tabletop

microcentrifuge at 13000 rpm for 10 min at 4 ^{o}C and the resulting supernatant was transferred to a Qiaprep spin column and centrifuged again at 13000 rpm for 2 min at 4 ^{o}C. 750 μL PE buffer (wash buffer containing 16 mM NaCl, 1.6 mM Tris-HCl, pH 7.5 and 80% ethanol) was added and then the column was centrifuged again at 13000 rpm for 2 min at 4 ^{o}C two times. 40 μL of MilliQ water was added to the centre of the spin column's filter in two 20 μL steps, with a 10 min incubation break after each addition. Finally, the purified plasmid DNA was eluted from the column with a final centrifugation step at 13000 rpm for 2 min at 4 ^{o}C.

For the plasmid sequencing, 5 μL of purified plasmid was mixed with 2.5 μL of 10 μM of the appropriate sequencing primer for the construct used. After addition of 2.5 μL MilliQ water, the plasmid sample was sent to GATC Biotech (Eurofins Genomics) for Sanger sequencing.

2. 1. 6. DNA gel electrophoresis

In order to ensure that the mutated plasmid DNA that resulted from the amplification reactions was suitable for use, DNA gel electrophoresis was performed, using a self – cast gel. Initially, 0.5 g of low grade agarose (Sigma – Aldrich) were dissolved in 50 mL of 0.5 x Tris – phosphate buffer (TPE buffer, containing 45 mM Tris base, 45 mM phosphoric acid and 1 mM EDTA) and heated in a microwave oven. Once cool enough to handle, but before it turned into gel, 1 μL of SYBR safe (Invitrogen, Thermo Fisher Scientific) was added to the solution and mixed thoroughly. The solution was poured in the electrophoresis chamber (Biorad) and left to cool down until the gel was properly set, at which point enough 0.5 x TPE was added to the chamber to cover the gel. Then, the prepared samples (10 μL of plasmid DNA sample mixed with 2 μL of DNA loading dye (Thermo Fisher Scientific)) along with DNA molecular weight marker (Thermo Fisher Scientific) (5 μL mixed with 2.5 μL of DNA loading dye) was loaded on to the gel and the electrophoresis was left to proceed for 35 – 40 min at a potential of 90 V. When the electrophoresis was finished, the gel was visualized using the default SYBR Safe imaging protocol on a ChemiDoc imaging system (Biorad).

2. 2. Bacterial culture growth, protein overexpression and cell viability assays

2. 2. 1. Typical conditions for WT and mutant TbMscL and EcMscL expression

The growth and overexpression conditions have been described previously[177]. In the case of single – transformed BL21 (DE3) cells, for both mutant and WT proteins, 10 mL of LB supplemented with the appropriate antibiotic was inoculated with either 1 colony from a freshly transformed plate or 3 – 5 μL of an existing cell glycerol stock, and incubated overnight at 37 ^{o}C and 200 rpm in a shaking incubator. Next morning, the pre – culture was prepared by addition of 4 mL of the overnight culture to 120 mL of fresh LB and it was incubated for approximately 1 – 1 ½ h at 37 ^{o}C and 200rpm, until it reached an $OD_{600} \approx 0.5$. Then, 50 mL of the pre – culture was transferred into 500 mL LB (main culture) and incubated at 37 ^{o}C and 200 rpm until the culture reached an $OD_{600} \approx 0.8$. At this point the incubator was cooled down to 25 ^{o}C and 500 μL of 1 M isopropyl – β – D – thiogalactoside (IPTG) (final concentration 1 mM) was added to induce protein overexpression. After 4h at 25 ^{o}C and 200 rpm, cell cultures were centrifuged for 17 min at 4000 *x* g at 4 ^{o}C using a Beckman – Coulter JLA – 8.1 fixed angle rotor. Finally, the supernatant was discarded and the cell pellet was transferred to Falcon tubes and stored at -80 ^{o}C until further use. Typical main culture growth volumes were either 4 or 6 L. In the case of the highly unstable quadruple mutant R98Q / K99Q / K100Q – Y87R1, the main culture volume was 16 L and the protein overexpression time was reduced to 2 h.

2. 2. 2. Conditions for WT – double-mutant TbMscL co - expression

The optimized cell growth protocol for the TbMscL WT – mutant co-expression experiments differed at some steps compared to the one described. Only single colonies from freshly prepared LB – agar dishes were used to inoculate the starting overnight cultures. The use of glycerol stocks resulted in unexpected and non – replicable WT – to – mutant monomer ratios in the protein's pentamers. In addition, due to the simultaneous presence of two different plasmids in the cells, protein induction conditions differed as well. In the optimized protocol, WT TbMscL (pJ411:140126) overexpression was induced with 1 mM IPTG for a total of 4h at 25 ^{o}C and 200rpm as described earlier, while double mutant TbMscL (pASK75) overexpression was induced 2 ½ h later than the WT, only for 1 ½ h under the same conditions, by the addition of 0.4 μg/mL of anhydrotetracycline.

2. 2. 3. Conditions for overexpression in the *E. coli* SuptoxD and SuptoxR strains

The *E. coli* strains used here were the MC1061, SuptoxD (MC1061 transformed with a pBAD33 plasmid containing the gene for the expression of the co – chaperone DnaJ – Like protein, DjlA) and SuptoxR (MC1061 transformed with a pBAD33 plasmid containing the gene for the expression of the regulator of ribonuclease activity A protein, RraA)[173]. Both vectors carry a chloramphenicol resistance gene and the effector protein (DjlA or RraA) co-expression is regulated by L – arabinose.

Freshly transformed *E. coli* cells were used to inoculate 10 mL LB overnight cultures supplemented with the appropriate antibiotic (100 μg/mL ampicillin for MC1061 cells expressing TbMscL or BR2 alone, and 40 μg/mL chloramphenicol and 100 μg/mL ampicillin for SuptoxR and SuptoxD cells co-expressing TbMscL and BR2 respectively). Next morning, the overnight cultures were diluted 1:50 in fresh sterile LB supplemented with 0.01% w/v (for the MC1061 and SuptoxD strains) or 0.2% w/v (for the SuptoxR strain) L – arabinose. These cultures were grown at 30 ^{o}C and 200 rpm until they reached an OD_{600} ≈ 0.3 – 0.5. At this point the temperature was decreased to 25 ^{o}C and TbMscL or BR2 overexpression was induced by addition of 0.2 μg/mL anhydrotetracycline. Protein overexpression was left to occur overnight in a shaking incubator at 200 rpm. Next morning the cell cultures were centrifuged at 3500 rpm for 15 min at 4 ^{o}C, the supernatant was discarded and the cell pellets were used for protein purification.

2. 2. 4. Conditions for MSP1D1 expression

In the case of the overexpression of the Membrane Scaffold Protein 1 D1 (MSP1D1), 10 mL LB supplemented with 50 mg/mL kanamycin was inoculated with 3 – 5 μL of BL21 (DE3) cell glycerol stock and left to grow overnight at 37 ^{o}C and 200 rpm. The cells used were transformed with the pMSP1D1 plasmid[178] (Addgene). Next morning, 4 mL of the overnight culture was used to inoculate 120 mL of fresh LB and this pre - culture was incubated at 37 ^{o}C and 200 rpm. When the OD_{600} = 0.4 – 0.6, 60 mL of the pre – culture was added to 500 mL of LB and the main culture was grown under the same conditions until it reached an OD_{600} = 0.8 – 1. At this point the temperature was reduced to 28 ^{o}C and MSP1D1 overexpression was induced by addition of 500 μL 1M IPTG (final concentration 1 mM) for 3.5 h at 200 rpm. Finally, cell cultures were centrifuged at 3500 rpm and 4 ^{o}C for 15 min, the supernatant was discarded and the cell pellets were stored at -80 ^{o}C until further use. The typical main culture volume preparation was 8 or 12 L.

2. 2. 5. Cell viability assays with osmotic downshocks

For the cell viability assays, the strain used was *E. coli* MJF612, which lacks the four major mechanosensitive ion channels (ΔmscL, ΔmscS, ΔmscK and ΔmscM)[63]. Cells were either transformed with WT or mutated TbMscL, or were not transformed. For the starting overnight cultures, 10 mL of LB (for non – transformed cells) or LB supplemented with 50 μg/mL kanamycin (for transformed cells) were inoculated with a single MJF612 colony from a fresh plate and grown at 37 ºC and 200rpm. Next morning, 100 μL of the overnight culture were added to 9.9 mL LB (1:100 dilution) and grown at 37 ºC and 200 rpm until the cells reached an $OD_{600} \approx 0.4$ - 0.5. At that point, 3 mL of the culture was combined with 3 mL LB supplemented with 1 M NaCl (final concentration 0.5 M, to increase the osmolarity of the medium) and 1 M IPTG (final concentration 1 mM, to induce TbMscL overexpression) and grown at 37 ºC and 200 rpm for a further 1 h. Then, the cultures were diluted 1:1000 in either 0.2 M NaCl (osmotic downshocks, all samples) or 0.5 M NaCl (mock shock, only non – transformed cells and samples transformed with the WT protein) and incubated in a static incubator at 37 ºC for 20 min. Finally, the samples were further diluted 1:100 in LB supplemented with 0.5 M NaCl, spread on LB-agar plates (either containing kanamycin or not) and incubated overnight at 37 ºC. Next morning the plates were collected and the number of colonies on each one was counted. The experiment was independently repeated 4 times and the average number of colonies ± standard deviation for each sample was calculated. Cell viability was calculated as the percentage of colonies per plate compared to those of the WT TbMscL mock shock plate (positive control, 100% viability). The plates of untransformed MJF612 cells acted as the negative control of the assay.

2. 3. Protein purification

2. 3. 1. Purification of TbMscL and EcMscL protein

Cell pellets were taken out of -80 ºC and thawed in a beaker filled with lukewarm water. Afterwards, approximately 20 – 25 mL of phosphate – buffered saline (PBS) per liter of main cell culture was added and the mixture was left to homogenize by stirring for 10 – 15 min (or until full homogenization) at 4 ºC. Once homogeneous, the cell suspension was lysed using a cell disrupter (ThermoFlex 1400, Thermo Fisher Scientific) at a pressure of 30 Kpsi. The sample was passed through the cell disrupter twice if it did not appear sufficiently lysed after the first passage. In order to remove intact cells and cell debris, the resulting lysate was centrifuged at 4000

rpm and 4 ºC for 20 min. The pellet was discarded and the supernatant was transferred to appropriate tubes and ultracentrifuged again at 100000 *x* g and 4 ºC for 1 h. The resulting supernatant was discarded and the membrane pellet was weighed and mixed with 25 mL of fresh solubilization buffer (containing 50 mM sodium phosphate at pH 7.5, 300 mM NaCl, 10% v/v glycerol, 50 mM imidazole and 1.5% w/v n – dodecyl β – D – maltoside, DDM (Glycon, GmbH)) per g of membrane, and mechanically homogenized using a glass homogenizer (Thermo Fisher Scientific). The membrane suspension was left to solubilize by gentle rocking at 4 ºC for 1 h. It was centrifuged at 5000 *x* g and 4 ºC for 10 min and afterwards the supernatant was filtered through 0.8 μm filters (Thermo Fisher Scientific) in order to remove any residual non – solubilized membrane particles. The solubilized membrane suspension was then subjected to immobilized metal affinity chromatography (IMAC). The sample was passed through a gravity glass column packed with 0.5 – 0.75 mL of Ni^{2+} - nitrilotriacetic acid (Ni^{2+} – NTA) resin, on which the 6 x His tagged protein binds, at an approximate flow rate of 0.5 mL / min at 4 ºC. The column was pre – equilibrated with 3 – 5 mL of solubilization buffer. Once all of the sample had passed through, the column was washed with 5 – 10 mL of degassed wash buffer (containing 50 mM sodium phosphate pH 7.5, 300 mM NaCl, 10% v/v glycerol, 0.05% w/v DDM and 50 mM imidazole) in order to dispose of undesired proteins bound to it. Lastly, the protein was eluted from the column with 5 mL of elution buffer (containing 50 mM sodium phosphate pH 7.5, 300 mM NaCl, 10% v/v glycerol, 0.05% w/v DDM and 300 mM imidazole).

As a final purification step, the eluted protein was subjected to size exclusion chromatography (SEC) using a Superdex S200 column (GE Healthcare) pre – equilibrated with fresh and degassed SEC buffer (containing 50 mM sodium phosphate at pH 7.5, 300 mM NaCl and 0.05% w/v DDM). The resulting protein fractions were collected and concentrated with Vivaspin 2 100000 kDa molecular weight cut – off centrifugal concentrators (Sartorius) to a concentration appropriate for the experiment they would be used for afterwards. For liposome, GUV and nanodisc reconstitution or EPR experiments (CW – EPR, PELDOR and ESEEM), a starting monomer concentration of ≈ 800 μM is sufficient. For single molecule planar lipid bilayer electrophysiology measurements, normally no concentration was required.

2. 3. 2. Spin labelling of cysteine mutants

In the case of cysteine mutants that would be used for EPR experiments, before the Ni^{2+} column elution step, the sample was labelled with S - (1 – oxyl - 2,2,5,5 –

tetramethyl - 2,5 – dihydro - 1H – pyrrol – 3 - yl) methyl methanethiosulfonate (MTSSL, paramagnetic spin label, obtained from either Toronto Research Chemicals Canada or Santa Cruz Biotechnology). Before labelling, 5 mL of degassed wash buffer supplemented with 3 mM tris - (2-carboxyethyl) phosphine hydrochloride (TCEP, Thermo Fisher Scientific) was passed through the column in order to ensure that all existing cysteines were fully reduced and, thus, available to react with the sulfhydryl moiety of the spin label. TCEP is preferentially used instead of other reducing agents (e. g. DTT or β – mercaptoethanol) because it does not reduce the Ni^{2+} ions of the resin. The column was then washed with 2 mL of degassed wash buffer to remove the excess TCEP. The spin labelling was performed with a total of 3 mL of degassed wash buffer supplemented with 1.5 mM MTSSL in two steps. In each step, 1.5 mL of the solution was added to the column, the column was capped to stop the flow and the labelling reaction was left to proceed first at room temperature for 10 – 15 min and then at 4 ^{o}C for 45 – 50 min. After the second labelling step the excess MTSSL was washed away with the addition of 5 mL of degassed wash buffer and finally the bound protein was eluted from the column with 5 mL of elution buffer (containing 50 mM sodium phosphate pH 7.5, 300 mM NaCl, 10% v/v glycerol, 0.05% w/v DDM and 300 mM imidazole).

2. 3. 3. Sample deuteration

In order for long distances (> 45 – 50 Å) to be measured with higher accuracy (needed in the case of some TbMscL WT – double-mutant hybrid samples for example) during PELDOR experiments, the measurement time window had to be increased, and this was achieved through deuteration of the PELDOR sample buffer (which helps by reducing magnetization dephasing). In that case, the protein was initially concentrated to lower volumes, typically 60 – 100 μL, depending on the amount of pure protein present in the sample. At the same time, the appropriate amount (typically 12 – 16 mL) of SEC buffer that did not yet contain DDM was heated to ≈ 80 ^{o}C until all water was evaporated. Then, a volume of deuterium oxide equal to that of the starting water volume that evaporated was added, along with 0.05% w/v DDM, and the solution was left gently stirring until all ingredients were fully dissolved. Subsequently, the protein's buffer was exchanged with the fresh deuterated one through 6 – 8 cycles of dilution with 2 mL of deuterated SEC buffer and concentration. In the final step, the protein was concentrated to the aforementioned monomer concentration of ≈ 800 μM.

2. 3. 4. BR2 purification

The protocol used for BR2 overexpressed in MC1061 and SuptoxD cells was similar to what is described in section 2. 3. 1, with the only difference being the use of different buffers. The solubilization buffer contained 10 mM HEPES at pH 7.2, 400 mM NaCl, 10% v/v glycerol, 30 mM imidazole and 0.5% w/v fos – choline 14, the wash buffer contained 10 mM HEPES at pH 7.2, 400 mM NaCl, 10% v/v glycerol, 30 mM imidazole and 0.05% w/v DDM, the elution buffer contained 10 mM HEPES at pH 7.2, 400 mM NaCl, 10% v/v glycerol, 300 mM imidazole and 0.05% w/v DDM, and the SEC buffer contained 10 mM HEPES of pH 7.2, 400 mM NaCl and 0.05% w/v DDM.

2. 3. 5. MSP1D1 purification

As for MSP1D1, the cell pellets were thawed in a beaker filled with lukewarm water, approximately 20 – 25 mL of lysis buffer (containing 40 mM Tris at pH 8.0 and 300 mM NaCl), and then was added per 1 L of main culture growth and the mixture was left stirring at 4 ^{o}C until fully homogenized. The homogeneous cell suspension was lysed using a cell disrupter at a pressure of 30 Kpsi. The lysed sample was ultracentrifuged at 100000 *x* g and 4 ^{o}C for 1 h. The resulting pellet (containing intact cells, cell debris and membranes) was discarded and the supernatant was first filtered through 0.8 µm filters and then it was passed through a gravity glass column packed with 3 - 4 mL of Ni^{2+} – NTA resin, at an approximate flow rate of 0.5 mL / min at 4 ^{o}C. The column was pre – equilibrated with 10 mL of lysis buffer. Once all of the sample had passed through, the column was washed with 20 mL of wash buffer (40 mM Tris pH 8.0, 300 mM NaCl and 50 mM imidazole) in order to get rid of unwanted proteins and then MSP1D1 was eluted by addition of 10 mL elution buffer (40 mM Tris at pH 8.0, 300 mM NaCl and 500 mM imidazole). The eluted protein was subjected to SEC using a Superdex S200 column pre – equilibrated with SEC buffer (40 mM Tris pH 8.0 and 300 mM NaCl). Finally, the pure protein was concentrated using Vivaspin 20 10000 kDa molecular weight cut – off centrifugal concentrators.

2. 3. 6. Cell membrane isolation of TbMscL mutant R98Q / K99Q / K100Q – Y87C

100 mL of cell cultures were grown and protein expression was induced as previously described in section 2.2.1, with the difference that the time window of the expression was reduced. At the specified time intervals of 1 h and 2 h, the cell cultures were centrifuged at 4000 *x* g for 10 min. The resulting cell pellets were

subsequently resuspended in 10 mL PBS and sonicated at 4 ^{o}C. The samples were then centrifuged again at 4000 *x* g for 15 min at 4 ^{o}C in order to get rid of intact cells and cell debris, and the supernatant was ultracentrifuged at 100000 *x* g for 1 h at 4 ^{o}C. The resulting membrane pellets were resuspended in 125 µL PBS.

2. 3. 7. Protein SDS - PAGE electrophoresis and anti – His tag Western blotting

Sodium dodecyl sulfate polyacrylamide gel electrophoresis (SDS-PAGE) and Western blotting was used to assess the purity and yield of the purified protein, respectively. Initially, 12 µL of the purified protein sample was mixed with 4 µL of NuPAGE lithium dodecyl sulfate (LDS) sample buffer (with final concentrations 141 mM Tris base and 106 mM Tris HCl pH 8.5, 2% w/v LDS, 10% v/v glycerol, 0.51 mM EDTA, 0.22 mM SERVA Blue G, 0.175 mM Phenol Red (Thermo Fisher Scientific), and incubated at 100 ^{o}C for 5 min for the protein to be denatured. During the incubation time, a pre – cast Bis – Tris gel (Thermo Fisher Scientific) was put in the electrophoresis chamber (Thermo Fisher Scientific) and enough MES SDS buffer (containing 50 mM 2 - (N – morpholino) ethanesulfonic acid (MES) and 50 mM Tris base at pH 7.3, 0.1% w/v SDS and 1 mM EDTA) was added inside the chamber to completely cover the gel. Subsequently, the denatured samples along with pre – stained Mark 12 molecular weight marker (Thermo Fisher scientific) were loaded into the gel's wells and the electrophoresis was carried out for 35 min at a potential of 200 V. Once the electrophoresis was finished and when no Western blotting would be carried out later, the gel was stained with Coomassie brilliant blue for 30 min, washed multiple times with double – distilled water until the stain was completely removed, and visualized on a ChemiDoc imaging system (Biorad).

Western blotting was used in the case of the quadruple mutant R98Q / K99Q / K100Q – Y87C to identify the expression conditions that were associated with maximum protein yield and minimum cell death rates. In this case, the cell membrane fraction was used, prepared as described in section 2.3.6. . The samples were subjected to SDS – PAGE gel electrophoresis as described above. Since the objective of the procedure was the Western blotting of those samples, the protocol was followed up to the electrophoresis step. At this point the gel was removed and gently washed with doubly – distilled water. At the same time, the appropriate number of Western blot transfer pads and filter papers, as well as the nitrocellulose transfer membrane, were soaked in freshly prepared 1 x Western blot Tris – glycine working transfer buffer (containing 25 mM Tris and 192 mM glycine of pH 8.3, and 20% v/v methanol). Afterwards, the Western blot sandwich was assembled as such (following the direction of transfer, from cathode (-) to anode (+)): cathode (-)

electrode, transfer pad, filter paper, protein gel, nitrocellulose membrane, filter paper, transfer pads and anode (+) electrode (Fig. 2. 1). The gel was briefly wetted with working transfer buffer too, prior to the assembly of the blotting sandwich. Care was taken so that there were no air bubbles trapped between the gel and the nitrocellulose membrane, since this would block the transfer of the proteins from the gel to the membrane. Finally, the inner chamber of the blotting module (Thermo Fisher Scientific), which contained the sandwich, was filled with working transfer buffer to promote the transfer, while the outer chamber was filled with double – distilled water (to dissipate heat). The transfer was initiated with application of a potential of 30 V (initial current of 170 mA) and was finished after 1 h (final current of ≈ 110 mA). After the transfer, the membrane was carefully removed from the blotting sandwich, placed in a container filled with blocking solution (PBST (phosphate – buffered saline with 0.1% v/v Tween – 20 detergent) supplemented with 5% w/v dried milk powder) and left on a rocker at room temperature for 1 ½ h until the blocking was completed. Afterwards, the membrane was washed 3 times with PBST for 15 min and then it was left incubating in blocking solution supplemented with 0.1 μg/mL of the primary mouse anti – (6 x His tag) antibody (Biorad) on a rocker, either at room temperature for 2 h or at 4 ^{o}C overnight.

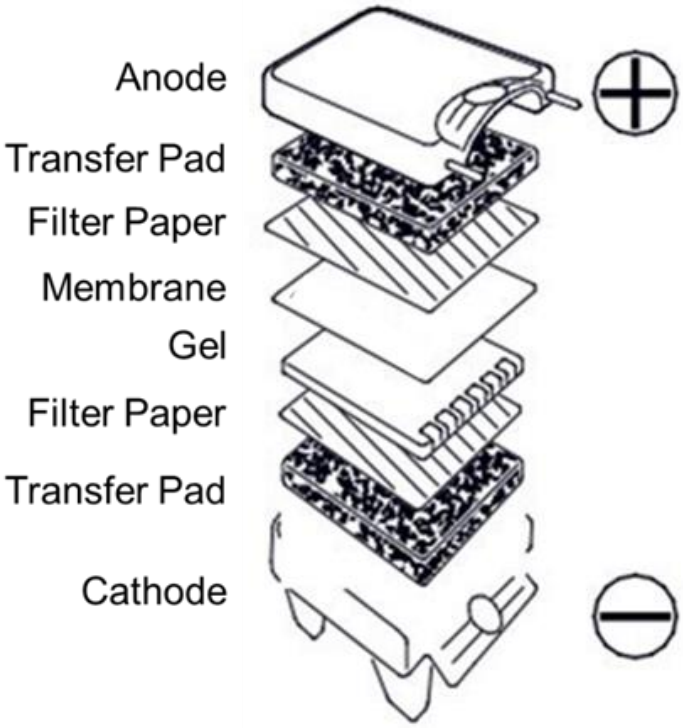

Figure 2. 1: Western blot assembly sandwich. Adapted from the Thermo Fisher Scientific web page.

Subsequently, the membrane was washed again 3 times with PBST for 15 min before being left incubating in blocking solution supplemented with 0.03 μg/mL of the secondary HRP - conjugated goat anti – mouse antibody (Biorad) on a rocker, again either at room temperature for 2 h or at 4 ^{o}C overnight. The membrane was then washed 5 times with PBST for 15 min. Finally, the membrane was incubated for 5 min with Pierce ECL plus Western blotting substrate (Thermo Fisher Scientific) and the results were visualized on a ChemiDoc imaging system (Biorad) using the standard protocol.

2. 4. MscL reconstitution in lipid bilayers

2. 4. 1. Reconstitution in liposomes for EPR measurements

The method used for the reconstitution of MscL in liposomes for the purpose of EPR measurements is an adaptation of a protocol previously described[164]. Firstly, the appropriate lipid in powder form (Avanti Polar Lipids) was dissolved in MscL lipid buffer (containing 50 mM sodium phosphate at pH 7.5 and 300 mM NaCl) to a concentration of 20 mg/mL and subjected to 10 – 15 cycles of freezing in liquid N_2 and subsequent thawing. The temperature at which the thawing step occurred depended on the specific kind of lipid used, since every lipid species has a unique phase transition temperature, T_m. At $T < T_m$, the lipid bilayer is in its ordered gel phase, with hydrocarbon chains fully extended and tightly packed. Liposome formation is much more efficient at $T > T_m$, since at such temperatures the lipid bilayer is in the liquid crystalline phase, where the hydrocarbon chains are fluid and lipid mobility is increased. Hence, the thawing temperature used for single lipid species was 15 ^{o}C for 1, 2 – dilauroyl – *sn* – glycerol – 3 – phospholcholine (DLPC 12:0, T_m = -2 ^{o}C), 37 ^{o}C for 1, 2 – dimyristoyl – *sn* – glycerol – 3 – phospholcholine (DMPC 14:0, T_m = 24 ^{o}C), 50 ^{o}C for 1, 2 – dipalmitoyl – *sn* – glycerol – 3 – phospholcholine (DPPC 16:0, T_m = 41 ^{o}C) and 60 ^{o}C for 1, 2 – distearoyl – *sn* – glycerol – 3 – phospholcholine (DSPC 18:0, T_m = 55 ^{o}C). For the *E. coli* polar lipid extract (Avanti Polar Lipids) liposome formation, the thawing temperature used was 50 ^{o}C, which is high enough for most lipids in the mixture to surpass their transition temperature. The lipid suspension was then subjected to cycles of sonication for 5 min and heating at the temperature used for thawing, until the formation of a homogeneous, milky – white opaque solution. Afterwards, 3 – 6 % v/v Triton X – 100 (Sigma – Aldrich) detergent was added, until the suspension turned into a pale but

transparent colour. The typical Triton X – 100 concentration used was 4.5 % v/v. The liposome suspension was heated again to the previous thawing temperature and purified protein was added to it at a 1:100 protein monomer to lipid molar ratio, and the protein – liposome mixture was left incubating at 50 ^{o}C for 30 min. The incubation was interrupted every ≈ 10 min and the mixture tube was put on a rolling shaker for approximately 2 min at room temperature. Once the incubation period was over, the sample was diluted by addition of 1:1 v/v of lipid buffer and 8 – 10 mg of Biobeads (Biorad) per µL of Triton X – 100 which was added to facilitate detergent (Triton X – 100 and DDM) removal. The mixture was left incubating overnight with gentle rotation on a rolling shaker at 4 ^{o}C. Next morning, a further ≈ 10 mg of Biobeads was added and the sample was left incubating on a roller for 30 min at room temperature. Afterwards the sample was separated from the Biobeads using a 0.8 µm filter and a syringe and ultra-centrifuged at 100000 *x* g for 50 min at 4 ^{o}C. The resulting supernatant was carefully discarded and the proteoliposome pellet was resuspended in 15 – 20 µL of lipid buffer by slow and gentle pipetting.

2. 4. 2. Reconstitution in MSP1D1 Nanodiscs

The method used for the reconstitution of MscL in MSP1D1 nanodiscs is an adaptation of a protocol previously described[178, 179]. The lipid of choice (in the case of nanodisc formation it could be DLPC, DMPC, DPPC, DSPC or *E. coli* polar lipid extract, depending on the experiment) in powder form was dissolved in lipid buffer supplemented with 1% v/v Triton X – 100 by cycles of sonication for 5 min, vortexing and heating at 42 ^{o}C for 2 min, until the suspension reached a transparent pale white colour. An appropriate amount of purified MSP1D1 was thawed from -80 ^{o}C and diluted with lipid buffer supplemented with 1% v/v Triton X – 100 to a concentration of 1 mg/mL. MSP1D1 and solubilized lipids were then mixed at a molar ratio of 1:70 (for DLPC), 1:80 (for DMPC and *E. coli* polar lipid extract, with a calculated average molecular weight of 803.6 Da), 1:90 (for DPPC) or 1:100 (for DSPC) and incubated at the appropriate temperature for the lipid used for 30 min. This is the temperature used for the thawing steps described in section 2.4.1. Afterwards, purified TbMscL was added to the mixture so that the TbMscL to MSP1D1 ratio was 1:2 and the sample was left incubating at the appropriate temperature for the lipid species used for a further 30 min. The incubation was interrupted every ≈ 10 min and the sample was put on a roller for 1 – 2 min. Once the incubation time was over, the sample volume was taken to 3 - 4 mL by addition of lipid buffer supplemented with 1% v/v Triton X – 100 and 0.8 – 1 g of Biobeads per mL of mixture was added. The sample was left on a rolling shaker for 4 – 4 ½ h at room temperature until full removal of the

detergents used. Biobeads were added stepwise (1/3 of the total weight in the first hour of the incubation in 3 steps, and the remaining 2/3 in two steps in the following 1 ½ h), so that the sample remained in contact with the total amount of Biobeads for the last 1 ½ - 2 h of the incubation. Finally, the sample was first separated from the Biobeads by filtering and then concentrated to ≈ 20 μL with Vivaspin 2 100000 KDa molecular weight cut – off centrifugal concentrators.

2. 4. 3. Reconstitution in giant unilamellar vesicles for electrophysiology experiments

The method used for the formation and reconstitution of TbMscL in giant unilamellar vesicles (GUVs) is similar to the one described above for the liposome reconstitution, with some adaptations that promote the size increase of the vesicles and renders them suitable for patch – clamp electrophysiology experiments[180]. The lipid system used for the formation of GUVs is asolectin (Avanti Polar Lipids), and a 10 mg/mL homogeneous suspension of asolectin in lipid buffer was prepared as described in section 2.4.1. In order to achieve clear, single – channel recordings during measurements, the protein monomer to lipid ratio was 1:1000 for TbMscL WT and L89R1, and 1:5000 for the highly active L89W mutant. The mixture was incubated at 50 ^{o}C for 30 min and then its volume was taken to 3 – 4 mL by addition of lipid buffer (described in section 2.4.1). 0.5 – 0.7 g of Biobeads per mL of the mixture was added stepwise (as described in section 2.4.2) and left incubating on a rolling shaker for 4 – 4.5 h. After removal of the Biobeads by filtering the sample was ultracentrifuged at 100000 *x* g for 50 min at 4 ^{o}C and the resulting pellet was resuspended in lipid buffer, so that the final lipid concentration was an estimated 50 mg/mL. At this point the sample could be aliquoted in 7 μL stocks and kept at -80 ^{o}C until further use. If patch – clamp measurements were scheduled for the next day, 7 μL of the sample would be placed in a desiccator and left to dry overnight at 4 ^{o}C (without vacuum). Next morning, the sample was rehydrated with rehydration buffer (lipid buffer supplemented with 400 mM sucrose) for 2 h at room temperature. The protein – containing GUVs were subsequently collapsed in working solution (5 mM HEPES adjusted to pH 7.2 with KOH, 200 mM KCl, and 40 mM MgCl2) before patch – clamp measurements could take place.

2. 5. EPR measurements and *in silico* distance modelling

2. 5. 1. *In silico* distance modelling

In silico spin labelling and distance modelling on the TbMscL crystal structure (PDB 2OAR)[109] was initially used in order to assess whether the distance between the amino acid residues picked for site – directed spin labelling was in the proper range for PELDOR measurements (from ≈ 15 Å to 60 – 70 Å). It was also used to compare the experimentally derived distance distributions with the expected ones from the closed state structure, so that the agreement with it would be assessed and potential discrepancies could be identified. In the case of the MscL orthologue from *Methanosarcina acetivorans*, MaMscL, distance modelling was used on certain amino acid residues to compare their positions and distance distributions between the pentameric closed (PDB 4Y7K) and pentameric expanded (PDB 4Y7J) states[117], in order to attempt and draw some conclusions regarding the expansion mechanism of TbMscL by analogy. *In silico* spin labelling and distance modelling was performed using the MTSSLWizard[181] GUI (integrated into PyMOL) for all Tb and MaMscL mutants, while the Matlab software package MMM[182] (Multiscale Modelling of Macromolecules) was also used in the case of the TbMscL N70R1 mutant in order to verify that the experimental PELDOR distance distributions obtained could not be corresponding to the TbMscL closed state. In both software used, all amino acid residues of interest were first mutated to cysteines (to ensure that the residue's side chain length and flexibility are taken into account) and then modified *in silico* with the MTSSL spin label, resulting in the R1 side chain. In MTSSLWizard, the "thorough search" option was selected for the R1 rotamers and van der Waals restraints were set to "tight". In cases where the search yielded ≤ 50 possible rotamers, van der Waals restraints were set to the "loose" option, in order to allow for a more descriptive image of the theoretical distance distribution. The results were plotted as histograms with OriginPro 2016 (Origin Lab), binned to 100 bins. In the case of MMM, labelling was performed at ambient temperature (298 K setting), since this option yields results that resemble experimental PELDOR distance distributions more closely.

2. 5. 2. Continuous Wave EPR spectroscopy

For room temperature continuous wave EPR (CW–EPR) measurements, 30 μL of purified and spin labelled TbMscL mutant sample was loaded in a glass capillary tube, at a monomer concentration of ≈ 450 μM. All CW–EPR spectra were recorded on a Bruker EMX 10/12 spectrometer equipped with an ELEXSYS Super High

Sensitivity probe head (Bruker ER4122SHQE), with a modulation frequency of 100 kHz and operating at ≈ 9 GHz. The magnetic field center was set to 350.5 mT (at roughly the centre of the typical 3 - peak nitroxide spectrum) and the magnetic field sweep width to 16 mT. The modulation amplitude was set to 0.2 mT. All spectra were averaged for 20 or 50 scans, in order to improve the signal – to – noise resolution for mutants with apparently low labelling efficiency, and the X – axis resolution was set to 512. Both the time constant and the conversion time were set to 40.96 ms, and the microwave bridge power to 1 mW. In room temperature CW – EPR measurements, the spectra obtained are the first derivatives of the absorption spectra.

In the case of low temperature (80 K, achieved with constant liquid N_2 flow) CW – EPR, 35 µL of purified detergent or reconstituted and spin labelled TbMscL mutant sample was mixed with another 35 µL of deuterated (d6) ethylene glycol (Santa Cruz Biotechnology or Sigma – Aldrich), which acts as a cryoprotectant, to a final monomer concentration of ≈ 400 µM. The resulting 1:1 diluted sample was mixed carefully and thoroughly until fully homogeneous, loaded in to 3 mm (OD) quartz tubes and flash – frozen in liquid N_2. Measurements were carried out using a Bruker ELEXSYS E580 X – band (≈ 9 GHz) spectrometer equipped with a Flexline probe head housing a 5 mm dielectric ring (MD5) resonator which was critically coupled for the duration of the measurements. Low temperatures and temperature control was achieved with an Oxford Instruments CF935 helium flow cryostat (operating with liquid N_2 for the purpose of these measurements). In this case, the magnetic field center was set to 346 mT, the magnetic field sweep width to 20 mT and the modulation amplitude to 0.2 mT. For these measurements, the time constant was set to 40.96 ms and the conversion time to 346 ms. The X – axis resolution was set to 1024 and the microwave bridge power to 1.5 µW. Due to the high apparent labelling efficiency of the samples measured and the low temperature used, spectra could be taken as single scans. The spectra obtained are the raw absorption spectra.

2. 5. 3. PELDOR measurements

Sample preparation for the Pulsed Electron – Electron Double Resonance (PELDOR or DEER, Double Electron – Electron Resonance) measurements is the same as described in section 2. 5. 2. All measurements were performed at a temperature of 50 K (using liquid He) with an ELEXSYS E580 pulsed Q – band (≈ 34 GHz) Bruker spectrometer equipped with a TE012 cavity. The frequency offset used between the detection (ν_A) and pump (ν_B) frequencies was 80 MHz, and the pulse sequence used was $(\pi/2)_A - \tau_1 - \pi_A - (\tau_1 + t) - \pi_B - (\tau_2 - t) - \pi_A - \tau_2 - \text{echo}$[183]. The pulses of the

detection frequency were set to 32 ns and 16 ns for π_A and $(\pi/2)_A$, respectively, and separated by τ_1 = 380 ns, whereas the pump π_B pulse was varied between 12 ns and 16 ns among samples, depending on which length resulted in the echo with the highest signal intensity. The most usual value for the pump π_B pulse was 14 ns. The short repetition time for all measurements was set to 3 ms.

2. 5. 4. PELDOR data analysis

The experimental data acquired were analyzed using the Matlab software package DeerAnalysis2016[184]. Raw time – domain traces were fitted with a mono – exponential decay function, then they were background – corrected and finally analyzed with the Tikhonov – regularization method[185]. The "L – curve" option was selected as well, and the value chosen always corresponded to the part of the L – curve that displayed the steepest slope. This way, in cases where the resulting distribution was made up of multiple individual distance peaks, these were appropriately grouped without the danger of over – smoothing the distribution, which would result in very broad and unreliable distances. In addition, due to the pentameric symmetry of MscL, the "ghost suppression for 5 spins" option was used to take into account the multi – spin effects that arise in the presence of more than two spin – labelled cysteines in relatively close proximity[161]. Afterwards, in order to calculate and visualize the error of the previous analysis procedure, the DeerAnalysis2016 validation tool was also employed in a way that has been described previously[186]. For each individual trace, the starting point of the background fitting function was varied between 5% and 80% of the total time length of the time – domain trace in 16 equal steps. On top of that, an extra 50% random noise was added too, with 50 random noise trials per fitting step, resulting in 800 trials in total. At the end of the validation analysis, trial data sets where more than 15% above the best root – mean – square deviation (RMSD, best value is considered the lowest one) were excluded using the default "prune" option.

In theory, a background fitting function with a positive slope corresponds to a negative spin concentration and, therefore, negative sample concentration, which is not physically possible. Such positive slopes may arise from artefacts at the very end of the time – domain trace. In the experimental data presented in this thesis, there are indeed samples where the background fitting function of the best RMSD was continuously rising, but those cases are associated with incomplete, though real, oscillations of the time – domain trace, rather than artefacts. In order to overcome these effects, either the time window of the measurement needs to be increased or the last part of the trace, where the incomplete oscillation is displayed,

needs to be truncated. The former is not possible due to the very low signal intensity of the echo as the time window is increased, and the intrinsic dephasing properties of the sample, while the latter would result in the substantial shortening of the time window of the measurement (since those oscillations are typically long), which in turn would greatly compromise the accuracy of the measurement and of the resulting distance distributions. Therefore, the best RMSD fit was consistently used for the full traces of all data sets, regardless of the slope of the fitting function. In all cases, this was found to not lead to significant changes to the distance distribution with respect to fitting the background to the latter two thirds of the trace.

2. 5. 5. ESEEM measurements and analysis

The sample preparation for both 2 – pulse (2p) and 3 – pulse (3p) Electron Spin Echo Envelope Modulation (2p – and 3p – ESEEM respectively) experiments was identical to the one described in section 2. 5. 2 for low temperature CW – EPR measurements. For all ESEEM measurements an ELEXSYS E580 X – band spectrometer (Bruker) was used, equipped with a Flexline probe head housing a 5 mm dielectric ring (MD5) resonator which was over – coupled. Measurements were conducted at a temperature of 80 K using an Oxford Instruments CF935 helium flow cryostat (operated with liquid N_2).

For the 2p - ESEEM measurements, the pulse sequence used was π/2 – τ – π – τ – echo. The π and π/2 pulses were set to 32 ns and 16 ns respectively and the time delay τ was incremented in 4 ns steps. For the 3p – ESEEM experiments, the pulse sequence used was π/2 – τ - π/2 – T - π/2 – τ – echo. Each π/2 pulse was set to 16 ns, the inter – pulse delay τ was kept constant at either 140 ns or 450 ns, corresponding to blind spots of the proton and the deuterium resonance, respectively, and the delay time T was incremented in 12 ns steps. The raw time – domain signal traces obtained from the measurements were then background – corrected through the subtraction of a fitted stretched – exponential decay function. Subsequently, they were apodized using a hamming window function and zero – filled to 1024 points. Finally, the time – domain traces were Fourier transformed to frequency – domain spectra. Frequency – domain spectra from 2 – pulse ESEEM measurements of MscL samples contain 4 prominent peaks: 2 corresponding to ^{2}H nuclei coupling (a primary one at ≈ 2.6 MHz and a secondary one at ≈ 5.2 MHz) and another 2 corresponding to ^{1}H nuclei coupling (a primary one at ≈ 14.8 MHz and a secondary one at ≈ 29.6 MHz). The solvent / ^{2}H accessibility can be calculated as the ratio of the deuterium peak intensity to the proton one. On the other hand, due to the existence of the extra pulse (which eliminates detection of the secondary

peaks) and the ability to utilize inter – pulse delay times τ that correspond to blind spots for specific nuclei species, frequency – domain spectra of 3 – pulse ESEEM measurements only contain one peak, either the main ^{2}H peak (≈ 2.6 MHz) or the main ^{1}H peak (≈ 14.8 MHz). In this case, the solvent / ^{2}H accessibility can be determined either from the modulation depth in the time – domain trace or the corresponding amplitude of the ^{2}H peak in the frequency – domain spectrum.

2. 6. Planar lipid bilayer electrophysiology experiments

Purified TbMscL WT and the L89R1 spin – labelled mutant were assessed with planar lipid bilayer (PLB) electrophysiology experiments. All measurements were conducted on a Newport RS2000 antivibration table (Newport Corporation). Initially, 15 μL of a 50 mg/mL stock of bovine heart phosphatidyl ethanolamine (Avanti Polar lipids) in chloroform was transferred into a glass vial and left to completely dry in an oven at 45 – 55 ^{o}C for ≈ 20 min. In the meantime, a pair of silver electrodes (made in – house) were stripped with a razor until their colour turned shiny and were dipped in bleach for 15 – 20 min, until they turned dark grey (full chlorination). Then, the dried lipids were dissolved in 21.5 μL of decane to a final working concentration of ≈ 35 mg/mL. Subsequently, a clean delrin perfusion cup (Harvard Apparatus) with a 200 μm diameter aperture was thoroughly dried using paper tissue and a small amount of the lipid solution was applied and painted with an in – house made brush (made from cutting clean plastic Pasteur pipettes) on the inner side of the aperture, so that a part of the lipid solution would leak on the outside of the perfusion cup. The cup was left to dry for 10 min and then the painting procedure repeated, followed by another 10 min drying step. When fully dry, the delrin perfusion cup was placed in the cis chamber of the measuring block (Harvard Apparatus) and both the cup and the trans chamber of the block were filled with 1 mL of PLB buffer (10 mM HEPES at pH 7.2 and 210 mM KCl) each. The two side wells of the block were also filled with 200 μL of 3 M $LiCl_2$ and the chlorinated electrodes were dipped in them. Afterwards, two agar salt bridges were used to bridge each of the two chambers with one of the $LiCl_2$ wells to close the circuit. Care was taken so that none of the silver electrodes came in direct contact with the agar bridges throughout the experiment. Once the amplifier (a BC - 525C amplifier, Warner Instruments) was warmed up and its offset was calibrated to 0, a further small amount of lipid solution was applied on the inner side of the perfusion cup's aperture, until the lipid film's electrical capacitance became measurable but ≤ 7 pF. From then on, the solution inside the

perfusion cup was slowly and carefully pipetted until the electrical capacitance gradually reached a value ≥ 70 – 75 pF, indicative of the formation of a proper, thin lipid bilayer. After a working planar lipid bilayer was established, the resting electrical current was measured to ensure that it is 0 (i. e. there is no leakage on the lipid bilayer) at applied electrode potential values of +30 mV and +200 mV (maximum).

The next step was the incorporation of the purified protein in the planar lipid bilayer. In order to ensure (or increase the chances) of single – channel recordings, small amounts (i. e. 0.5 μL) of very low protein concentrations (typically ≈ 1 – 2 μg/mL) were added in the perfusion cup stepwise under gentle stirring. For this reason, the concentrated protein was first diluted with PLB dilution buffer (50 mM sodium phosphate at pH 7.5, 300 mM NaCl and 0.025% w/v DDM) that contains a DDM concentration which is lower than the one normally used, since detergents disrupt lipid bilayers and higher amounts would cause leakage. After each addition of 0.5 μL of the diluted protein, the electrode potential was increased to +30 mV and the bilayer incorporation process was observed for 5 min under these conditions. Due to the very low activity of the channel (since no mechanical bilayer tension was applied), if no incorporation was observed by the end of the 5 min, the applied potential was increased to +200 mV to identify whether there was indeed no incorporation of the protein in the planar lipid bilayer, or if the channel's opening activity was too low to yield measurable electrical current values at low potential. If no current could be measured at +200 mV either, up to two more protein addition steps (i. e. a total of 1.5 μL) followed, since adding more than that would also result in the addition of higher amounts of DDM, which would compromise the measurements. If incorporation was observed, the electrical current at +30 mV applied potential was recorded for 15 min using the WinEDR 3.6.4 software (Strathclyde University, Glasgow). All recordings were low - pass filtered at 10 kHz with a 4 - pole Bessel filter, and digitized at 100 kHz using a NIDAQ - MX acquisition interface (National Instruments). The recordings were subsequently filtered at 800 Hz (−3 dB) using a low – pass digital filter implemented in WinEDR 3.6.4. Experiments were performed at room temperature (20 – 22 °C). Again, due to the very low activity of the channel, at the end of every 15 min recording at + 30 mV, the applied potential was increased to +200 mV to ensure that the protein remained incorporated in the lipid bilayer during the measurement. If no activity could be detected, the recording was discarded. Finally, the channel's open probability P(o) at +30mV was calculated using the Axon Clampfit 10.2 software (Molecular Devices, Sunnyvale).

2. 7. Giant *E. coli* spheroplasts preparation

Giant *E. coli* spheroplasts were prepared according to previously established procedures[187, 188]. *E. coli* MJF612 cells (lacking the major mechanosensitive channels) with either TbMscL WT or the L89W mutant plasmid freshly transformed into them were grown overnight in 10 mL LB supplemented with 50 μg/mL kanamycin in a shaking incubator at 37 ^{o}C at 200 rpm. Next morning, 200 μL of the overnight culture was used to inoculate 20 mL fresh LB supplemented with 50 μg/mL kanamycin and the main culture was grown at 37 ^{o}C and 200 rpm until it reached an $OD_{600} \approx 0.4 – 0.5$. At this point, 6 mL of the main culture was added to 54 mL LB (elongation culture), which had been pre – warmed at 42 ^{o}C. The "snake" formation / elongation was then initiated by addition of 360 μL of freshly prepared and filter – sterilized cephalexin solution, to a final concentration of 60 μg/mL. Snake formation and elongation was left to occur for 2 h in a shaking incubator at 42 ^{o}C and 120 rpm. After the 2 h had passed, the incubation temperature was reduced to 25 ^{o}C and protein expression was induced for 30 min at 120 rpm by addition of 1 mM IPTG. The elongated and induced culture was stored overnight at 4 ^{o}C.

Next morning, the culture was centrifuged at 3000 *x* g for 5 min at 4 ^{o}C. The supernatant was discarded and the cell pellet was gently resuspended by swirling (no pipetting) in 2.5 mL of 0.8 M sucrose. The centrifugation and resuspension in 0.8 M sucrose steps were repeated one more time. Subsequently, the following reagents were added sequentially to the cell suspension, in order to initiate cell wall digestion: 300 μL of 1 M Tris – HCl at pH 7.2, 240 μL of fresh 5 mg/mL lysozyme solution, 100 μL of fresh 5 mg/mL DNase I solution and 300 μL of 0.125 M EDTA. After the addition of each ingredient, the suspension was swirled carefully and thoroughly. The lysozyme digestion reaction was left to occur for 25 min, at which point it was terminated by addition of 2 mL of fresh stop solution (containing 0.7 M sucrose, 20 mM $MgCl_2$ and 10 mM Tris – HCl at pH 7.2). Giant spheroplast sample aliquots were subsequently cooled down to 4 ^{o}C and then flash frozen and stored at -80 ^{o}C until used for patch – clamp measurements.

CHAPTER 3: ALLOSTERIC ACTIVATION AND ELUCIDATION OF THE GATING MECHANISM OF THE MECHANOSENSITIVE ION CHANNEL OF LARGE CONDUCTANCE

3. 1. A brief introduction

MscL is omnipotent in all prokaryotic cells and it plays the crucial role of their last – resort safety valve. By opening its large pore when the turgor pressure of the cytoplasm increases close to the point of the lytic limit of the cell membrane, it rescues the cell from lysing. Hence, it is no surprise that MscL is the mechanosensitive channel with the highest pressure activation threshold, which poses an important difficulty in the search for a trigger of the channel's activation and opening. In addition, the exact mode through which mechanosensation is mediated through mechanosensitive ion channels in general is not known in its molecular detail, which makes the identification of the "binding site" of mechanosensitivity, through which MscL's activation would be triggered, even more challenging.

Thus, in the case of most previous attempts to activate the channel and stabilize an expanded or open state, the pore constriction site of the protein was being modified and tampered with[121, 189, 190]. However, those modified sites lie far from the transmembrane part of the channel, which is the one coming in direct contact with the bulk of the lipid bilayer and the annular lipids and that is expected to be the link between the lateral tension of the bilayer and the channel's gating response. This means that such modifications are not able to provide us with any insight into either the physiological gating of MscL, as this naturally occurs in the cell membrane, or mechanosensation itself in a more broad sense. Alongside these attempts, other studies conducted have linked the sensitivity and activation threshold of MscL with some of the properties of the bulk of the lipid bilayer, such as its composition, its curvature and its thickness[133, 135, 136, 191-194]. The exact route through which such bilayer properties affect MscL's gating, as well as the extent of those effects, though, is not clear yet.

So far, the most comprehensive and detailed model that has been proposed in order to explain the mechanosensitivity of ion channels is the "lipid moves first" principle[128]. According to it, as long as the nano – pockets of a mechanosensitive ion channel (which can be found on the transmembrane surface of those channels) remain occupied by bilayer lipid acyl chains, the channel remains closed. When bilayer lateral tension drives the acyl chains away from those crevices, voids are created inside them, which naturally need to be eliminated. In order for this to happen, the channel adapts its conformation and these structural changes lead gradually to the

opening of its pore. Detailed as it may be, this model has not been tested for its accuracy to date, and this is the main scope of the present project. The means through which this was attempted was site – directed mutagenesis, mostly targeting the region in and around those nano – pockets, coupled with spin labelling which introduces paramagnetic centers on the protein, that can then be investigated using EPR spectroscopy. In addition, two previously proposed strategies for triggering the channel's activation, namely the neutralization of the positively charged cluster of amino acid residues at the bottom end of TM2[34] and the introduction of histidine mutations in the pore restriction site[190], were also coupled with site – directed spin labelling and their efficacy was assessed with pulsed EPR techniques.

3. 2. Experimental results

3. 2. 1. The choice of the protein and of the mutagenesis sites

The reason why MscL was the mechanosensitive ion channel of choice is because this is the channel with the highest activation threshold. Furthermore, there are two reasons behind the choice of the MscL orthologue from *Mycobacterium tuberculosis*, TbMscL. The first reason is that, among all of the MscL orthologues, this is the one with the highest activation threshold[106, 108], a feature that possibly derives from the microorganism it is found in and its lipid composition[136]; this makes it the most challenging, but at the same time the most interesting target to test the "lipid moves first" hypothesis on. The second reason is the availability of the TbMscL crystal structure in its pentameric closed conformation (PDB 2OAR)[109], which was the only such structure available at the time this project was started. This is a great advantage since it allows the *in silico* spin labelling and distance modelling of TbMscL, which can then be compared to the experimentally obtained PELDOR distance distributions. This comparison can then (a) verify that the state of the protein used in these experiments is the appropriate one, meaning that it is pentameric and closed, and (b) help identify possible discrepancies between the expected distance distributions for the closed pentameric channel and the experimental ones, when targeting potentially sensitive parts of the protein.

The total number of cysteine mutants generated on TbMscL for the purpose of mapping the channel spectroscopically and targeting its nano – pockets was 20 (Fig. 3. 1 a & b). Those 20 cysteine mutants were designed to span most of the length of the channel and, with respect to the nano – pockets, they can be divided into four distinct categories: a) mutations inside the nano – pockets (I23C and F79C), b) mutations at the entrance of the nano – pockets (F5C, A85C, Y87C and L89C), c) mutations in proximity to the nano – pockets (L2C, F34C, F84C and F88C), and d)

mutations at sites not associated with the nano – pockets ("control" sites L42C, V48C, N70C, L72C, L73C, R98C, K99C, K100C, E102C and V112C). The three amino acid residues of the positively charged cluster that binds anionic lipid head groups, R98, K99 and K100, were also included in the "control" sites category.

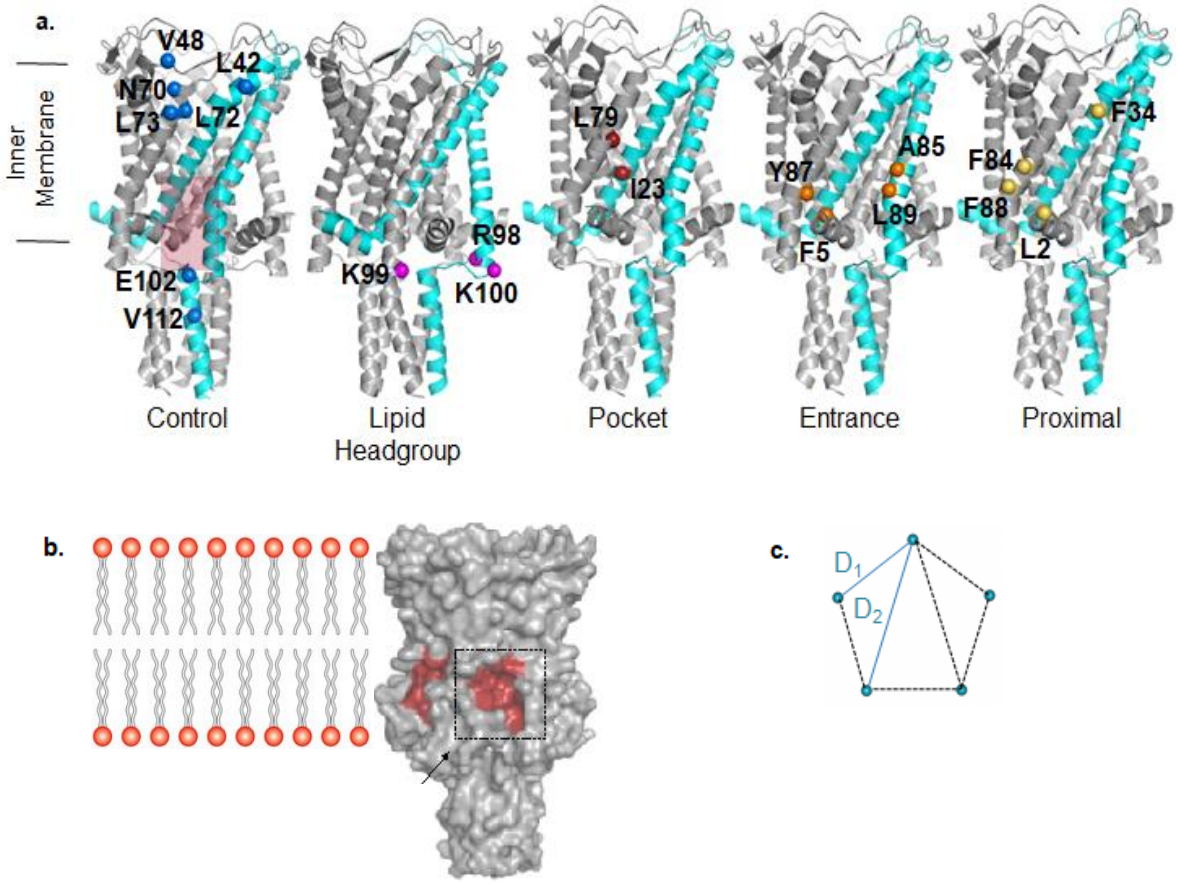

Fig. 3. 1: a. Mutation sites on TbMscL, with the monomer shown in cyan. The nano – pockets region is shown in transparent red. Spheres of different colours represent the generated mutants with respect to their distance from the nano – pockets. The colour coding is: blue for control mutants, with their lipid head group binding sub – category shown in magenta, dark red for mutants inside the pockets, orange for pocket entrance mutants and yellow for mutants proximal to the nano – pocket's entrance. **b.** Location of the nano – pockets (red surface, highlighted in the black square) on TbMscL, on the cytosolic leaflet – side of the protein, and that of the channel with respect to the lipid bilayer. **c.** The two distinct distances that are seen in PELDOR measurements and in silico modelling for TbMscL due to its pentameric symmetry. Figure adapted from Kapsalis *et al., Nat Commun*, 2019.

In silico spin labelling and distance modelling played an important role in choosing the exact residue to be mutated. Due to the pentameric symmetry of TbMscL (Fig. 3. 1 c), the 4 individual distances are identical pairwise, so this gives rise to 2 distinct distances in the experimental and simulated distance distributions. Furthermore, PELDOR has a practical useful range of measurable distances between roughly 15 – 70 Å. This means that if, during the *in silico* distance modelling, a candidate mutant had a distance that was ≤ 18 Å and / or a second distance that was ≥ 65 – 70 Å, this mutant was abandoned from further investigation. In addition, for PELDOR distance distributions to be more informative, accurate and useful, they need to be relatively narrow. *In silico* spin labelling was thus also used qualitatively for the rough estimation of the broadness of the expected distance distributions. This was not relied upon too much though, since these predictions are not of high accuracy, especially in the case of transmembrane mutants, as the simulation procedure does not take into account the detergent micelle and co-extracted lipids that covers that part of the protein and can significantly alter the spin labelling efficiency properties of such sites. Nevertheless, in hydrophilic parts of the channel the estimation is much more accurate and it was thus taken into account. Labelled mutants with very broad distance distributions, especially when that resulted in a high overlap between the two distinct distances, were also discarded from further investigation.

3. 2. 2. Initial characterization of the mutations, the purity of the protein and its labelling efficiency

Site – directed mutagenesis was performed on the plasmid containing the TbMscL gene and the resulting products of the PCR amplification procedure were assessed initially through DNA agarose gel electrophoresis (Fig. 3. 2) for the first set of mutants generated and subsequently sent for sequencing to verify that (a) the desired mutation was indeed introduced, and (b) no other accidental mutations were present in the gene. After the first set of mutations were generated and once the protocol procedure had been established and verified, mutant plasmids were no longer assessed by DNA agarose gel electrophoresis, but were directly sent for sequencing. Mutant plasmids that had been verified through DNA sequencing were transformed into two different *E. coli* strains: BL21(DE3) and MJF612. Transformed cells of the latter were used for the assessment of the *in vivo* functionality of the mutant proteins during hypo – osmotic stress shock assays (Fig. 3. 3). All single – cysteine TbMscL mutants demonstrated the ability to protect the *E. coli* cells from a hypo – osmotic shock as much as the wild type protein. Despite that, and in accordance with previous studies[195], TbMscL in general was shown to not be efficient enough at rescuing *E. coli* cells from such an osmotic shock, a fact that, as explained before, might have to do with the adaptation of TbMscL in different

microorganism with a different cell membrane lipid composition. Nevertheless, the assays (repeated independently 3 times for each of the conditions) showed that there is no significant *in vivo* functional difference between those mutants and the wild type TbMscL.

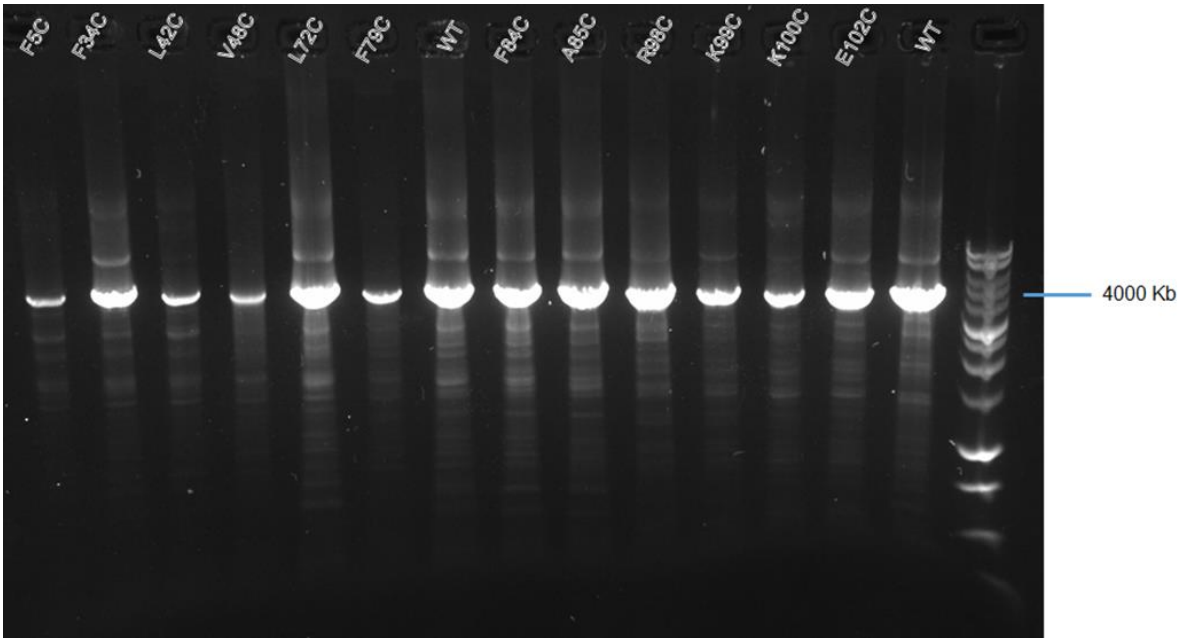

Fig. 3. 2: DNA agarose gel of the first set of mutants generated (F5C, F34C, L42C, V48C, L72C, F79C, F84C, A85C, R98C, K99C, K100C and E102C) plasmid DNA. All plasmids migrated equally at the correct size, which is approximately 4000 kb. Two of the lanes correspond to the WT plasmid, which was used as a form of internal standard.

E. coli BL21(DE3) cells transformed with TbMscL mutant plasmids were used for the overexpression and subsequent purification of the channel. Due to the nature of the EPR techniques that were to be used later on, the purity and monodispersity of the protein sample are considered to be very important factors. Hence the samples' monodisperity was always assessed through the separation method of size exclusion chromatography for all samples produced (Fig 3. 4) and purity was assessed, for selected samples, by SDS – PAGE as well, especially until the full establishment of the protein purification procedure. As evident from the size exclusion chromatography profiles, in the case of many of the TbMscL mutants (the most prominent example being the V48R1 mutant, with R1 designating a cysteine mutant modified with MTSSL spin label), the main peak of what is expected to be (according to the molecular weight) the 6 x His – tagged pentameric channel is preceded by a higher molecular weight peak.

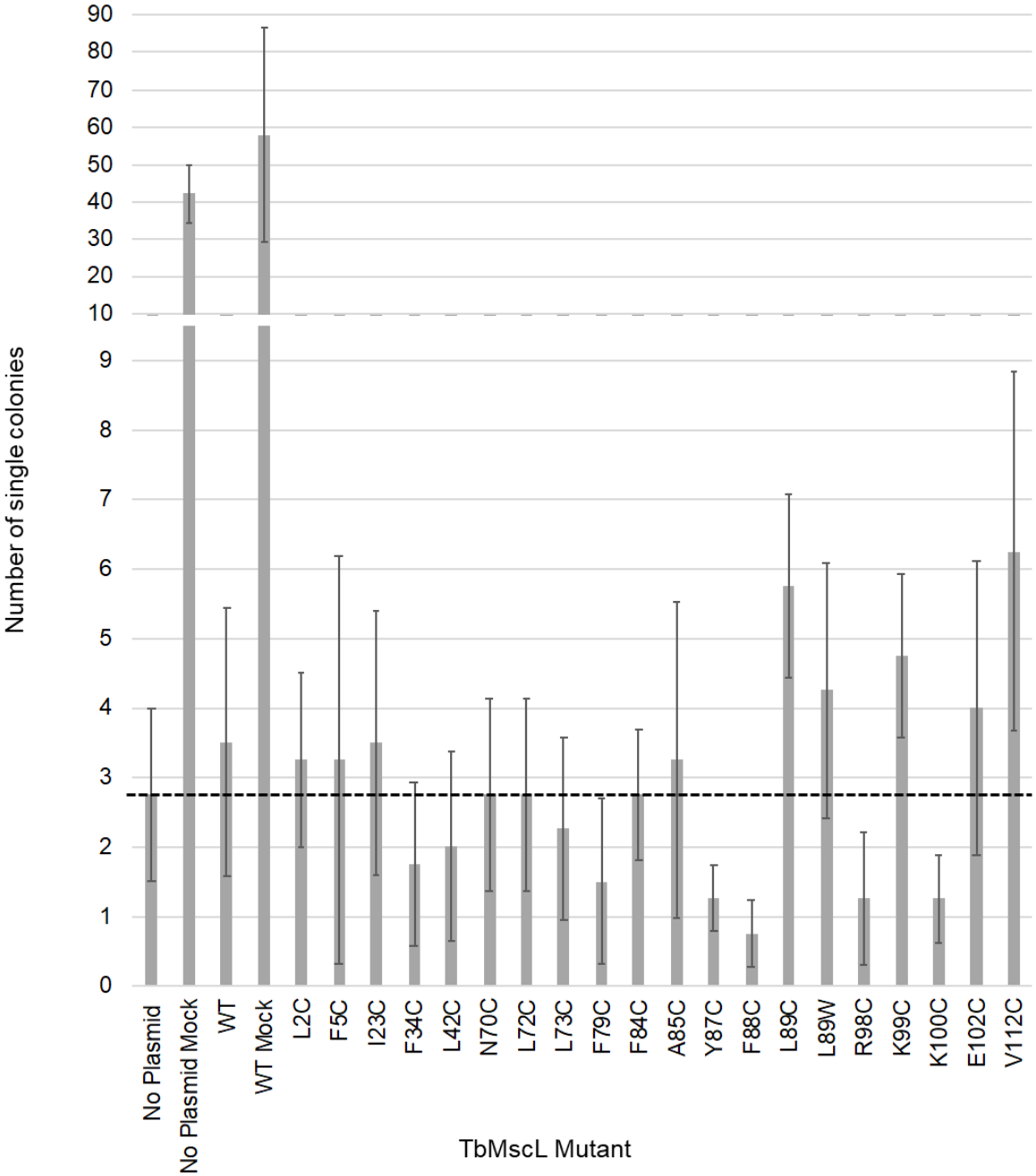

Fig. 3. 3: Hypo – osmotic shock survival of MJF612 *E. coli* cells. Cells were transformed with a plasmid expressing WT or mutant TbMscL, or non – transformed. Bars represent the mean ± SD of the number of colonies counted from 3 independent preparations and assays. The dotted line is the threshold of the average survival of untransformed cells after a hypo – osmotic shock, i.e. the baseline survival that cannot be attributed to the action of MscL. Figure adapted from Kapsalis *et al., Nat Commun*, 2019.

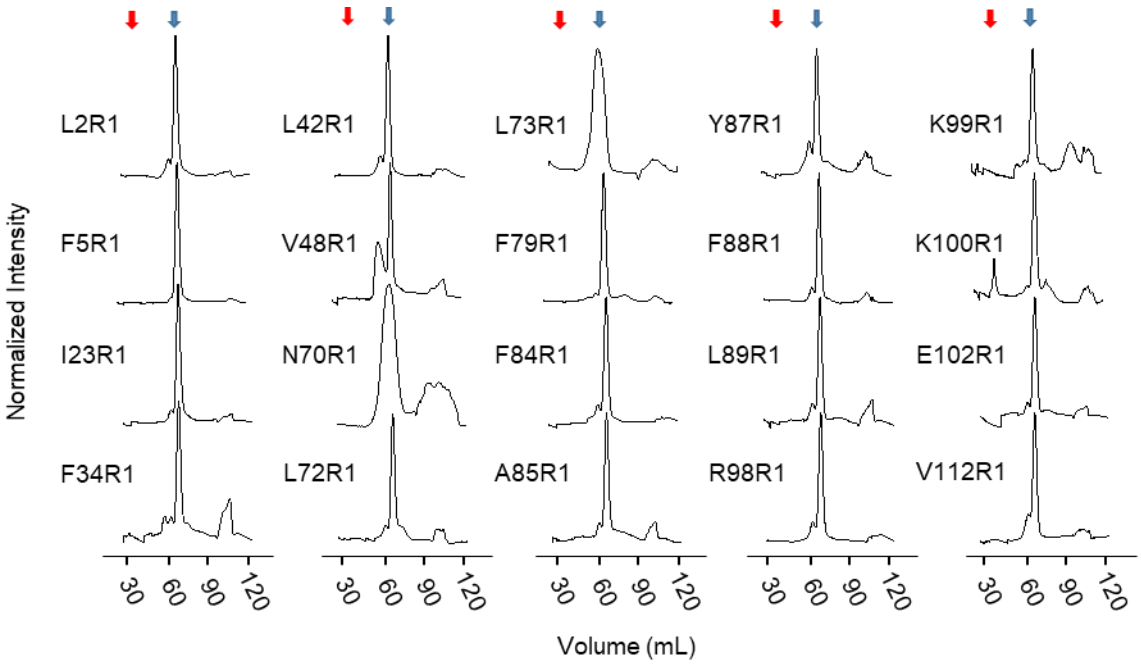

Fig. 3. 4: Size exclusion chromatography profiles of purified single cysteine TbMscL mutants. Red arrows denote the void volume (≈ 25 mL) and blue arrows denote the main pentameric TbMscL peak (≈ 65 mL). The higher molecular weight peak, when visible, shows up at ≈ 57 mL. Figure adapted from Kapsalis *et al., Nat Commun*, 2019.

This peak was investigated using SDS – PAGE in the case of mutant K100R1 (Fig. 3. 5) and it was shown to be pure TbMscL, just as in the main peak, and its adequately defined shape and elution volume indicates that it does not represent randomly aggregated protein, but rather a more defined structure. It is thus possible that this higher molecular weight peak is a product of accidental cross – linking between individual pentamers through some of the introduced cysteine residues that did not get labelled with MTSSL. The fact that these peaks seem to be more prominent in the case of mutants that are more exposed to the aqueous buffer (the highest mutant with the percentage of this peak when compared to the main peak is V48R1, which is situated on the periplasmic loop that connects the two transmembrane helices (Fig. 3 .1 a) and is the most exposed mutant generated) could act to support this view.

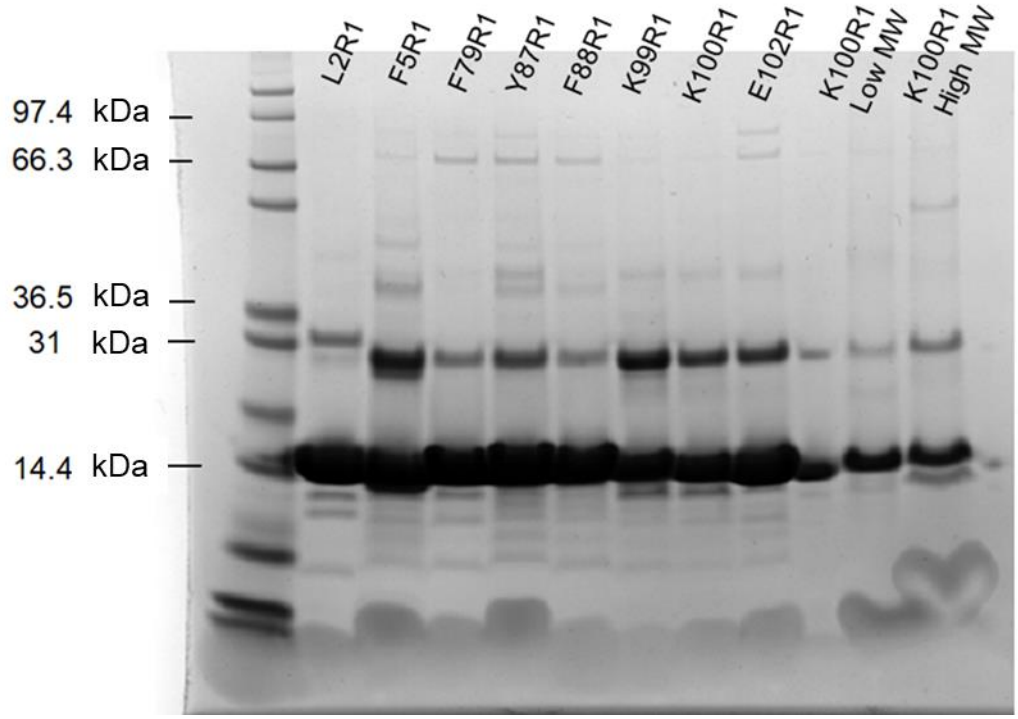

Fig. 3. 5: SDS – PAGE gel of TbMscL MTSSL – modified cysteine mutants. Apart from the very strong monomer bands (≈ 15 kDa), bands corresponding to high oligomeric states (e. g. at ≈ 31 kDa) are also visible. Products of TbMscL's degradation can also be seen as bands of lower molecular weight than that of the monomer. High concentrations of sample were used in order for such bands to be visible.

Before PELDOR and ESEEM measurements, spin – labelled TbMscL cysteine mutants were also assessed through CW – EPR spectroscopy (Fig. 3. 6). CW – EPR spectra can provide us with important information regarding both the label's environment and mobility, and the spin – labelling efficiency of the individual mutants. Regarding the spin label's mobility, the narrower and sharper the first – derivative peaks of the spectrum, the more mobile the label is, which is usually an indication of it being exposed to the aqueous solution or, at least, being situated in a part of the protein where there is not much steric clash with either other amino acid residues of the protein itself or the detergent micelle covering the hydrophobic parts of the protein. Good examples of highly mobile spin labelled mutants generated on TbMscL are V48R1 (on the loop that connects the two transmembrane helices), K99R1 and K100R1 (part of the positively charged cluster at the C – terminal end of TM2, expected to be exposed to the aqueous buffer) as well as E102R1 and V112R1 (mutants of the highly exposed cytosolic C – terminal α – helix of the protein).

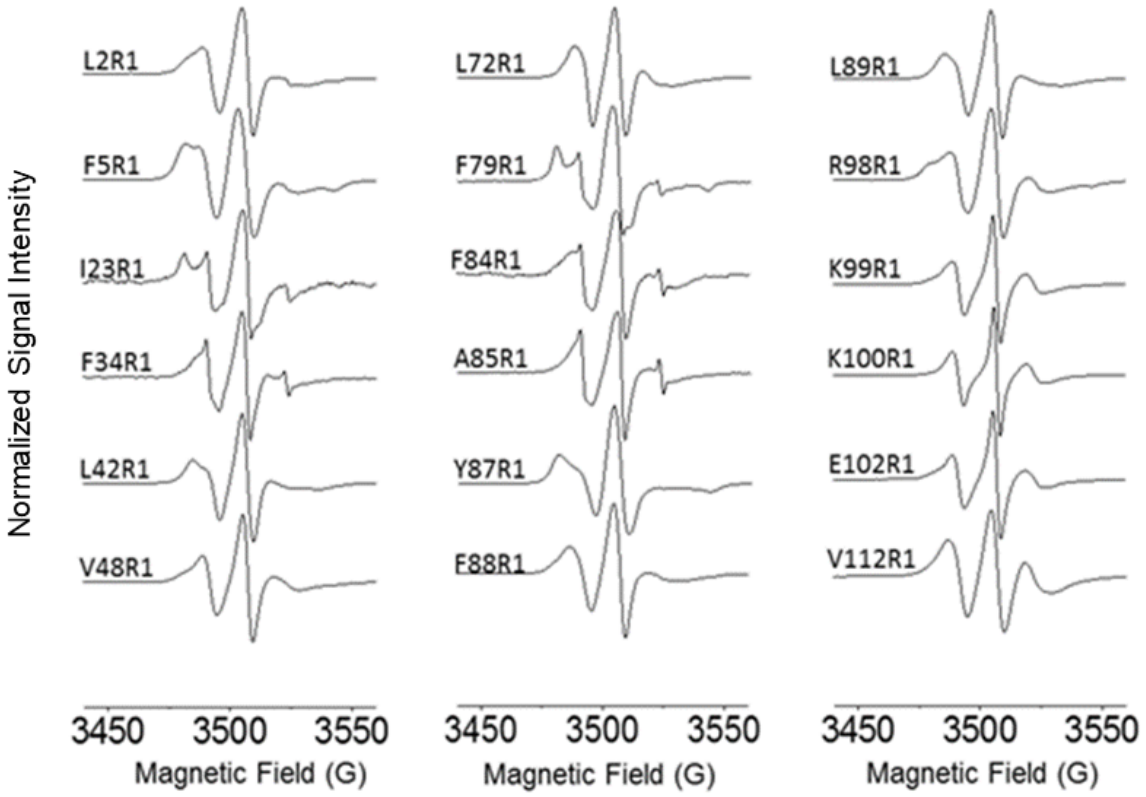

Fig. 3. 6: CW – EPR spectra of TbMscL's single cysteine mutants. High mobility spin labels (e.g. V48R1 and K100R1) can easily be distinguished from low mobility ones (e. g. F5R1 and Y87R1). Signal resembling that of a free spin label can be observed in the form of very sharp and narrow peaks in samples such as I23R1, F34R2, F79R1, F84R1 and A85R1. Figure adapted from Kapsalis *et al., Nat Commun*, 2019.

On the other hand, CW – EPR spectra with spread – out and broad first – derivative peaks are indicative of spins labels of reduced mobility, and such spectra are usually expected from mutants in the transmembrane part of the protein, where the label's mobility is hindered by the tertiary structure of the protein itself or the detergent micelle. L2R1, F5R1, L42R1 and Y87R1 are some of the least mobile mutants in the present dataset. In many such cases, the low – field peak (i. e. the left – most one) can manifest as a double peak, which can be an indication of the existence of two distinct conformers of the spin – label that show up as the two separate components of the peak: a more restricted (the one on the left side of the peak) and a more mobile (the one on the right side). In the data presented here, prominent examples of those double peaks can be seen in the spectra of mutants such as F5R1, L42R1, Y87R1 and R98R1. In the case of the first one, the two components are of roughly equal contribution to the peak. In the L42R1 and Y87R1 spectra, the rigid component is more prominent than the mobile one, while in the case of R98R1 it is the other way

around. Furthermore, in the spectra of mutants such as I23R1, F34R1, F79R1, F84R1 and A85R1, a very sharp set of very high mobility first – derivative peaks are visible. This is typically a sign of the existence of “free” spin label (spin labelling that is non – specifically bound) in the sample, which is randomly and non – specifically attached to the protein and / or the detergent micelles that are present. It is highly improbable that in the present dataset these peaks arise from actual free spin label in the solution, due to the large number of rigorous washing steps that took place between the spin – labelling step and the final CW – EPR measurement, and which also include the size – exclusion chromatography procedure that involves large dilution of the protein in high volumes of aqueous buffer. Moreover, since in the data presented this high – mobility, free spin label peak only manifests in the spectra of mutants with very low labelling efficiency, it is very possible that this component might be present in the cases of all modified mutants but is only visible in the cases mentioned due to the very low signal of the sample itself. In all other cases the signal is strong enough to hide the contribution of the free spin label.

As mentioned, apart from the investigation of the spin label’s mobility, CW – EPR is also employed for the (usually qualitative, but possibly quantitative too) assessment of the spin – labelling efficiency of modified cysteine mutants as well. This can give a preliminary idea of the potential quality of the PELDOR data that will be obtained later. High labelling efficiency is a prerequisite for good quality PELDOR data since this way the probability that A and B electron species will be an adequate distance to be coupled to one another increases drastically. For the purposes described here, a very rough and qualitative estimation of the labelling efficiency is more than adequate, and it can be performed by qualitatively assessing the signal – to – noise ratios. A more quantitative assessment was also performed for selected samples with the use of the paramagnetic molecule 4-hydroxy-2,2,6,6-tetramethyl-piperidine-1-oxyl, TEMPOL[196, 197] (Table 3. 1).

As it can be seen in the labelling efficiency calculated for selected mutants, those inside and at the entrance or in proximity to the nano – pockets, for example L2R1, F5R1, F34R1, F79R1 and A85R1, display reduced to minimal (≤ 30%) labelling efficiency, which can be explained because these mutants are buried in the hydrophobic transmembrane core of TbMscL. Despite that, along with the very exposed mutant like E102R1, some transmembrane mutants displayed high (≥ 60%) labelling efficiency as well and, interestingly, a number of them are also associated with the hydrophobic nano – pockets targeted (F88R1 is found in their vicinity while Y87R1 and L89R1 are situated right at their entrance).

TbMscL modified mutant	Labeling efficiency (%)
L2R1	3
F5R1	15
F34R1	3
F79R1	6
A85R1	8
Y87R1	79
F88R1	67
L89R1	62
E102R1	81

Table 3. 1: Spin labelling efficiency of selected TbMscL mutants as calculated from their CW – EPR spectra. Table adapted from Kapsalis *et al., Nat Commun*, 2019.

In order to put some biochemical and methodological meaning to the labelling efficiency percentages presented, we need to take two facts into consideration. Firstly, TbMscL is a homo – pentamer, which can be roughly described thus: each 20% - increase step in the spin – labelling efficiency means that one more subunit per protein pentamer gets labelled (for example, 50% labelling efficiency means that, on average, 2.5 subunits of the protein are spin labelled on any given pentameric protein). Secondly, and as explained earlier, due to the pentameric symmetry of TbMscL, two distinct distances can be measured with PELDOR and, in order for each of those distances to be measurable on every single and individual protein molecule, at least 3 of the pentamer's subunits need to be spin – labelled at all times. Those two facts can be translated in order to set two important spin – labelling efficiency thresholds. The first one is that when the labelling efficiency is ≤ 20 %, no more than one subunit per channel's pentamer is labelled at the same time on average, which means that PELDOR measurements cannot probably produce any useful data (at the very least 2 spin labels are needed per pentamer). The second one is that, for the purpose of PELDOR measurements and in the case of pentamers such as TbMscL, any spin – labelling value of ≥ 60 % is, in practice, virtually equivalent to full labelling of the protein, since only 3 out of 5 subunits need to be labelled in order for both distances to be measurable in every pentamer of the protein. In reality, the optimum labelling efficiency for TbMscL should be exactly 60 %, because the larger the number of paramagnetic centers on a molecule, the greater the multi – spin effects that arise and that can affect the quality of the obtained data[161]. This means that a 60 % labelling efficiency of a homo – pentamer

is the ideal compromise between maximizing the useful spin concentration while minimizing the multi – spin effects that arise from it.

3. 2. 3. Assessment of TbMscL' s oligomeric state and structure with pulsed EPR spectroscopy

Despite the low labelling efficiency (≤ 30%) that was evident for some, mostly transmembrane, cysteine mutants, PELDOR measurements were performed for all of the 20 generated mutants. 2 of them (L2R1 and F5R1) are on the N – terminal helix, 3 are on the TM1 helix (I23R1, F34R1 and L42R1), 1 (V48R1) on the periplasmic loop that connects the two transmembrane helices, 12 of the mutants (N70R1, L72R1, L73R1, F79R1, F84R1, A85R1, Y87R1, F88R1, L89R1, R98R1, K99R1 and K100R1) are on the TM2 helix and the remaining 2 (E102R1 and V112R1) are on the cytosolic C – terminal part of the protein. This means that 17 out of those 20 belong, to a greater or lesser extent, in the transmembrane core of the protein (the 3 that do not are V48R1, E102R1 and V112R1), which is of the highest interest and importance for a mechanosensitive ion channel. In the case of 7 of those 17 mutants, namely L2R1, F5R1, I23R1, F34R1, L79R1, F84R1 and A85R1 (Fig. 3. 7), the raw time – domain PELDOR traces acquired were not of good quality. This is not surprising, since those were the mutants with the lowest labelling efficiency and, in their case, there was not enough (i. e. two or more) paramagnetic centers per protein pentamer for dipolar coupling to be present between them. The very low modulation depth of the signal in most of those cases is highly indicative of this. In addition, the low labelling efficiency also leads to a very poor signal – to – noise ratio which, with the exception of L2R1 and F5R1, is evident in all of those cases. The most important problem that arises in the time – domain traces of those mutants, though, is the absence of any visible oscillation of their signal.

With the exception of the corrected trace of L2R1, where a shallow and very broad oscillation can be observed, the rest of the traces in question are essentially unremarkable exponential decay functions. As explained before, the oscillations of the PELDOR signal are a product of the dipolar coupling between the two electron species involved. This means that the distances between the unpaired electrons and, hence, the intra – molecular distances on the protein, can only be calculated accurately and reliably when such oscillations are both present and well – defined. Consequently, the distance distributions that are derived from these raw time – domain traces are very broad and, hence, highly unreliable (Fig. 3. 7). Thus, those mutants were excluded from any further investigation, since they could not be relied upon to either verify the closed state of the protein or be used to probe potential induced conformational changes of the channel.

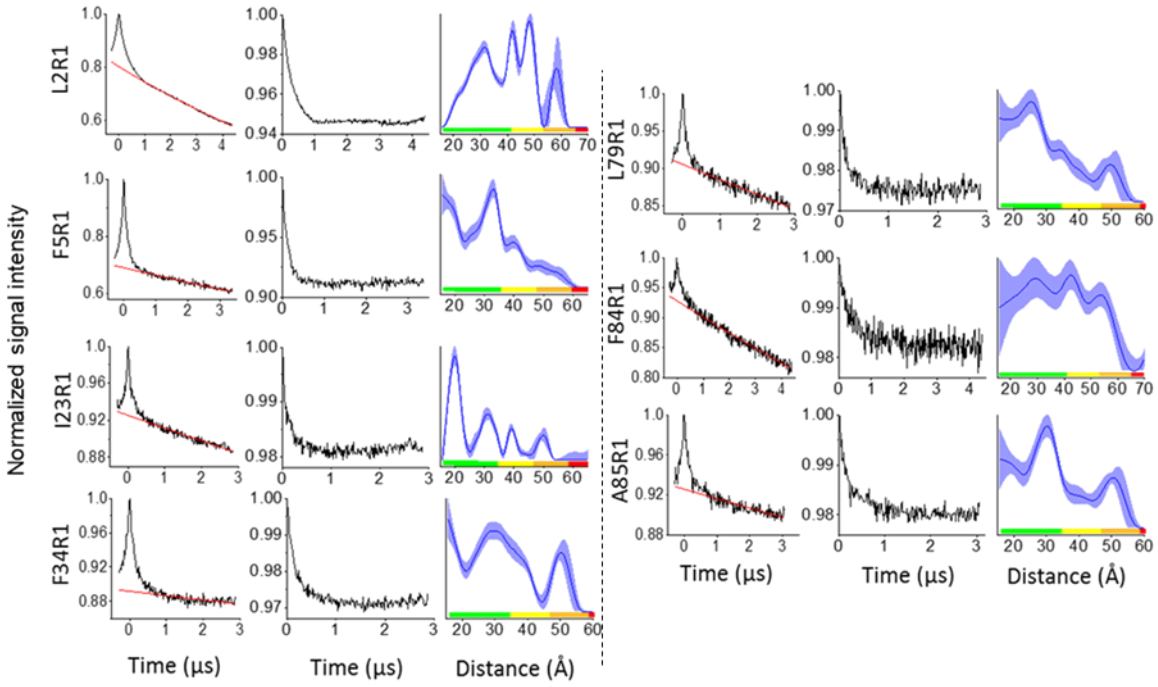

Fig. 3. 7: PELDOR data of TbMscL mutants with low labelling efficiency. For each mutant the raw, uncorrected time domain trace (black line) and the background function (red line) are shown on the leftmost column, the background corrected time – domain trace is shown in the middle column and the calculated distance distribution is shown on the rightmost column. Regarding the latter, blue shaded areas correspond to mean ± 2σ confidence intervals of the distance distributions (as calculated by the DeerAnalysis validation tool) and rainbow colour bars indicate the reliability of the measured distance ranges (as calculated by DeerAnalysis: green, shape reliable; yellow, mean and width reliable; orange, mean reliable; red, no quantification possible) The confidence intervals depend on the experimental time windows used. Figure adapted from Kapsalis *et al., Nat Commun*, 2019.

On the contrary, for the 3 buffer – exposed mutants and for the remaining 10 out of 17 transmembrane helix mutants, the acquired raw time – domain PELDOR data were of very high quality (Fig. 3. 8), with their modulation depths ranging from adequate (e. g. for L73R1) to very deep (e. g. for L42R1, L89R1 and K100R1), and with their oscillations ranging from adequately visible (e. g. for N70R1 and L73R1) to very prominent even before background correction of the traces (e. g. L42R1, L89R1 and V112R1). As a result of this, in most cases their distance distributions were also very well – defined and reliable (Fig. 3. 9). The broader one is that of V48R1, but that mutant is situated on the highly flexible loop that connects the two transmembrane helix. Spin labels found on such flexible and mobile domains are expected to naturally be very mobile themselves, and this is the reason behind the

very broad distance distribution exhibited here. The broadness of the peaks is, thus, not a result of a methodological problem or poor labelling efficiency, but rather a result of the structure of the protein itself and this means that, while it cannot be confidently used for the comparison between conformational states sought in the present project, it is still able to provide us with valuable information regarding the structural mobility of TbMscL's periplasmic loop.

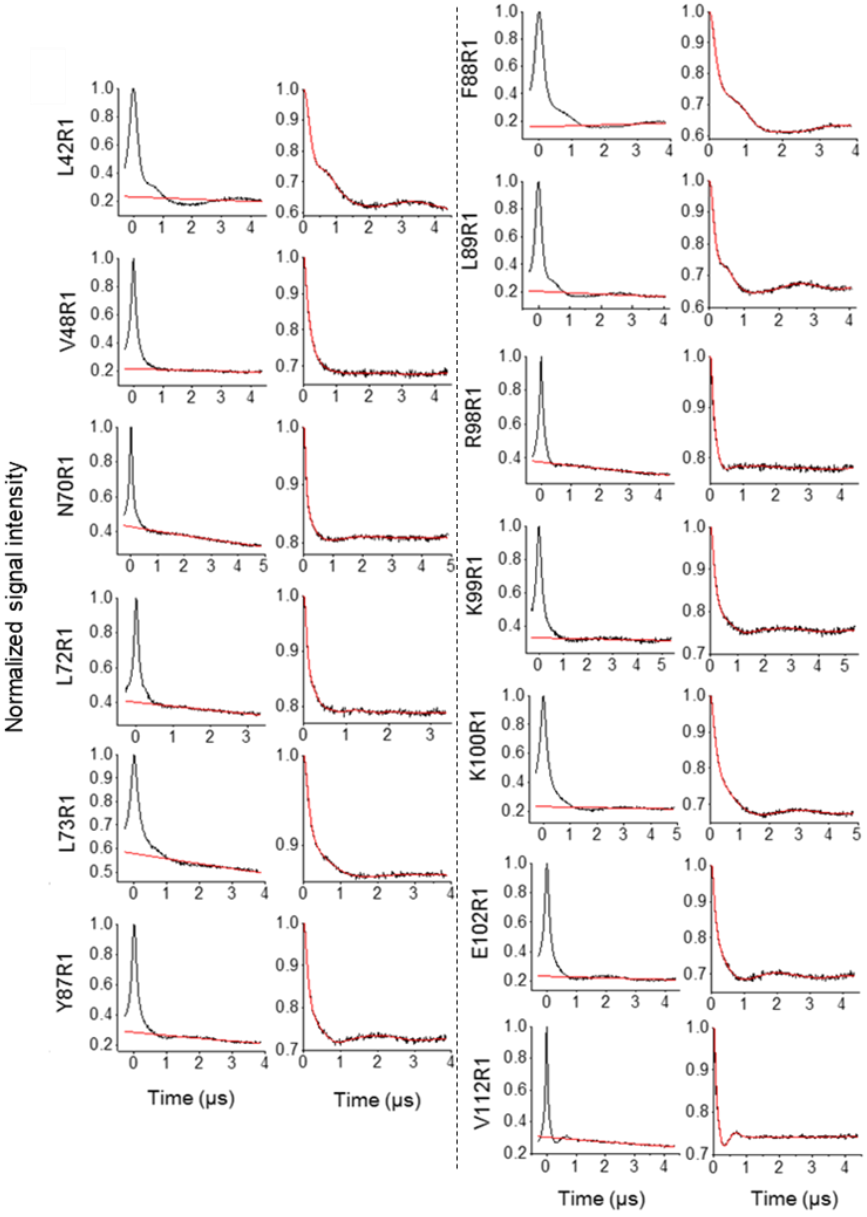

Fig. 3. 8: PELDOR data of TbMscL mutants with good labelling efficiency. For each mutant the raw, uncorrected time domain trace (black line) and the background function (red line) are shown on the left and the background corrected time – domain trace is shown on the right. Figure adapted from Kapsalis *et al., Nat Commun*. 2019.

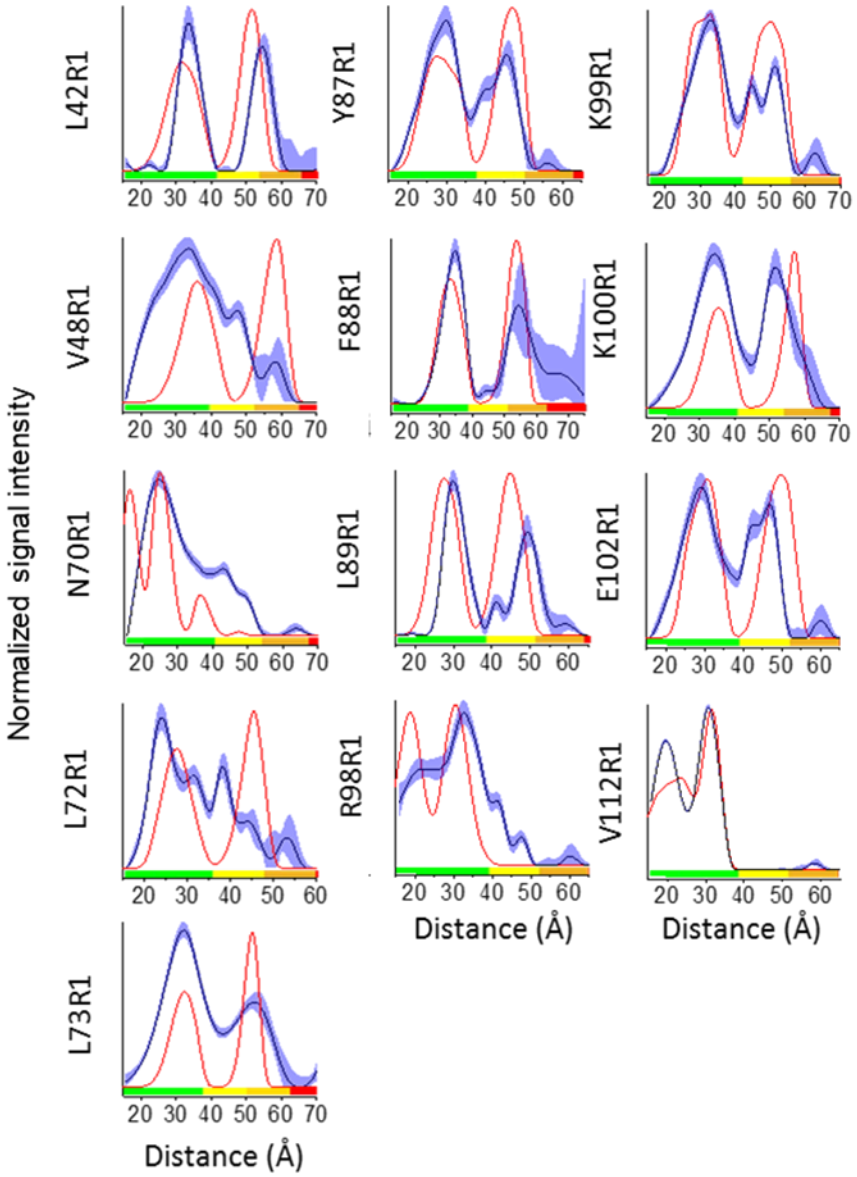

Fig. 3. 9: PELDOR distance distributions of TbMscL mutants with good quality raw time – domain traces. Blue shade areas correspond to mean ± 2σ confidence intervals of the distance distributions (as calculated by the DeerAnalysis validation tool) and red lines correspond to the *in silico* modelled distance distributions using MTSSLWizard. Rainbow colour bars indicate the reliability of the measured distance ranges (as calculated by DeerAnalysis: green, shape reliable; yellow, mean and width reliable; orange, mean reliable; red, no quantification possible). The confidence intervals depend on the experimental time windows used. Figure adapted from Kapsalis *et al., Nat Commun*, 2019.

Regarding the rest of the mutants with reliable raw time – domain PELDOR traces, their well – defined distance distributions can be used not only for the assessment of the structural state of TbMscL, but also for probing its oligomeric state. Through simple geometry it can be calculated that the ratio between the second (D_2) and first (D_1) distance for a symmetric pentagon is $D_2 / D_1 = 1.6$, while the corresponding values for a symmetric tetramer and hexamer would be 1.4 and 1.7, respectively. In all of the mutants with a well – defined distance distributions, the D_2 / D_1 ratio agrees quite well with what is expected for pentameric TbMscL (Table 3. 2). The mutant with the greatest divergence from this value is mutant R98R1, however the distance distributions are relatively broad, with a calculated $D_2 / D_1 = 1.50$, but which still agrees well with what is expected for a symmetric pentamer. The mutant with the best agreement is E102R1, with the calculated value of its D_2 / D_1 ratio being exactly 1.6.

TbMscL modified mutant	D_1 (Å)	D_2 (Å)	Ratio (D_2/D_1)
L42R1	33.5	54.5	1.62
L73R1	32.1	52.2	1.63
Y87R1	29.7	45.4	1.53
F88R1	34.6	54.5	1.57
L89R1	30.0	49.3	1.64
R98R1	21.7	32.6	1.50
K99R1	32.9	51.3	1.56
K100R1	34.2	51.7	1.51
E102R1	29.2	46.7	1.60
V112R1	19.6	30.6	1.56

Table 3. 2: Second-to-first distance (D_2/D_1) ratios of cysteine mutants. Values of ≈1.6 correspond to that expected for a pentameric protein, due to its symmetry. Table adapted from Kapsalis *et al., Nat Commu n*, 2019.

Despite the oligomeric state being a useful collateral piece of knowledge, the most important information derived from the PELDOR experiments is regarding the structural and conformational state of TbMscL. In the subset of “well – behaving” mutants presented above, the experimentally measured distance distributions (blue

shaded areas) seem to agree very well with the *in silico* simulated ones (using MTSSLWizard, red lines) for all but 4 mutants: L42R1, N70R1, L72R1 and L89R1 (Fig. 3. 9). For a discrepancy between the experimental and simulated distance distributions to be considered significant, it needs to be present both in the first and second distance, since an inconsistent difference in the second distance alone can most probably easily be attributed to the PELDOR measurement time – window not being long enough and, hence, the longer second distance being relatively less reliable. Of the four aforementioned mutants, the first three belong to the category of "control" mutants, located in regions of the protein unrelated to the hydrophobic nano – pockets, while the last one, L89R1, is situated right on their entrance. The case of L42R1 is perhaps the easiest to explain: this residue lies very close to a region of TbMscL, spanning from G47 to I56, where the original electron density map for the crystal structure was not very clear and, for the purposes of a later study, has since been remodeled[109, 117]. This means that the discrepancy observed between the experimental and simulated distance distributions could be a result of the uncertainty of the exact location of residue L42 in the original crystal structure.

The case of the following two mutants, N70R1 and L72R1, can be more complicated. In the case of N70R1, during *in silico* spin labelling using MTSSLWizard, the R1 side chain seems to adopt two distinct conformations: one pointing towards the inside of the pore and one pointing towards the outside (Fig. 3. 10 a). This leads to the splitting of each one of the distances into two and, consequently, this gives rise to the 4 distinct peaks in the *in silico* simulated distance distribution (Fig. 3. 9). The same splitting of the R1 side chain rotamer population into two distinct conformations is exhibited by the MMM site – directed spin labelling software too (Fig. 3. 10 a), resulting in a splitting of distances similar to the one produced by MTSSLWizard (Fig. 3. 10 b). On the contrary, no such splitting of the distance peaks is observed in the experimentally obtained distance distributions. Rather the two peaks, albeit slightly broadened, seem to agree very well with the longer set of distances (i. e. the second and fourth peak) predicted by MTSSLWizard (Fig. 3. 9). Hence, the discrepancy observed here can be explained as such: although in silico modelling predicts two distinct conformations (one inside and one outside of the pore) for the rotamer population of N70R1, in reality only one of these conformations (namely, the one pointing towards the outside of the pore, since this is the one corresponding to the longer set of distances) is adopted. On the other hand, in the case of L72R1, it seems like the discrepancy observed could be explained similarly, but the other way around: although the in silico modelling predicts only one conformation for the whole R1 side chain population, in reality L72R1 adopts two distinct conformations which give rise to the experimentally observed splitting of the distances. This could also explain why the simulated distances seem to coincide with the pair – wise average of the experimentally obtained ones (Fig. 3. 9). Finally, in the case of L89R1, an increase of ≈ 3 Å for the first and of ≈ 5 Å for the second distance can be observed.

Unlike the previous 3, this discrepancy cannot be explained by any means and, since this mutant is situated at the entrance of TbMscL's nano – pockets, it is a case worth investigating further.

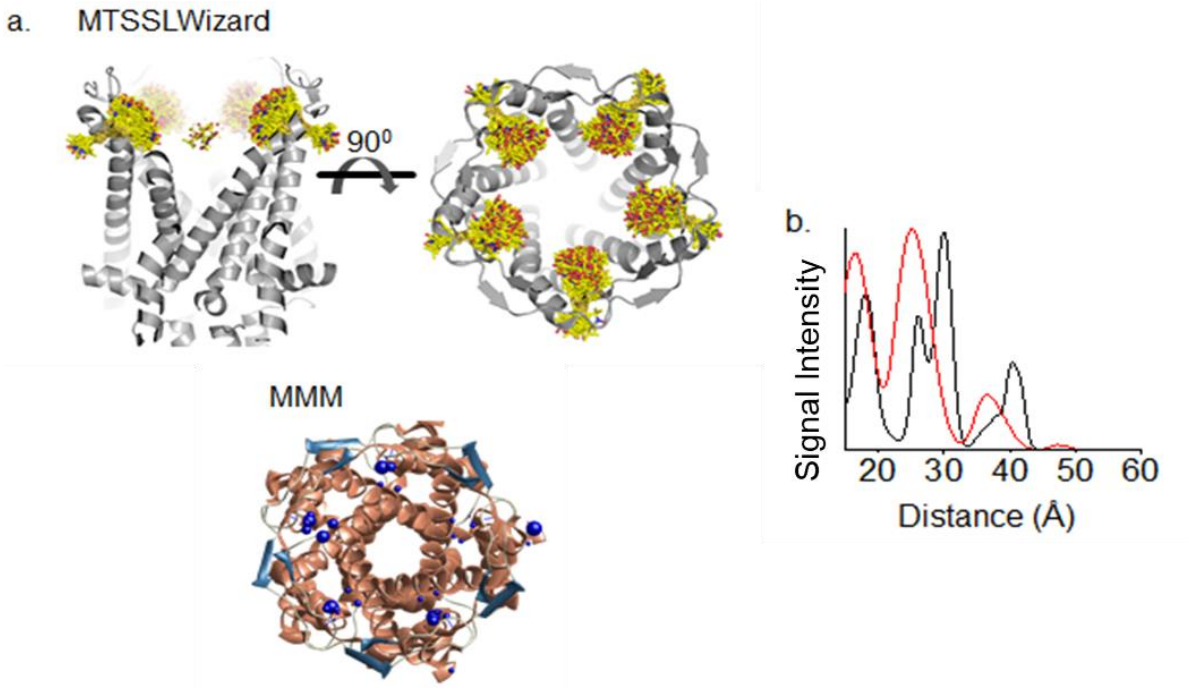

Fig 3. 10: a. Rotamers of the R1 side chain of N70R1 as predicted from MtsslWizard (yellow sticks, top) and MMM (blue spheres, bottom left). In both cases, N70R1 rotamers are split between two conformations: one pointing to the inside and one to the outside of the pore. **b.** MtsslWizard (red line) and MMM (black line) simulated distance distributions. The two distinct R1 conformations result in the appearance of multiple distance peaks. Figure adapted from Kapsalis *et al., Nat Commun*, 2019.

In addition, the modified cysteine mutants that were generated and purified were also probed using 3 – pulse ESEEM, which is capable of providing important information regarding the solvent accessibility of individual mutants. The buffer that the purified mutants are in for the purpose of low temperature EPR measurements (such as PELDOR and ESEEM) contains 50 % v/v deuterated ethylene glycol, and solvent accessibility can thus be estimated through the extent of the interactions between the paramagnetic center of the spin label and the ^{2}H nuclei that may be surrounding them. As expected, the mutants that are situated at the transmembrane parts of the protein, and especially the ones that displayed low labelling efficiency, were not readily accessible by the ^{2}H nuclei that are only present in the solution surrounding the protein (Fig. 3. 11), with the most "buried" of all mutants being L72R1. The mutants of the periplasmic loop (V48R1) and cytosolic C – terminus

(E102R1, V112R1) were, not surprisingly, highly exposed to the buffer, while the same stands true for the 3 mutants of the positively charged cluster of amino acid residues at the C – terminal end of the TM2 helix, R98R1, K99R1 and K100R1. Regarding transmembrane mutants, the ones closer to the two edges of the transmembrane helices (e.g. L42R1, R98R1 and K100R1) are more exposed compared to those closer to their middle (e.g. F79R1 and Y87R1).

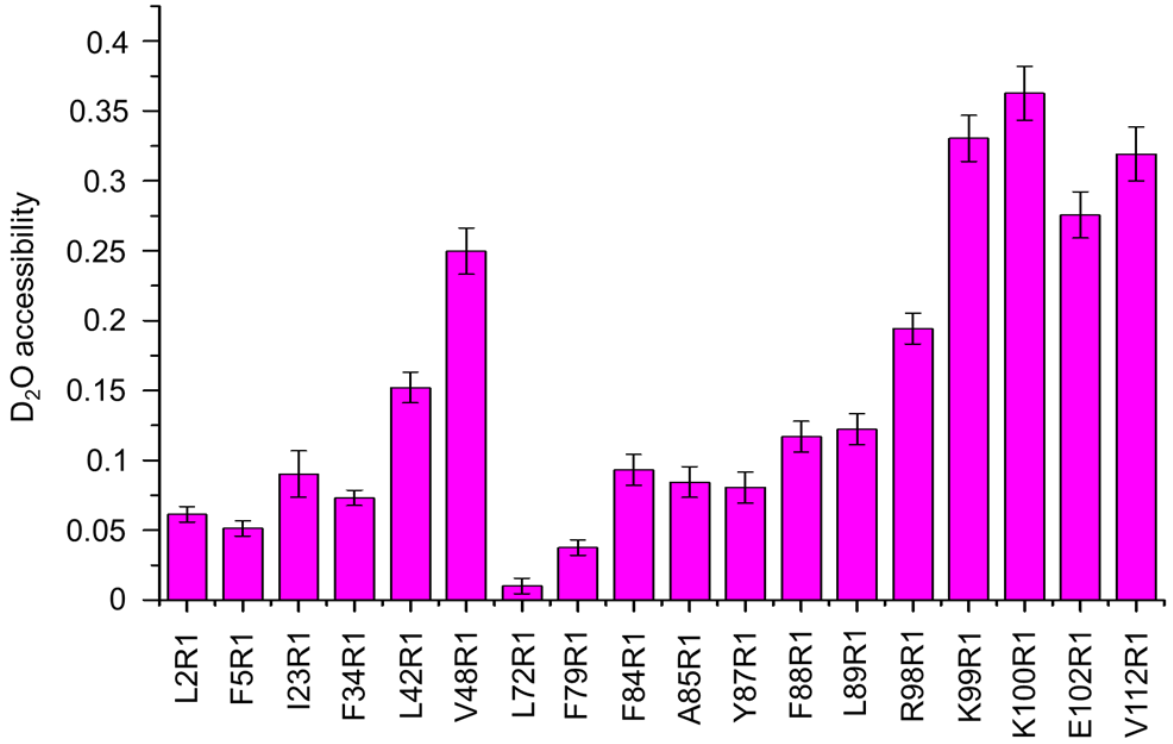

Fig 3. 11: D_2O accessibility of single cysteine TbMscL mutants as calculated from the modulation depth of their ^2H – interaction time – domain traces. Error bars arise from the fitting of the time domain trace with a simulation function, after correction by subtraction of a background stretched exponential decay function.

3. 2. 4. Assessment of the channel's structure in lipid bilayers

In order to further investigate the discrepancies observed in the PELDOR distance distributions for L42R1 and L89R1, those two TbMscL mutants were reconstituted into lipid bilayers. Along with them, mutants Y87R1, F88R1, R98R1, K100R1 and E102R1 were also reconstituted in the same artificial bilayer systems, since their experimentally determined distance distributions did not differ significantly from the *in silico* simulated ones, and could thus act as control samples. The reasoning behind reconstituting the mutants of interest in lipid bilayers to assess the effect of these mutations lies in the "Lipid moves first" principle. If these mutations, and

especially L89R1 which lies at the entrance of the nano – pockets, somehow hinder the close interactions between the bilayer and the channel, and more specifically if they manage to deny access of the annular lipids inside the nano – pockets, it is possible that the lateral pressure applied from the artificial lipid bilayer on the transmembrane part of TbMscL could force the lipids back inside the hydrophobic crevices. This way, the artificial lipid bilayer could act in a manner similar to the natural cell membrane and force the channel to open, if indeed the discrepancy observed is a product of some conformational change.

Since, as explained earlier, it has been suggested that specific lipid species might have an effect on the channel's function and could, thus, affect the conformational state of TbMscL, before reconstituting the protein in artificial bilayers it was of interest to investigate whether there are any endogenously derived *E. coli* lipids towards which the channel exhibited some kind of preference. It is known that during the purification process, endogenous lipids of the cell membrane are indeed co – extracted with membrane proteins[128]. Thus, we relied on two techniques, ^{31}P – NMR (measurements performed by Dr Jason Schnell, University of Oxford) and electrospray mass spectrometry (ES – MS) (measurements performed by Prof Terry K. Smith, University of St Andrews) in order to probe those co – extracted lipids. In the case that any kind of preference could be observed, the specific lipid or lipids would be included in the reconstitution lipid mixture. Through ^{31}P – NMR three distinct characteristic peaks were observed, which were consistent with lyso – phosphatidyl ethanolamine, phosphatidyl ethanolamine and phosphatidyl glycerol (Fig. 3. 12 a). The result is not surprising, since phosphatidyl ethanolamine and phosphatidyl glycerol together make up the vast majority of lipid head group species naturally found in the *E. coli* cell membrane. Furthermore, even more importantly, the ratio of the signal intensities of the two head group species is very similar to the one reported for the *E. coli* cell membrane, where phosphatidyl ethanolamine and phosphatidyl glycerol are found in a ratio of approximately 3:1[198]. This is already a good suggestion that TbMscL does not exhibit any strong preference or specificity for a specific lipid species. This view is also supported by the identification of the endogenous lipids extracted from both wild type and mutant samples of TbMscL, using ES – MS. In the majority of samples the aforementioned two lipid species, phosphatidyl ethanolamine and phosphatidyl glycerol, along with the negatively charged phosphatidic acid head group, were present (Table 3. 3). Nevertheless, no lipid binding specificity could be observed through this method either, so there was no need to dope the artificial bilayers with any kind of extra lipid.

TbMscL modified mutant	PA 29:0/:1	PG 30:1	PG 32:0/:1	Extra
WT	✓		✓	PE 30:0/:1
L2R1		✓	✓	
F5R1	✓	✓	✓	
L23R1	✓	✓	✓	
F34R1			✓	
L42R1	✓	✓		
V48R1		✓	✓	
L72R1	✓	✓	✓	
F79R1	✓	✓		
F84R1	✓	✓	✓	PE 29:0
A85R1		✓		
Y87R1	✓	✓		PG 24:1
F88R1	✓	✓	✓	
L89R1		✓		
		✓	✓	PG 33:1 PG 34:1 PG 37:2
R98R1		✓		
K100R1				PE 33:1 PG 36:2
E102R1		✓		PG 33:1
V112R1		✓	✓	

Table 3. 3: ES – MS analysis of endogenous *E. coli* lipids co – extracted during the purification of wild type and MTSSL – modified mutants of TbMscL. Measurements were performed by Prof Terry K. Smith, University of St Andrews. Figure adapted from Kapsalis *et al., Nat Commun*, 2019.

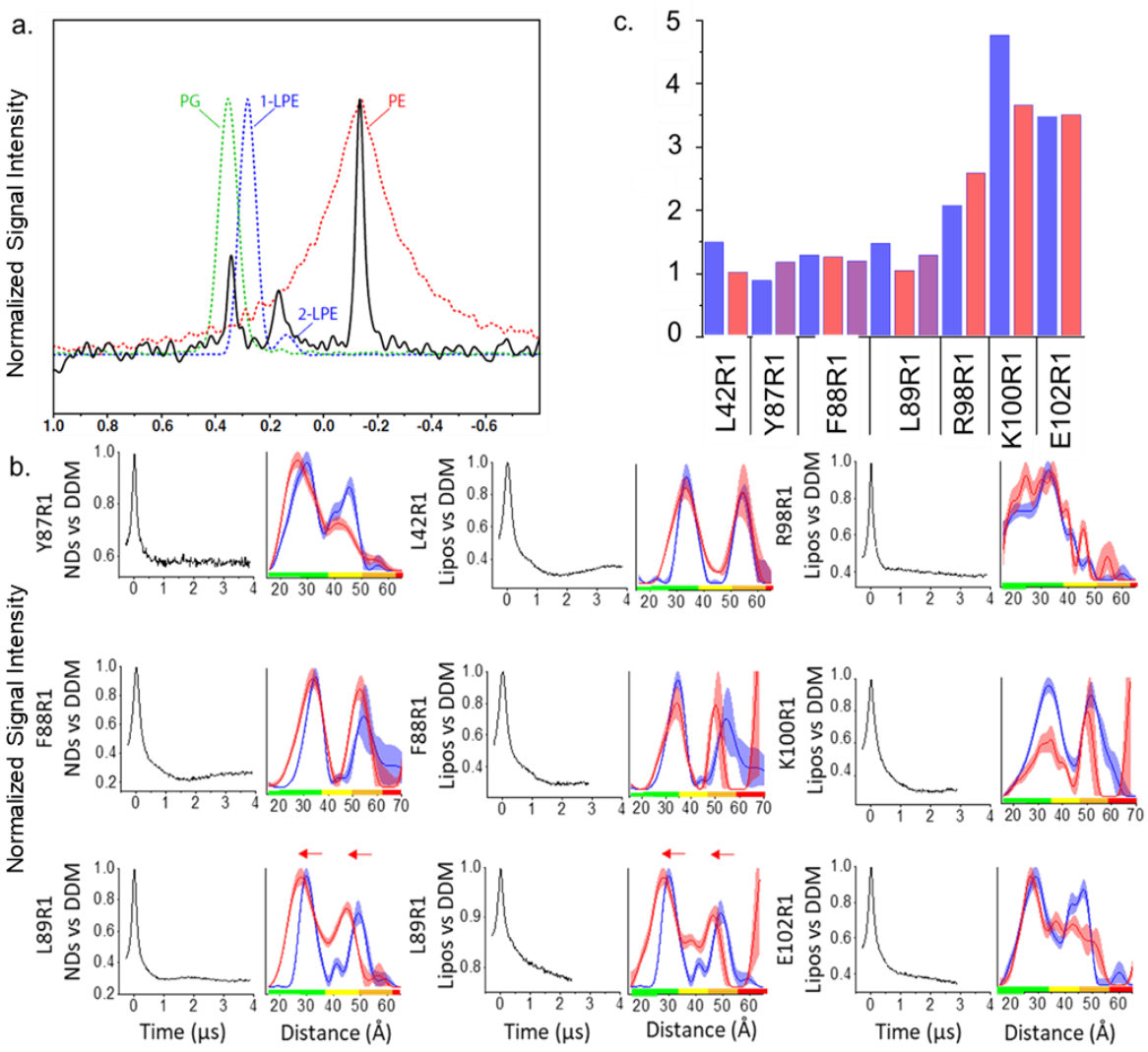

Fig 3. 12: a. ^{31}P – NMR spectrum of wild type TbMscL (black line) with characteristic peaks corresponding to phosphatidyl glycerol, phosphatidyl ethanolamine and 2 – lyso phosphatidyl ethanolamine. Coloured lines correspond to the spectra of those individual lipid standards as indicated. **b.** Background corrected PELDOR time domain spectra of reconstituted TbMscL mutants (left) and the corresponding distance distributions (right) (red shaded areas) compared to those of the same mutant in detergent solution (blue shaded areas). Colour coded confidence intervals correspond to the measurement with the shortest time window, which is in all cases that of the reconstituted sample. **c.** D_2O accessibility of detergent – solubilised (blue) and reconstituted (red for liposomes and purple for nanodiscs) TbMscL mutants as calculated by their 2 – pulse ESEEM ^{2}H / ^{1}H frequency peak intensity ratios. NMR measurements were performed by Dr Jason Schnell, University of Oxford. Figure adapted from Kapsalis *et al., Nat Commun*, 2019.

Two different lipid mixtures were used in two different reconstitution systems. The channel was reconstituted in either liposomes composed of *E. coli* polar lipid extract or nanodiscs composed of (the single lipid species) dimyristoyl phosphatidyl choline (DMPC) and the membrane scaffold protein 1 D 1 (MSP1D1). Liposomes are curved bilayers, resembling more of a natural membrane, while nanodiscs are planar and flat. MSP1D1 was the scaffold protein of choice due to its length and, hence, the nanodisc diameter that it can accommodate, which would ensure the presence of a single TbMscL pentamer per nanodisc, significantly reducing the effect of molecular (and, more importantly, paramagnetic center) crowding during PELDOR measurements.

The “control” mutants Y87R1, F88R1, R98R1, K100R1 and E102R1 span a good portion of the protein, sampling both the transmembrane (Y87R1, F88R1, R98R1 and K100R1) and cytosolic (E102R1) part of the channel, and the first four are situated on regions of high interest on TbMscL: Y87R1 and F88R1 are on and close to the nano – pocket entrance respectively, while the other two, R98R1 and K100R1, are part of the positively charged cluster at the end of TM2. Nevertheless, it can be seen in the PELDOR data, no significant change can be observed when comparing their distance distributions in detergent solution (Fig. 3. 12 b, blue shaded areas) with that after reconstitution (Fig. 3. 12 b, red shaded areas), and this consistency is independent of whether the reconstitution system is curved *E.* coli polar lipid extract liposomes or planar DMPC MSP1D1 nanodiscs. The same seems to be true in the case of L42R1, the distance distribution of which remains unchanged after reconstitution in liposomes (Fig. 3. 12 b). This is a strong indication that the channel’s conformation remains unchanged.

This was, though, not the case for the nano – pocket entrance mutant L89R1. Upon reconstitution, the distance distributions become shorter for both distances and, very importantly, they end up coinciding with the distance distribution predicted from the *in silico* modelling. Interestingly, the distance peaks shift equally towards shorter distances in the case of both liposomes and nanodiscs. This is an indication that neither the lipid mixture (*E. coli* polar lipid extract vs DMPC) nor the reconstitution system (curved liposomes vs flat nanodiscs) affect the channel’s state on their own. The same conclusion can be drawn for the F88R1 modified mutant as well, where both reconstitution systems seem to leave the distance distributions unaffected equally. Thus, it can be concluded that the existence of a lipid bilayer in general is, in its own right, adequate for the reversal of the effect observed in the L89R1 modified mutant. Furthermore, these findings also suggest that the influence L89R1 has on the channel’s conformation and structure seems to be completely reversible upon reconstitution, which is enough to revert TbMscL from the induced expanded state back to its closed one. The lateral pressure exerted from the lipid bilayer on

the transmembrane part of the protein is enough to force annular lipids back inside the channel's nano – pockets and, consequently, close TbMscL.

3. 2. 5. The effect of nano – pocket entrance mutations on the global structure of TbMscL

As explained, the L89R1 mutation and modification at the entrance of TbMscL's nano – pockets does indeed have a local effect on the protein conformation, which is readily reversible upon reconstitution in lipid bilayers. The question that still remained though is whether the obstruction of the nano - pocket entrance on its own, without the assistance of the channel's main trigger which is the lateral tension of the bilayer, is capable of causing a global conformational change, which can structurally affect other parts of the protein as well. In addition, if such an effect was to be observed, it would decisively and strongly support the argument that the discrepancies and alterations observed in the case of L89R1 between in silico modelled, detergent solution and bilayer – reconstituted distance distributions are indeed caused by a change in the structural state of the channel and are not merely artefacts that randomly arise due to the interactions between the detergent molecules and / or lipids with the attached spin labels, which could affect the measured distances. Hence, a new L89 mutation was generated, L89W, with a tryptophan replacing the R1 side chain of the previous L89R1, and it was paired with 4 EPR – reporter mutants from the TM2 helix: N70R1, L72R1, L73R1 and K100R1. A mutation to tryptophan was chosen because this is the amino acid with the bulkiest hydrophobic side chain. This means that, if the spin label acted by sterically hindering the penetration of annular lipids inside the nano – pockets due to its relatively flexible and bulky structure, the same effect could possibly be achieved by substituting it with the side chain of a tryptophan, which has similar physical and chemical characteristics. The 4 EPR – reporter mutants were chosen because of the good quality PELDOR data acquired for the single cysteine mutants, the parts of the protein where they are found (spanning the whole length of the important TM2 helix but without being too close to, and thus possibly interacting with, the nano – pockets and their entrance) and the fact that their single – cysteine distance distributions between the detergent – solubilized and bilayer – reconstituted samples did not show any significant differences, while at the same time they were in agreement with what expected from the in silico modelling. In addition a second tryptophan mutation, F88W, which is adjacent to the important L89 residue but is not expected to have any effect on the channel's conformation, was paired with K100R1 in order to be used as a control.

All five W – C double mutants (L89W- N70R1, L89W – L72R1, L89W – L73R1, L89W – K100R1 and F88W – K100R1) were purified as for the WT and they all eluted as

single homogeneous peaks during size exclusion chromatography (Fig. 3. 13 a), without any problems arising. Afterwards, the PELDOR measurements that were conducted showed very little to no change in the distance distributions for 3 out of the 5 double W – C mutants. In the cases of L89W – N70R1 (Fig. 3. 13 b) and F88W – K100R1 (Fig. 3. 14 a), the distance distributions did not differ when compared to those of the single – cysteine, detergent – solubilized N70R1 and K100R1, while in the case of L89W – K100R1 a slight discrepancy could be observed when its distance distribution is compared to that of K100R1 (Fig. 3. 13 b).

Nevertheless, the differences observed are too small and subtle to be individually interpreted unequivocally as some form of a conformational change. However, a very strong and significant change could be observed in the case of the two remaining double W – C mutants, L89W – L72R1 and L89W – L73R1: for both mutants a shortening of the distances could be observed (Fig. 3. 13 b). In fact, the distance distributions of those two mutants shortened so much that the individual distance peaks could not be properly resolved through PELDOR measurements, which means that they became shorter than the technique's lower distance limit, which is approximately 18 – 20 Å. Such short distances at that part of the channel (i. e. the upper bilayer – leaflet side of the transmembrane part of the protein) could only possibly arise and be explained structurally due to a turn of the TM2 helix, capable of turning the two modified residues L72 and L73, so that they face the inside of the pore. Initially, when the channel is in its resting closed state, those two residues lie on the bilayer – associated transmembrane surface of the protein, which means that they face away from the pore's center. Very interestingly, such a rotation that brings amino acid residues at structurally equivalent positions facing towards the inside of the pore can also be observed in the MaMscL expanded state crystal structure. But the most important observation was that, when L89W – L72R1 and L89W – L73R1 were reconstituted in lipid bilayers (this time only nanodiscs), the effect was reversed and the distance distributions of the reconstituted double W – C mutants coincided once again with the ones of their respective single – cysteine mutant (fig 3. 13 b). Interestingly, in the case of L89W – L72R1, after reconstitution in nanodiscs the distance distribution is identical to the one predicted from the in silico modelling, and it does no longer display the separation of each of the two distances into a further two individual ones, resulting in a total of 4 separate distance peaks, as it was observed for L72R1.

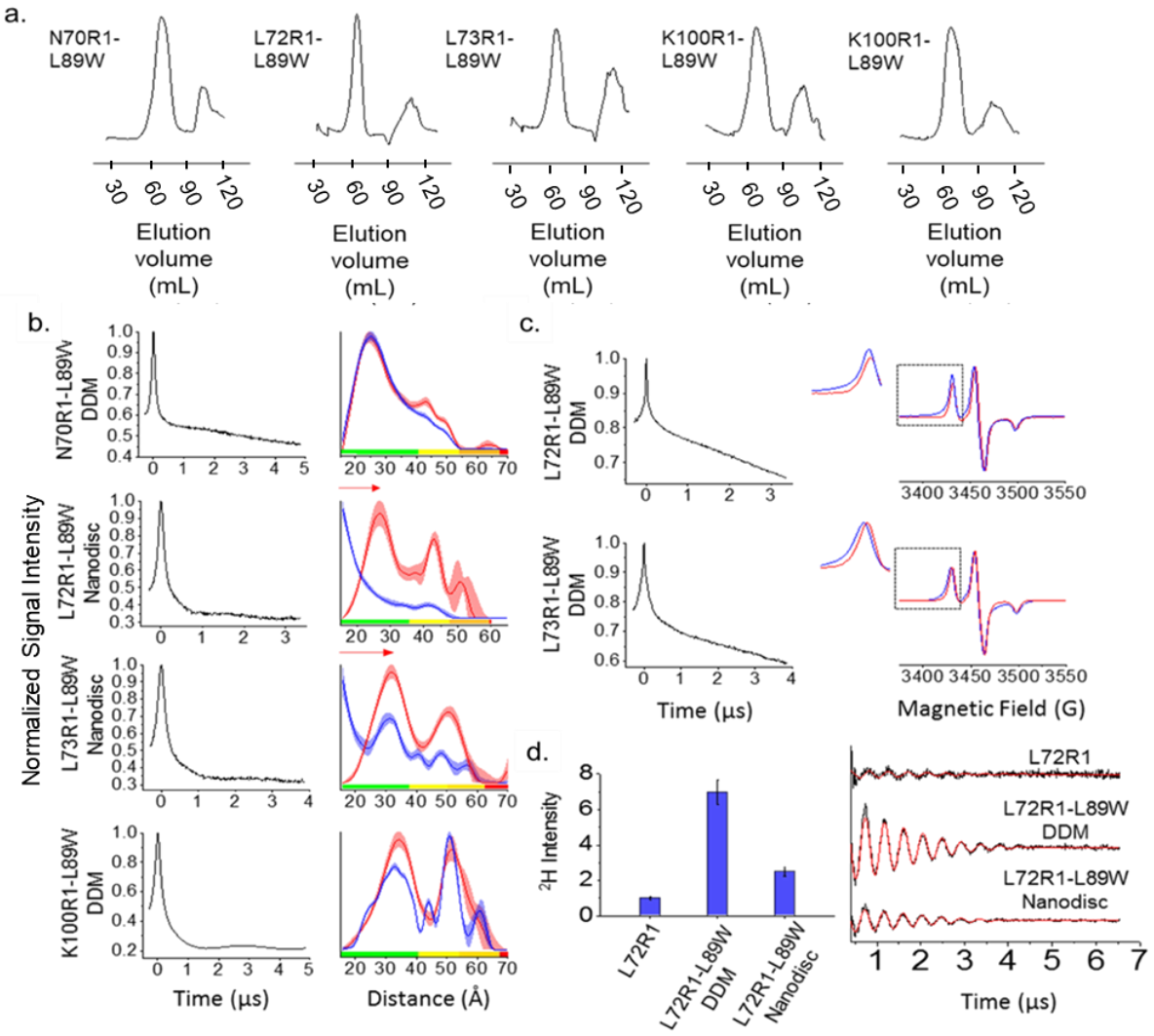

Fig 3. 13: a. SEC profiles of double TbMscL mutants. The main peak is the one at ≈65 mL. **b.** Left: Background corrected PELDOR time domain spectra of reconstituted double mutants. Right: Distance distributions of DDM - solubilized double mutants (blue shaded areas) compared to the same mutants in nanodiscs (red shaded areas). Coloured confidence intervals correspond to the measurement with the shortest time window (the reconstituted sample in all cases). **c.** Left: Raw time domain traces of the two double mutants that displayed very short distances. Right: Comparison of low – temperature CW – EPR spectra in detergent (blue line) and nanodisc (red line) of L89W – L72R1 (top) and L89W – L73R1 (bottom), displaying the characteristic line width broadening associated with dipolar interactions at very short distances. **d.** Left: D_2O accessibility of DDM – solubilised L72R1 and L89W – L72R1 and reconstituted L89W – L72R1, calculated by their 3 – pulse ESEEM ^2H nuclei coupling. Right: Background – corrected ^2H 3 – pulse ESEEM time domain spectra of the samples (black lines) and the simulated fitted functions (red lines) from which the error bars in the left hand panel arise. Figure adapted from Kapsalis *et al., Nat Commun*, 2019.

This observation could possibly support the argument that the original multiple distances exhibited by L72R1 were indeed a result of the spin label adopting two distinct conformations, which arise due to some form of steric hindrance of the modification site by detergent molecules, endogenous co – extracted lipids, or potentially both of them. With the simultaneous presence of the disruptive tryptophan mutant L89W, the L72C cysteine residue faces the inside of the pore rather than the transmembrane surface of the protein. Hence, the spin – labelling disruptions are no longer present and the spin label adopts one homogeneous conformation. When the channel reverts to its original closed state, the R1 side chain's conformer population remains homogeneous (since the spin label is already present) and the distance distribution is no longer "fractured", resembling the one expected from the in silico labelling procedure which does not take into account detergent and lipid molecules that surround the protein.

Unlikely as it may be, there is still a possibility that a change in the distance distributions such as the one observed for L89W – L72R1 and L89W – L73R1 could also arise from the unfolding and / or dissociation of the protein. In order to completely rule out this possibility, these two mutants were also investigated with low temperature (80 K) CW – EPR, and the spectra acquired for the detergent – solubilized samples were compared to those of the respective bilayer reconstituted ones (Fig. 3. 13 c). When compared to the reconstituted ones, the detergent samples of both mutants displayed the characteristic line – width broadening of the spectrum which is associated with close dipolar interactions between paramagnetic centers at very short distances of ≤ 15 Å. The only way that the spin labels attached to the cysteines of those two mutants, L72C and L73C, could end up being so close to each other is if the TM2 helix rotated adequately so that those two residues found themselves facing the inside of the channel's pore. Moreover, in order to further verify the structural stability of the protein, one of the samples of interest, namely L89W – L72R1, as well as a sample to be used as control, E102R1, were thawed, removed from the PELDOR measuring tubes and subjected once again to size exclusion chromatography. Both mutants eluted as well – folded pentamers (Fig. 3. 14 b), which minimizes the possibility that the short distances measured for the two double W – C mutants L89W – L72R1 and L89W – L73R1 could be a result of protein unfolding or denaturation.

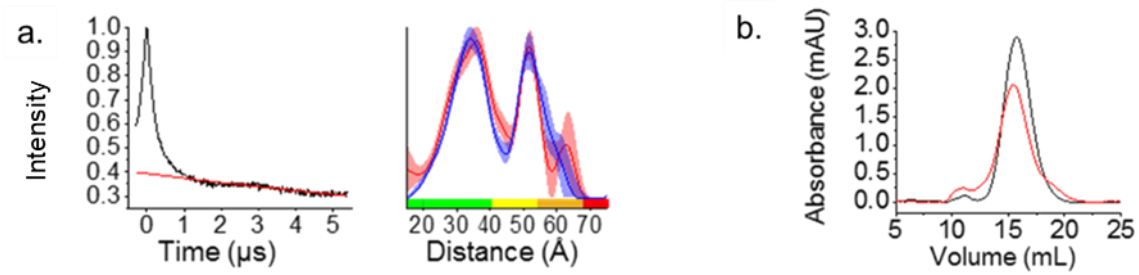

Fig 3. 14: a. Left: Uncorrected time domain PELDOR trace of F88W – K100R1 (black) and the background function (red). Right: Distance distribution of F88W – K100R1 (red shaded area) compared to that of single cysteine K100R1 (blue shaded area). **b.** Size exclusion chromatography profiles of L89W – L72R1 (black) and E102R1 (red, control) after thawing their respective PELDOR samples. Figure adapted from Kapsalis *et al., Nat Commun*, 2019.

The structural changes observed through PELDOR were also further supported by 3- pulse ESEEM measurements, which are capable of providing us with important information regarding the solvent accessibility of individual modified mutants. Indeed, the most buried of all single – cysteine mutants L72R1 (Fig. 3. 10), becomes highly accessible to the buffer upon the introduction of the disruptive L89W mutation (Fig. 3. 13 d). Once again, the effect that L89W has on the properties of L72R1 is reversed when the channel is reconstituted in a lipid bilayer (Fig. 3. 13 d). This means that the incapability of the acyl chains to penetrate the channel's nano – pockets, caused by the tryptophan side chains that block their entrance, promotes a conformational change (at least at the top bilayer – leaflet part of the TM2 helix that is probed here) that results in a drastic increase in the solvent exposure of that part of the protein. Such a change in solvent accessibility is very consistent with a rotation of the helix that brings those residues inside the buffer – filled pore of the channel.

Overall, when combined, PELDOR, 3 – pulse ESEEM and low temperature CW – EPR data indicate that the state of the L89W TbMscL in detergent solution closely resembles that of L89R1 TbMscL, with both mutations hindering lipid acyl chain penetration of the channel's nano – pockets. Especially the data acquired regarding double W – C mutants L89W – L72R1 and L89W – L73R1 point towards a conformational change that includes a TM2 helix rotation, at least partially at its top part. Interestingly, such a conformational change with an anti – clockwise rotation of the TM2 helix can be observed by comparing the crystal structures of the closed and expanded states of MaMscL (Fig. 3. 15 a). Unfortunately, due to the relatively low resolution of the expanded state, the equivalent residues between TbMscL and MaMscL, as predicted by their amino acid sequences, cannot be seen on that crystal structure. Nevertheless, "structurally" equivalent residues, which means that they are (a) found at the equivalent part of the protein, and (b) they have a similar

orientation, can be found on MaMscL and, at least for the purpose of this comparison, they are more descriptive than the sequence equivalents.

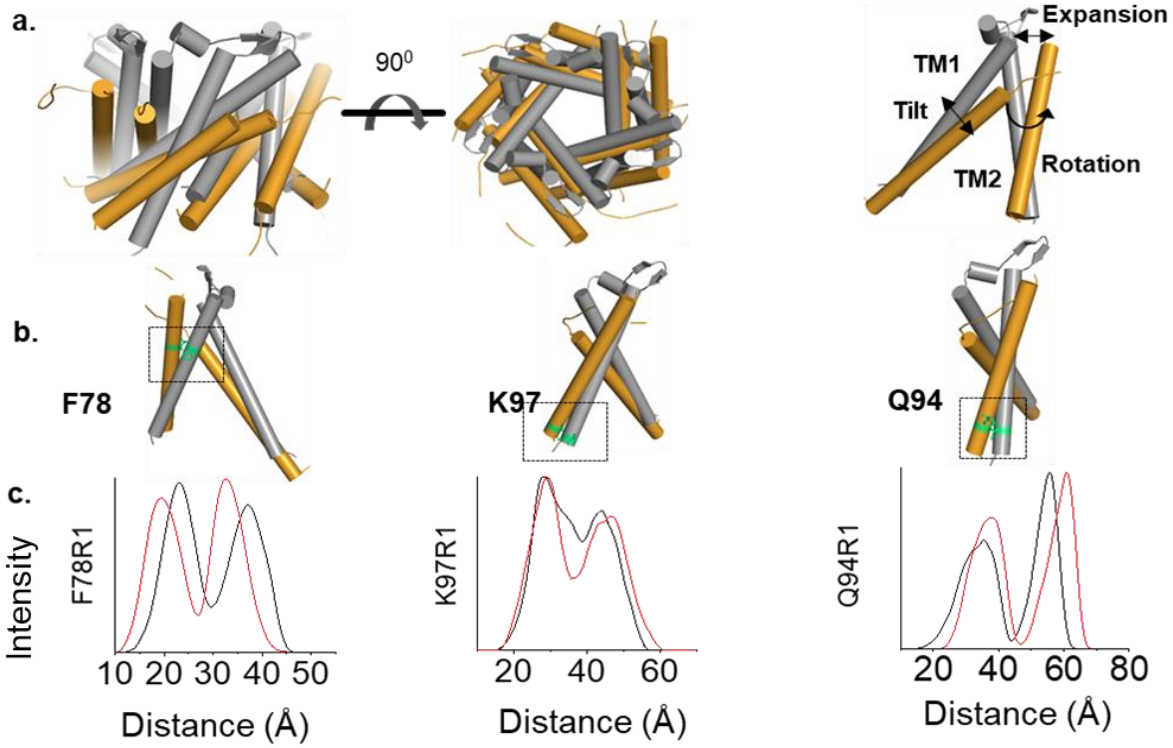

Fig 3. 15: a. Left: Side and top view of MaMscL in its closed (gray) and expanded (orange) state. Right: TM helices' movements between the two states shown in a monomer of the protein. **b.** The sites of the three equivalent residues (F78, K97 and Q94, shown in green) on both the closed (gray) and expanded (orange) states. **c.** Comparison of the distance distributions of the three residues in the closed (black) and expanded (red) states of MaMscL, as simulated with MTSSLWizard. Figure adapted from Kapsalis *et al., Nat Commun*, 2019.

Thus, MaMscL residue F78 was selected as the structural equivalent of TbMscL residues L72 and L73, and MaMscL residues Q94 and K97 were picked as the structural equivalents of TbMscL residue K100 (Fig. 3. 15 b). Those MaMscL residues were spin – labelled *in silico* and their distance distributions were simulated in the close and expanded state (Fig. 3. 15 c). Finally, their differences were compared to the experimental differences observed in the PELDOR distance distributions obtained for their structurally equivalent TbMscL residues. For MaMscL, upon expansion, the distances of F78R1 become shorter, which is the case of its equivalent TbMscL mutants L72R1 and L73R1. In the case of TbMscL mutant K100R1, only a small and subtle difference could be observed upon expansion (in

the case of L89W – K100R1), and this is more or less the same for the two equivalent MaMscL residues Q94 and K97. The above comparisons demonstrate that the transition we observe for TbMscL upon expansion seems to closely resemble the one observed through the crystal structures of its MaMscL orthologue.

3. 2. 6. The effect of the nano – pocket entrance modifications on TbMscL's function

So far it has been established that mutations and modifications of residue L89, which lies right at the entrance of TbMscL's nano – pockets, cause the channel to change its structural state and possibly adopt a more expanded conformation that would potentially be more prone to gating. But in order for the effect this altered expanded state has on the channel's function and activation to be elucidated, single molecule electrophysiology experiments had to be performed. Such experiments would allow us to monitor changes in the activation threshold of TbMscL upon introduction of the L89R1 and / or L89W mutations and modifications, by measuring the electrical currents that can pass through the pore of a single TbMscL molecule and, hence, its single – channel conductance. Two different single – molecule electrophysiology techniques were used: planar lipid bilayer electrophysiology and patch – clamp electrophysiology. The former has been recently successfully utilized for the investigation of the effect specific lipids (namely, lyso phosphatidyl choline) have on MscS[128], while the latter is the state – of – the – art technique for the identification and characterization of mechanosensitive ion channels in general, and it has been heavily used for the investigation of the functional properties of MscL in particular[64, 95, 104, 195, 199].

For planar lipid bilayer electrophysiology experiments, the channel is reconstituted inside a flat bilayer of relatively small surface, somewhat resembling a nanodisc, and each side of the bilayer comes in contact with a reservoir that contains the appropriate buffer system of choice. This technique is ideal for ligand- or voltage-gated channels, since (a) the appropriate ligands or other chemicals (e. g. lyso phosphatidyl choline, as mentioned before for MscS) can be selectively added on either the cytosolic or periplasmic side of the bilayer and the channel, and (b) the applied voltage can be easily changed at will. No external pressure can be applied, which means that the bilayer's tension cannot be altered and it is very stable. This may seem counter – intuitive in the case of a solely mechanosensitive channel such as MscL but, in reality, it could provide us with important insight regarding the resting state of the L89R1 mutant in physiological conditions. As described before, PELDOR measurements revealed that reconstitution in lipid bilayers forces the L89W and L89R1 mutants to revert to the closed state. Nevertheless, PELDOR measurements are conducted at very low temperatures (50 K in our case) and, thus, it is not known whether such a response (the mutant channel closing upon reconstitution) is still relevant in conditions resembling the physiological ones and, also importantly, in real

time. In addition, PELDOR and EPR techniques in general are ensemble techniques, where the average behavior of a large number of individual channel molecules is observed, while planar lipid bilayer, as well as patch – clamp, electrophysiology are single – molecule techniques that allow the probing of one protein at a time.

Hence, the planar lipid bilayer electrophysiology experiments conducted here were fairly "passive": the channel was incorporated inside the bilayer and then its function was monitored, without the application of any external stimuli. Both the wild type protein and the L89R1 modified mutant were used for the measurements, which were all conducted at room temperature. In the case of both samples, only some very rare opening could be observed under the experimental conditions used, with the activity presented being relatively similar to that exhibited by the first, low sub – conducting state(s) of the activation of EcMscL[200]. Such low conducting functional states are consistent with spontaneous opening that has previously been described in the absence of any form of externally applied pressure for both MscL and MscS[106, 128]. Once incorporation of the channel in the planar lipid bilayer was verified, the channel's activity was monitored at an applied voltage of + 30 mV for 15 consecutive minutes. Four independent measurements were performed for each sample (wild type and L89R1) from two independent preparations, with the results being very similar for both of them: 1 out of the 4 traces for wild type and L89R1 displayed any kind of spontaneous channel activity (Fig. 3. 16 a), while the other 3 out of 4 for each did not show any form of activity at + 30 mV (Fig. 3. 16 b). The conductance calculated for both channels was very similar and ≈ 70 pS (Fig. 3. 16 c). However, due to the overall probability of an open conformation for both channels was very close to zero (0.01 ± 0.008 % for L89R1 and 0.07 ± 0.059 % for the wild type TbMscL), the calculation of their conductance is not very reliable. Open probability (P_o) was calculated as the time during which the channel was conducting (t_O) divided by the total time of measurement (t_t), $P_o = t_o / t_t$.

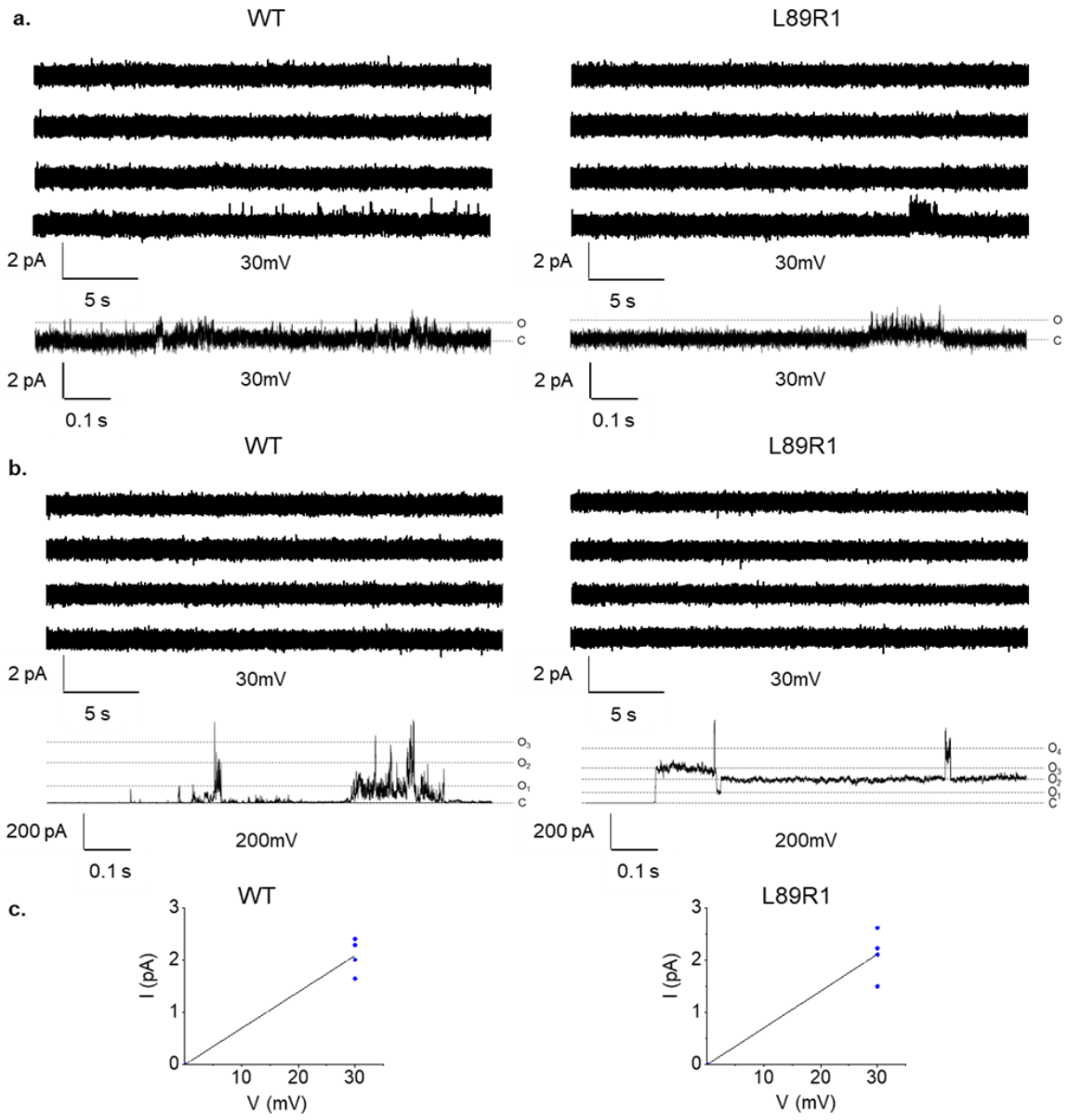

Fig 3. 16: Representative planar lipid bilayer recordings of WT (left) and L89R1 (right) TbMscL. **a.** 2 consecutive minutes of recording showing low levels of spontaneous activity (30mV, 1 out of 4 15-min recordings for each channel). Bottom traces show channel activity in an expanded timescale. **b.** 2 consecutive minutes of recording showing no activity (3 out of 4 recordings for each channel). Bottom traces show representative activity at +200mV applied at the end of each trace to verify that channels remained incorporated in the bilayer throughout the recording. **c.** Current-Voltage plots for WT and L89R1 TbMscL at +30mV.

After the verification of the resting state inside lipid bilayers being the closed conformation for wild type and L89R1 under physiological conditions, the next step was to investigate the effect that the L89 mutation and modification with MTSSL have on the channel's activation threshold and whether the structural changes observed through the PELDOR measurements are translated into an increase in the channel's functionality as well. The ideal technique for this to be probed is patch – clamp electrophysiology. For the purpose of these experiments, the channel first has to be reconstituted in giant unilamellar vesicles, similar to the liposomes prepared for PELDOR measurements but larger in size. Unilamellar vesicles of such large diameter ensure that there is enough surface for the patch pipette, through which the negative pressure is applied, to attach to the vesicle. The negative pressure, or suction, applied on the giant liposome simulates the lateral tension of the bilayer experienced by a mechanosensitive channel during an osmotic shock and, thus, forces the channel to open. The goal of these measurements (which were performed and analyzed at the University of Leeds by Dr Jonathan Lippiat) was to investigate whether the L89R1 and L89W mutant channels are more prone to gating, meaning that they are activated with the application of less negative pressure, when compared to the wild type. It is of interest to mention again that MscL is activated when the lytic tension threshold of the cell membrane is approached. EcMscL has been shown to be activated at such high pressure that liposomes tend to rupture before gating occurs, while at the same time TbMscL's activation threshold is known to be almost double than that of EcMScL[108, 188].

The effect of the L89R1 modification on the channel function was obvious before even any application of negative pressure occurred. All patches containing a L89R1 channel (13 independent patches) exhibited, just by the attachment of the pressure pipette, background short electrical current bursts with a macroscopic conductance of 15.8 ± 2.3 nS. In cases where true single – channel openings could be resolved from the background current, they had a unitary conductance of 0.273 ± 0.039 nS (this was the case for 7 out of the 13 excised patches of L89R1) (Fig. 3. 17). The same effect was observed for the wild type channel too, but the measured average macroscopic conductance for it was only 1.68 ± 0.89 nS (4 independent patches). However, no spontaneous unitary single – channel openings could be resolved as in the case of L89R1. Upon application of negative pressure, single – channel openings were observed in 3 out of the 4 patches containing WT protein, with a conductance of 2.74 ± 0.10 nS. In order for this to happen, a pressure of at least -140 mm Hg had to be applied (Fig. 3. 17). In the case of L89R1, single – channel electrical currents similar to those observed for the wild type channel occurred in 4 out of the 13 patches, with a similar calculated conductance of 2.98 ± 0.07 nS, but this time the activation threshold was much lower, ranging from -30 mm Hg to -120 mm Hg (Fig. 3. 17). All results obtained were analyzed by Dr Jonathan Lippiat, at the University of Leeds.

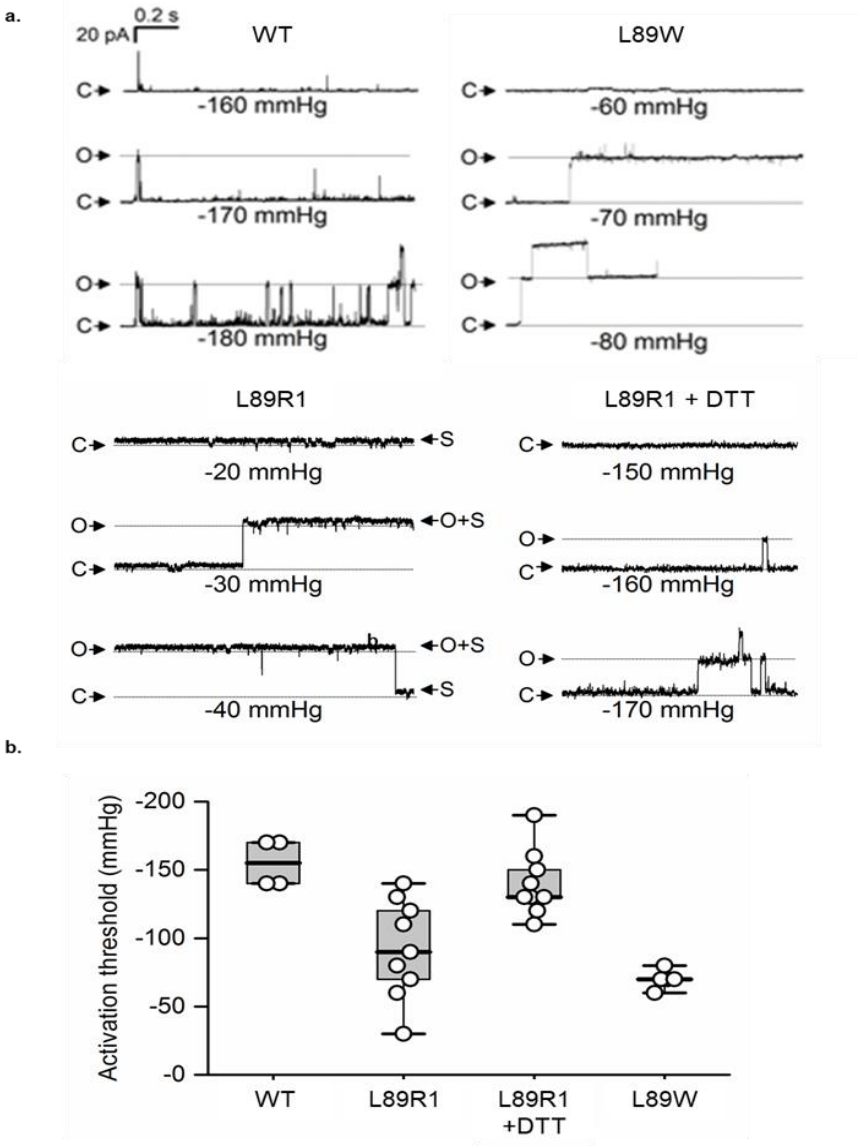

Fig 3. 17: a. Representative patch clamp recordings at 20 mV of WT, L89R1 (± DTT) and L89W TbMscL. Applied pressure is indicated below each trace and the measured current levels representing the closed ("C") and fully opened ("O", ≈ 60 pA for WT, L89R1 and L89W, ≈ 50 pA for L89R1 plus DTT) channels are also shown. Channels opening to a sub - conducting level ("S", approx. 5 pA) contribute to the traces in the case of L89R1. **b.** Threshold pressure values of full opening, applied at 10 mmHg intervals. Data points are individual measurements, bars show the full range of values, boxes represent 25 - to - 75 percentile range, and the horizontal line is the median. Samples are significantly different ($p < 0.001$, Kruskal-Wallis ANOVA), with 7/9 L89R1 and 5/5 L89W values below the median ($p < 0.005$, Moody Median test). All analysis and measurements were performed by Dr Jon Lippiat, University of Leeds. Figure adapted from Kapsalis *et al., Nat Commun*, 2019.

Furthermore, and since the increased activation sensitivity of L89R1 TbMscL compared to that of the wild type had been demonstrated, it was of interest to investigate whether it was the MTSSL modification that caused the modified mutant's increased functionality, or the cysteine mutation alone would suffice. With this question in mind, giant unilamellar vesicles containing L89R1 were incubated with 5 mM DTT in order to reduce the mutant channels' cysteines and remove the spin labels. Subsequently, the measurements performed on the unmodified L89C channels (4 independent patches) resulted in a calculated mean channel conductance of 2.30 ± 0.17 nS, but this conductance was only achieved after the application of much higher negative pressure than the one needed for the activation of the modified L89R1 mutant, with pressure values ranging from -120 mm Hg to -190 mm Hg (Fig 3. 17). This is a very strong indication that it is the MTSSL modification, rather than the cysteine mutation itself, that causes the structurally expanded and functionally more sensitive state of TbMscL. Finally, the single L89W mutant was also tested with patch – clamp experiments. Similar to the L89R1 modified channel, patches containing the L89W mutant channel exhibited high background levels of electrical current before the application of any negative pressure, as well. In all 11 patches measured, single – channel closures occurred which allowed the calculation of the unitary conductance in the absence of pressure at 0.248 ± 0.022 nS (Fig. 3. 17), similar to the one calculated for L89R1. Due to the high spontaneous activity of the patches, the patch – clamp experiments were quite difficult to perform. Nevertheless, in 5 out of the 11 patches, application of negative pressure was successful and caused channel openings with a mean conductance of 2.43 ± 0.27 nS, with the applied pressure ranging between -60 mm Hg and -80 mm Hg (Fig. 3. 17).

In addition, patch – clamp measurements of wild type, L89R1 and L89W TbMscL were also attempted in giant *E. coli* spheroplasts. Spheroplasts are, in essence, swollen *E. coli* cells that are devoid of their protective cell wall, being thus enclosed only by their inner membrane, which leaves the mechanosensitive channels embedded in it exposed to the pressure pipette used for the patch – clamp electrophysiology experiments. Their preparation is initiated by restricting the *E. coli* cells at some point during their growth from being able to produce their cell wall during cell division. This causes them to fuse into elongated, snake – like formations that share a common external cell wall. Subsequent treatment of these snakes with lysozyme causes the digestion of the common cell wall and the final formation of swollen *E. coli* cells that are devoid of their outer membranes. Preparation of *E. coli* spheroplasts large enough to be used in patch – clamp experiments is quite tricky and demanding. Nevertheless, such giant *E. coli* spheroplasts with the wild type TbMscL overexpressed and embedded in their inner membrane were successfully

produced (Appendix, Section B) and patch – clamp electrophysiology measurements were attempted on them. However, partly due to the very high activation threshold of the channel, the attempts were not successful in yielding any measurable and meaningful results.

Despite that, the results obtained from the patch – clamp electrophysiology measurements on giant unilamellar vesicles clearly demonstrated that the mutation and modification of residue L89 which lies at the entrance of TbMscL's nano – pockets has a direct effect, not only on the channel structure, but on its function as well. Both L89R1 and L89W are shown to be activated at much lower pressure thresholds compared to the wild type protein, which means that they are much more sensitive to the bilayer's lateral tension. Moreover, in the case of L89R1, it has been demonstrated that it is the MTSSL modification, rather than the cysteine mutation alone, that increases the channel gating sensitivity, since the reduced L89C mutant channel seems to be activated at applied negative pressure with values similar to that needed for the activation of the wild type protein.

3. 2. 7. Investigation of other modes that could trigger TbMscL's expansion

3. 3. Discussion and conclusions

It has been clearly demonstrated that the principles of the “lipid moves first” model for the mechanical activation of mechanosensitive ion channels do apply and describe TbMscL’s gating mechanism. Hindering the penetration of lipid acyl chains inside the channel’s nano – pockets through the mutation and modification of a residue that lies right at their entrance is sufficient to cause a conformational change in the protein structure. Equally interesting, the initial hypothesis that, if such a conformational change is indeed caused by the hindrance of the protein – lipid interactions (as they are dictated by the “lipid moves first” model), it would be reversible upon reconstitution of the channel in a lipid bilayer, has also been shown to be valid. The lateral compression exerted on the transmembrane part of the channel from the surrounding bilayer, and the fact that such a compression could cause the lipid acyl chains to enter the nano – pockets once again, forces TbMscL to revert back to its original closed state when it finds itself inside an artificial membrane. Furthermore, neither cysteine mutations and MTSSL modifications on other parts of the protein’s structure (covering most of the protein’s length), nor the neutralization of the positively charged amino acid clusters on the channel that act as binding spots for negatively charged lipid head groups, nor the introduction of high positive charge density right at the constriction site of TbMscL’s pore, were proven to be sufficient to cause a conformational change and the activation of the channel. This clearly showcases the high importance of the nano – pockets in the channel’s gating mechanism (Fig. 3. 23). The big question that remains is, thus, why are those nano – pockets so important? And how exactly are the voids that are created inside the nano - pockets during extreme lateral tension associated with and translated into the opening of the channel’s pore?

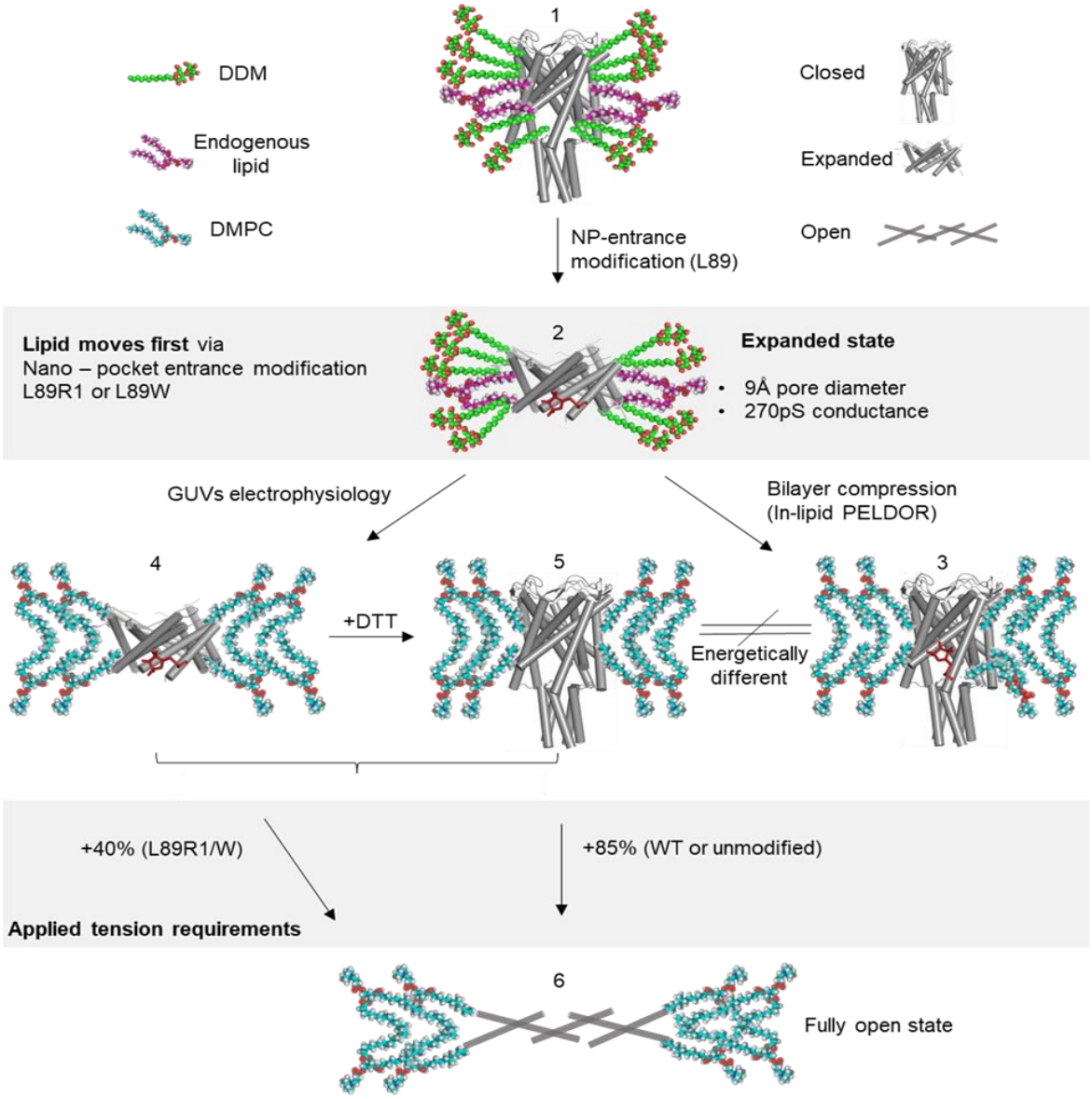

Fig 3. 23: The proposed mechanism of TbMscL's expansion and activation after modification of the nano – pockets' entrance. Upon the introduction of the modification the channel adopts an expanded state but it reverts to its closed one upon reconstitution in a lipid bilayer, as witnessed through PELDOR measurements. Nevertheless, the modified and wild type closed states do not have the same tension requirements for opening, because they are not energetically equivalent; the former gates more easily during patch – clamp electrophysiology experiments. The stored free energy of L89R1/W, due to hindrance of lipid chain access to the nano – pockets, is significantly increased. Thus, TbMscL L89R1/W acts as a Jack – in – the – box, with the box being the surrounding bilayer and its lateral compression. Figure adapted from Kapsalis *et al., Nat Commun*, 2019.

The answer to this question may lie in the combination of the accommodation of lipid acyl chains in the nano – pockets, their acyl chain – capacity, and the stored elastic energy within the structure of each individual mechanosensitive channel. In this case, the term “stored elastic energy” is used as an umbrella term that includes the accumulated, stored energy that is a result of all complex interactions (hydrophobic interactions inside the protein and between the protein and the annular lipids, hydrophobic mismatch between charged amino acid residues in the transmembrane part of the protein and the bilayer etc.). Such interactions have been shown to have a very important contribution in the free energy of membrane proteins and especially their transmembrane parts[201, 202], and stored elastic energy has already been proposed to be implicated in the gating mechanism of mechanosensitive channels in a study where MscS is very accurately likened to a “Jack – in – the – box”, and this channel might be the best example to demonstrate the importance of the bilayer’s lateral pressure and stored elastic energy[203]. This is because in the case of MscL, which is the most stiff and hardest to open mechanosensitive channel, all crystal structures (with the exception of the expanded MaMscL structure) obtained show it to be in its closed state (which means that it is not only the lateral compression of the bilayer that keeps the channel closed) and they are not of high enough resolution to reveal the acyl chains that occupy the nano – pockets (hence, their function and capacity are not obvious). On the other hand, MscS has a much lower activation pressure – threshold and an important result of this fact is that, according to biophysical experiments on the channel in detergent solution and most of its crystal structures[128, 142, 151, 196, 204], the channel normally adopts an expanded (if not completely open) conformation when it is not embedded in a lipid bilayer. This could be explained as such: for MscS, unlike MscL, the mere removal of the lateral compression exerted from the lipid bilayer on the channel is enough to allow MscS to adopt an expanded conformation, hence the comparison of it to a Jack – in – the – box. This seems to imply that the most energetically favorable, relaxed, “ground” state of the channel is the expanded one and the transition from the closed state to this ground state is achieved by the release of the stored elastic energy upon removal of the surrounding lipid bilayer. This has never been shown to be the case with the wild type MscL, which remains closed inside lipid bilayers or removed from them. The L89R1 TbMscL mutant though, as clearly demonstrated here, does display an identical behaviour: it adopts an expanded state in detergent solution but reverts to the closed one when compressed by the lipid bilayer. This means that the tryptophan mutation and the R1 mutation and modification of L89 of TbMscL alone is sufficient to increase the stored elastic energy, or free energy, adequately enough, so that the channel’s ground state is no longer closed, but rather an expanded conformation. According to the definition of this stored energy as given before, the question that arises from this, is whether the mode of action of these mutations and

modifications is through an increase in the hydrophobic mismatch between the protein and lipids or through steric hindrance of acyl chain penetration in the nano – pockets. And, if it is the latter, why does it play such an important role?

As observed in the patch – clamp electrophysiology experiments, despite cysteines being relatively polar amino acids, the cysteine mutation alone is not enough to lower the pressure activation threshold of TbMscL. The modification with MTSSL, which is of similar polarity to the cysteine but more bulky and flexible, is needed for the increase in the channel's gating sensitivity. Moreover, the mutation of L89 to a tryptophan has similar (or even more pronounced) effect on the protein function to that of L89R1, but tryptophans are hydrophobic amino acids, and certainly more hydrophobic than the cysteine or the R1 modification. They do, though, have a bulky and relatively flexible side chain. This suggests that the increased activation sensitivity is probably a result of the steric clash between bulky side chains and annular lipids, which does not allow the acyl chains of the latter to enter the nano – pockets, rather than the result of increased hydrophobic mismatch. Nevertheless, what needs to be explained is how does the inability of lipid acyl chains to penetrate the nano – pockets affect and increase the stored free energy of the channel enough, in order to shift its ground state from the closed to the expanded conformation.

The easiest and most logical explanation, taking into account the data presented here as well as pieces of evidence regarding other mechanosensitive channels, is that some form of hydrophobic mismatch still plays a role, but instead of the bulk of the channel's transmembrane surface, it manifests mainly inside the nano – pockets. By default, as shown in the crystal structures, the closed state of MscL (as well as those of other mechanosensitive channels) is characterized by crevices in the transmembrane part of the protein that are lined by hydrophobic amino acid residues. In high – resolution structures of MscS in both the open and closed state, those crevices have been shown to be occupied by acyl chains. But, very importantly, the number of acyl chains per nano – pocket differs between conformations: in the closed state they are penetrated by two acyl chains each[205], while in the open state only by one[128]. In the open state though, the space that was occupied by the second acyl chain does not remain empty, as this would be highly energetically unfavorable. Rather, the protein has adapted its conformation in order to fill up the void that was created. But structures are only snapshots of the protein in its different states and, while they can demonstrate correlation between the existence or absence of one acyl chain and the conformational state of MscS, they cannot demonstrate causation. If judged only by this, the mechanism could as easily work the other way around, especially in the case of MscS where removal of the lateral pressure of the bilayer alone allows the channel to open: the protein opens its pore by altering its state and the conformational change is what forces the acyl chain out of the nano – pocket.

Here lies the importance of investigating this phenomenon on MscL. A relationship of a one – way causation, rather than mere correlation, between nano – pocket penetration by acyl chains and the channel's expanded state, is described by the data presented here. As shown by the L89C electrophysiology data, the mutation on its own does not affect the protein's function, thus it is not possible that an initial step of a conformational change forces the acyl chains out of the nano – pockets. Thus, it must be the other way around: the acyl chains' inability to enter the nano – pockets forces the channel to alter its conformation and expand, in order to fill up the void. Furthermore, it looks like the placement of the nano – pockets, which can be found only on the lower and not on the upper bilayer leaflet side of the transmembrane part of the protein, is not by chance. There seems to be some form of "rational design" behind their placement on the protein structure: the acute - pressure point of the nano – pocket lies right behind the constriction site of the pore (residue L17 is on the constriction site of the pore and its adjacent residue A18 lies at the very bottom / end of the nano – pocket) and those two very crucial regions for the protein function are separated in space just by one or two residues. Hence, it looks as if the lipid acyl chains, through full penetration of the nano – pockets, "push" the constriction of the pore, keeping it closed. Parallels can be drawn between this observation and the way lipid acyl chains bind to eukaryotic K2P channels: the acyl chain fully penetrates the channel's nano – pockets and end up physically blocking the pore conduction pathway themselves[145]. This is probably the reason why, despite being potassium – dependent channels, they still need application of the bilayer lateral tension for their activation[206]: the lipid acyl chains need to be mechanically pulled away from the pore.

According to the discussion so far, it becomes obvious that the gating mechanism of mechanosensitive ion channels is more "mechanical" / "physical" and less "biochemical" than for most other proteins and channels. In addition, individual annular lipids, and especially their acyl chains, seem to play a much more complicated and multimodal role than what was expected and theorized until now. Nevertheless, and regardless of the underlying mechanism, the data presented here clearly demonstrate that the obstruction of TbMscL nano – pocket's entrance causes a conformational change in the channel. Furthermore, this conformational change is not restricted to the area in and around the nano – pockets but it is propagated at least through the top part of the TM2 helix, as demonstrated by the very short distances observed in the distance distributions of double W – C mutants L89W – L72R1 and L89W – L73R1. The appearance of such short distances is compatible with a rotation of helix TM2, which brings the two EPR reporter modified residues facing the inside of the pore (Fig. 3. 24 a). A simultaneous expansion of the pore is also highly possible, but cannot be unequivocally demonstrated by the data acquired. Such a move of the TM2 helix would be consistent with the activation mechanism as it can be implied by the closed and expanded crystal structures of the MaMscL orthologue. A comparison with them also allows us to explain the very small

difference observed in the distance distributions between K100R1 and L89W – K100R1, as the same behaviour is observed at the bottom of MaMscL TM2 helix. Moreover, a rotation of the helix can also explain the case of L89W – N70R1, where the distance distribution remains almost identical to that of the single – cysteine mutant N70R1: an appropriate angle of symmetric rotation among the TM2 helices of all of TbMscL subunits is certainly capable of bringing residue N70R1 at a place where, while its absolute position has changed, the relative position, and thus the distance, between those residues from different subunits remains the same (Fig. 3. 24 b). Furthermore, through simplified calculations (which, in the site of the pore's restriction, take only a symmetric expansion into account) that make use of the experimentally acquired (for the expanded state) and the *in silico* modelled (for the closed state) distances of TbMscL L89R1, the diameter of the channel's pore in the expanded state can be estimated as ≈ 9 Å[177]. Since the diameter of the pore in TbMscL closed state is approximately 4 Å, the net increase in the pore diameter caused by this conformational change can be calculated as ≈ 5 Å. This is another similarity between TbMscL and MaMscL, since a similar pore opening can be measured in the expanded structure of the latter. A pore opening of ≈ 9 Å should be sufficient to allow small substances, such as small hydrated ions, to pass through the pore. Despite that fact, the expanded MaMscL state is thought to not be conductive, but this might be a result of fusing the full length MaMscL with a pentameric soluble protein through the former's C – terminus, which is the end closest to the pore[117].

As mentioned earlier, the way through which the expanded MaMscL crystals were formed remained unclear to the authors of the study[117]. All methods of the protein purification procedure were identical to the ones followed for the acquisition of the closed MaMscL crystals, so obtaining crystals of the channel in two different conformations was surprising and difficult to explain. The only difference that can be identified is the different crystallization conditions through which each of the crystals developed. Since through the present study an expanded state of TbMscL has been provoked through controlled experiments that were designed to cause this, and since this state seems to strongly resemble the expanded state of MaMscL, it is possible that the findings of that study could be explained by analogy to the experimental design and conditions presented here. The striking features of the crystallization procedure of the expanded state, when compared to those of the closed one, are: the long time it took for the expanded MaMscL crystals to form (5 months vs 1 week for the closed crystals) and the presence of $(NH_4)_2SO_4$ in its crystallization condition[117]. $(NH_4)_2SO_4$ can catalyze the degradation of lipids and, in addition, over such a long period of time, lipids can spontaneously hydrolyze on their own. It is, thus, possible that MaMscL's expanded state was, by pure coincidence, obtained through the same mode of action that was, on purpose and by experimental design,

applied in this study in order to provoke TbMscL's expansion: through depletion of the lipid acyl chains from the channel nano – pockets.

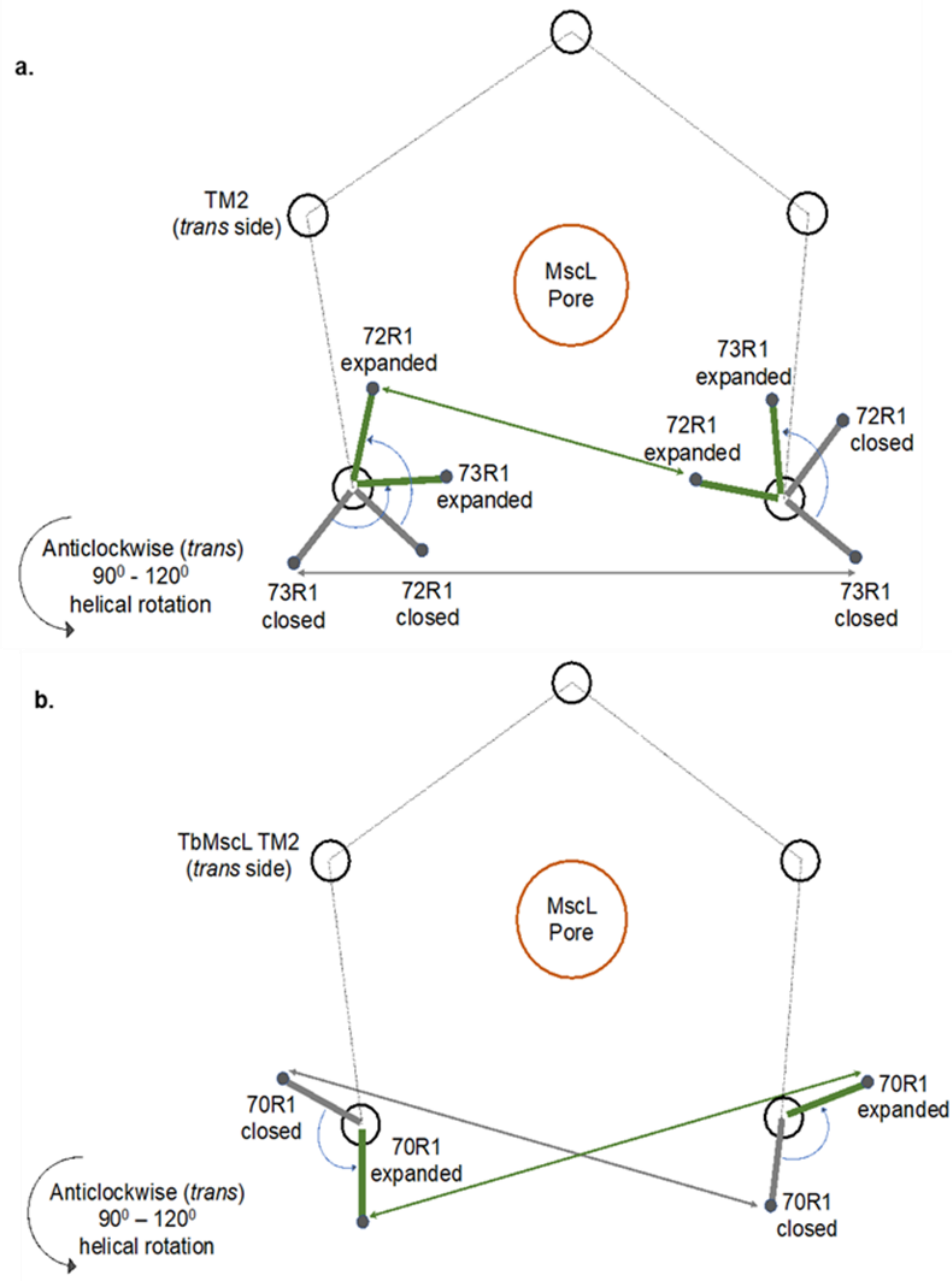

Fig 3. 24: a. A rotation angle of 90 – 120º of the top (trans) part of the TM2 would bring residues L72 and L73 inside the pore, which explains the short PELDOR distances. **b.** A similar rotation angle value would force residues N70 to move to such relative positions so that the absolute distance between them remains the same, again explaining the PELDOR data. Figure taken from Kapsalis *et al., Nat Comm*, 2019.

Overall, here it has been demonstrated that hindrance of the penetration of lipid acyl chains inside a mechanosensitive ion channel's nano – pockets is an important step of its gating mechanism, which causes the activation of the channel and forces it to adopt an expanded state. This finding sheds light on the mechanism of mechanosensation itself and can pave the way for further in – depth investigation of mechanosensation in general and of MscL in particular. Now that the "active site" of mechanosensitive ion channels has been unveiled, site – directed mutagenesis can be utilized for the careful rational design of mechanosensitive channels that exhibit specific traits, e. g. increased or reduced activation sensitivity, and which could be controlled at will and employed for specific nanotechnological and pharmacological applications. In addition, these attempts could be aided by the *de novo* synthesis and utilization of chemical molecules specifically designed to interact with the nano – pockets in various positive or negative ways. Finally, such approaches could also help completely elucidate the gating mechanism and the mode of action of mechanosensitive ion channels, which mediate one of the most widespread and primal cellular responses known in all kingdoms of life, mechanotransduction.

CHAPTER 5: OPTIMIZATION OF RECOMBINANT MEMBRANE PROTEIN OVEREXPRESSION IN ENGINEERED *E. COLI* STRAINS

5. 1. A brief introduction

Membrane proteins are abundantly found in living cells from all kingdoms of life[41] and play crucial roles in a large number of highly diverse physiological and pathological responses[222]. This makes membrane proteins extremely potent pharmacological targets and the research on drug development often focuses on them[223]. Hence, the close investigation and elucidation of the structure and function of this class of proteins is of high scientific importance. Generally, in order for a protein to be properly and thoroughly investigated, it needs to be isolated in a highly pure form and in relatively large quantities. While this can usually be achieved reasonably easily for water – soluble proteins, the successful overexpression of well – folded and functional recombinant membrane proteins in prokaryotic cells often proves to be much more challenging and problematic[44, 224]. The most common and significant problem faced is the aggregation of the overexpressed protein molecules in the host cell's cytoplasm, which not only leads to the production of non – usable protein, but also causes the death of the host cell[224]. This results in greatly reduced yields of the recombinant membrane protein, while it can also affect the proper folding and functionality of the protein produced, with the latter largely depending on the overexpression host organism and strain of choice[45]. Since the most widely used prokaryotic organism used for this purpose is *E. coli*[225], a number of *E. coli* strains, e. g. BL21 and C43, have been engineered with the sole purpose of being able to carry the burden of overexpressing recombinant membrane proteins effectively and efficiently. However, even in this case, the overexpression of "demanding" membrane proteins, e. g. eukaryotic ones, can still easily lead to the same kind of obstacles already mentioned[226-229].

Recently, a new set of *E. coli* strains, SuptoxD and SuptoxR, have been engineered, which have been shown to be capable of withstanding the cell toxicity induced by membrane protein overexpression and are simultaneously able to yield high levels of protein production[173]. This is achieved through the co – expression of single bacterial genes which encode proteins that act as suppressors of the aforementioned overexpression – induced cell toxicity[173]. Each of the two engineered *E. coli* strains co – expresses one toxicity – suppressing protein: SuptoxR co – expresses RraA, which is an inhibitor of the mRNA – degrading activity of the RNase E of *E. coli*[230], and SuptoxD co – expresses DjlA, which is a membrane – associated DnaK co – chaperone[231]. These strains have been shown to combine significantly increased final biomass levels (i. e. significantly higher cell survival

during overexpression) with greatly enhanced recombinant membrane protein yields[173, 232]. Hence, the purpose of the present project was to further investigate and, most importantly, optimize the cell growth and protein overexpression conditions for these two engineered *E. coli* strains, during large – scale protein production. For this purpose, two different membrane proteins were chosen, a prokaryotic (TbMscL) and a eukaryotic (the human bradykinin receptor 2, BR2, a G – protein coupled receptor) one[174].

5. 2. Experimental results

5. 2. 1. Overexpression of TbMscL in the engineered *E. coli* SuptoxR strain

E. coli SuptoxR (co – expressing RraA) and MC1061 (negative control, not expressing any toxicity – suppressing protein) cells were transformed with a pASK75 vector containing the 6 x His – tagged TbMscL F88C mutant gene. Cells were grown and both suppressor and membrane protein overexpression was induced as described in the Methods section 2. 2. 3. The protein was extracted from the cells, purified and spin – labelled as described in the Methods sections 2. 3. 1 and 2. 3. 2. Overexpression of TbMscL F88C in SuptoxR cells resulted in a greater than 10 – fold increase in protein yield compared to MC1061 cells (Fig. 5. 1 a). During size – exclusion chromatography, the maximum peak intensity for TbMscL F88C overexpressed in SuptoxR cells was ~ 5.40 mAU, while that of MC1061 cells only reached up to ~ 0.47 mAU (Fig. 5. 1 a). In both cases, but especially in the case of protein expressed in SuptoxR cells, the peak corresponding to pure TbMscL (at ~ 69 mL) is single, monodisperse and highly homogeneous. The calculated yield of protein from SuptoxR and MC1061 cells was 0.33 and 0.03 mg per L of culture, respectively. The protein purity was also assessed by SDS – PAGE (Fig. 5. 1 b), while the identity of the bands corresponding to TbMscL was also verified by mass spectrometry (Fig. 5. 1 c). In the SDS – PAGE gel, the existence of a double band at the expected molecular weight of the monomer is probably due to some form of degradation or proteolysis.

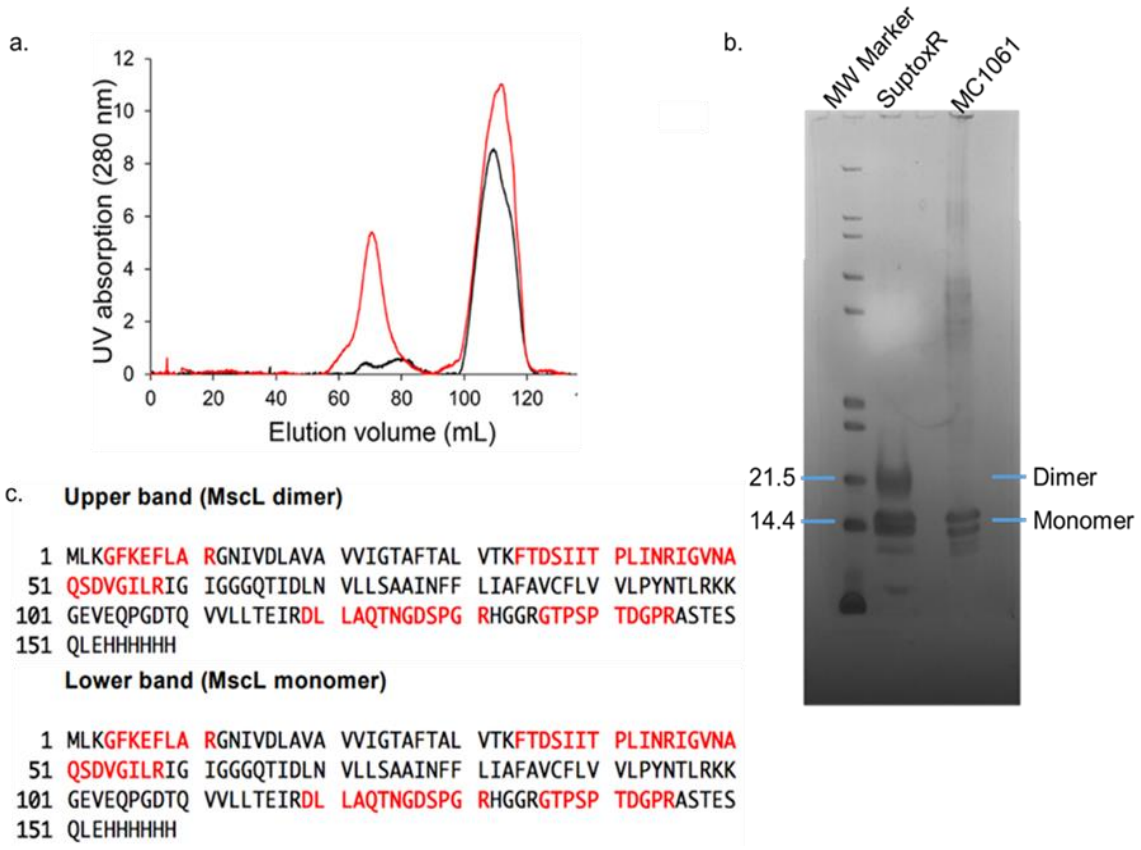

Fig. 5. 1: a. Size – exclusion chromatography profiles of TbMscL F88R1 expressed in MC1061 (black line) and SuptoxR (red line) cells. **b.** SDS – PAGE gel of the two TbMscL F88R1 samples. Bands corresponding to the protein monomer and dimer are visible. **c.** Mass – spectrometry data of the two TbMscL bands (denoted as monomer and dimer) visible in the SDS – PAGE gel, from the SuptoxR protein expression. Positively identified regions are highlighted in red.

Furthermore, in order to confirm that the protein was properly folded, the spin – labelled TbMscL F88R1 mutant was subjected to PELDOR measurements (Fig. 5. 2 a & b). Measurements were only performed on the labelled mutant overexpressed in SuptoxR cells, as the quantity of protein extracted from the MC1061 cells was not sufficient. As expected, the experimental distance distribution obtained for the SuptoxR – derived protein agrees very well with what was expected from the *in silico* spin labelling and distance modelling from the crystal structure with MTSSLWizard (Fig. 5. 2 c). This result strongly suggests that the protein obtained from the engineered strain is not only high in yield, but also properly folded.

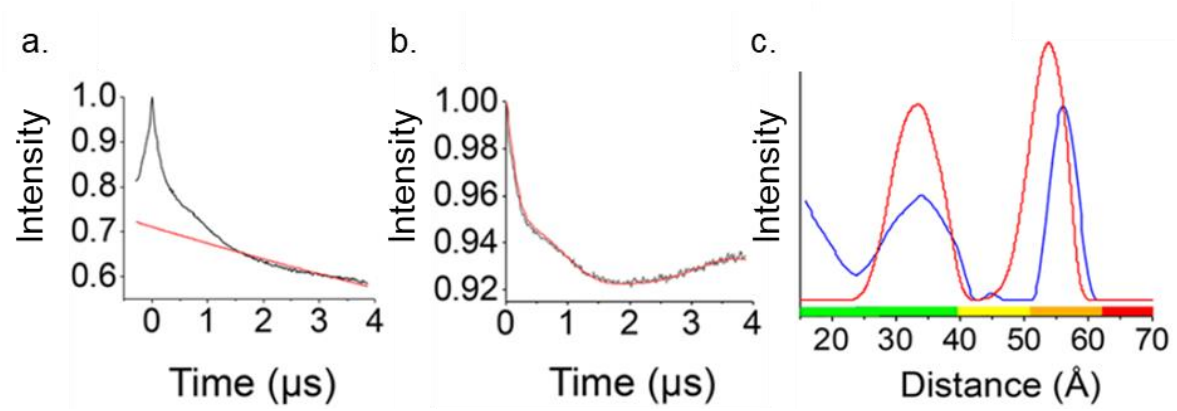

Fig. 5. 2: a. PELDOR time – domain raw data of TbMscL F88R1. **b.** Background – corrected data of TbMscL F88R1. **c.** Experimental distance distribution (blue line) is compared to the MTSSLWizard – modelled one (red line) . Figure adapted from Michou, M. *et al*, *ACS Synth. Biol.,* 2019.

5. 2. 2. Overexpression of BR2 in the engineered *E. coli* SuptoxD strain

E. coli SuptoxD (co – expressing DjlA) and MC1061 (negative control, not expressing any toxicity – suppressing protein) cells were transformed with a pASK75 vector containing the 6 x His – tagged WT BR2 gene. The protein was extracted from the cells using Fos – choline 14 as detergent. Contrary to the usual practice described in Chapters 3 and 4, at the end of the purification procedure the protein was subjected to 2 subsequent rounds of SEC. In the first one, the whole sample that was eluted from the IMAC column was used. In the second SEC, only the BR2 monomer peak of the 1st SEC round (denoted as 2 and 2* in Fig. 5. 3 b & c, respectively) was used. Similarly to TbMscL overexpressed in SuptoxR cells, overexpressing BR2 in SuptoxD cells resulted in a great increase, of approximately 14 – fold, in protein production compared to the MC1061 cells, with the yield for the former being ≈ 1 mg per L of culture. This can easily be seen in the 2nd size – exclusion chromatography profiles of the two proteins (Fig. 5. 3 a), where the maximum absorption peak intension for SuptoxD BR2 is ≈ 47.4 mAU, while that of MC1061 BR2 is only ≈ 3.5 mAU (Fig. 5. 3 a). In the 1st size – exclusion chromatography profiles, the peaks denoted as 1st possibly correspond to BR2 dimers, as the roughly estimated apparent molecular weight fits with the mass for the BR2 dimer (Fig. 5. 3 b & c).

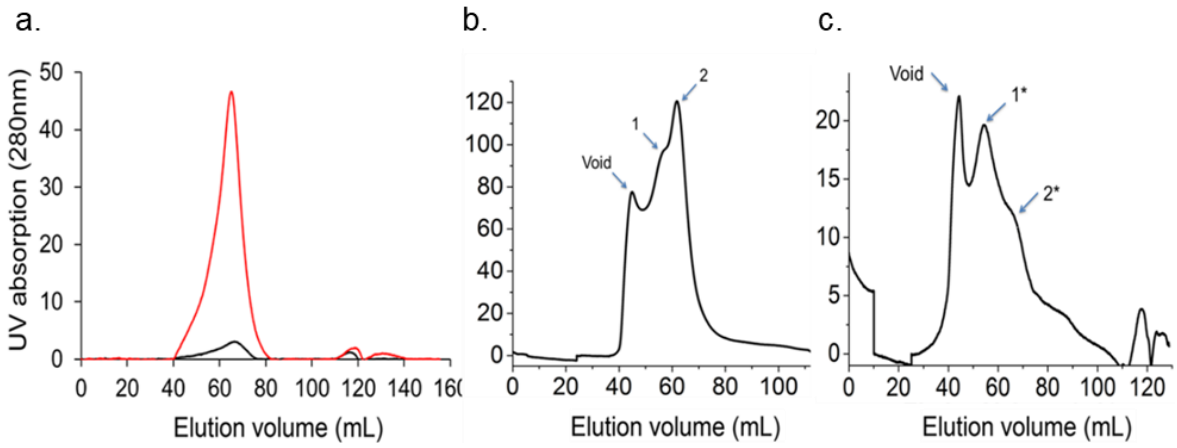

Fig. 5. 3: a. Comparison of the 2nd size – exclusion chromatography profiles of BR2 produced in MC1061 (black line) and SuptoxD (red line) cells. **b.** 1st size – exclusion chromatography profile of BR2 overexpressed in SuptoxD cells. **c.** 1st size – exclusion chromatography profile of BR2 overexpressed in MC1061 cells. In both cases, peak 1 is the putative dimer peak and peak 2 is the monomer peak. Figure adapted from Michou, M. *et al*, *ACS Synth. Biol.,* 2019.

In order to assess the purity of the protein in each case, the samples were subjected to SDS – PAGE gel electrophoresis, Western blotting and mass – spectrometry measurement after trypsin digestion (Fig. 5. 4). As seen on the SDS – PAGE gels (Fig. 5. 4 a & b), the protein purity is not perfect (mainly visible in the case of the samples that were highly concentrated before being subjected to SDS-PAGE, in Fig. 5. 4 a), but it is adequate enough for the purpose of initial characterization and screening. In any case, the yield is evidently much higher in SuptoxD cells compared to the MC1061 cells (Fig. 5. 3 a and 5. 4 b & c). The identity of BR2 was further verified through Western blotting (Fig. 5. 4 c) and mass – spectrometry after trypsin digestion (Fig. 5. 4 d).

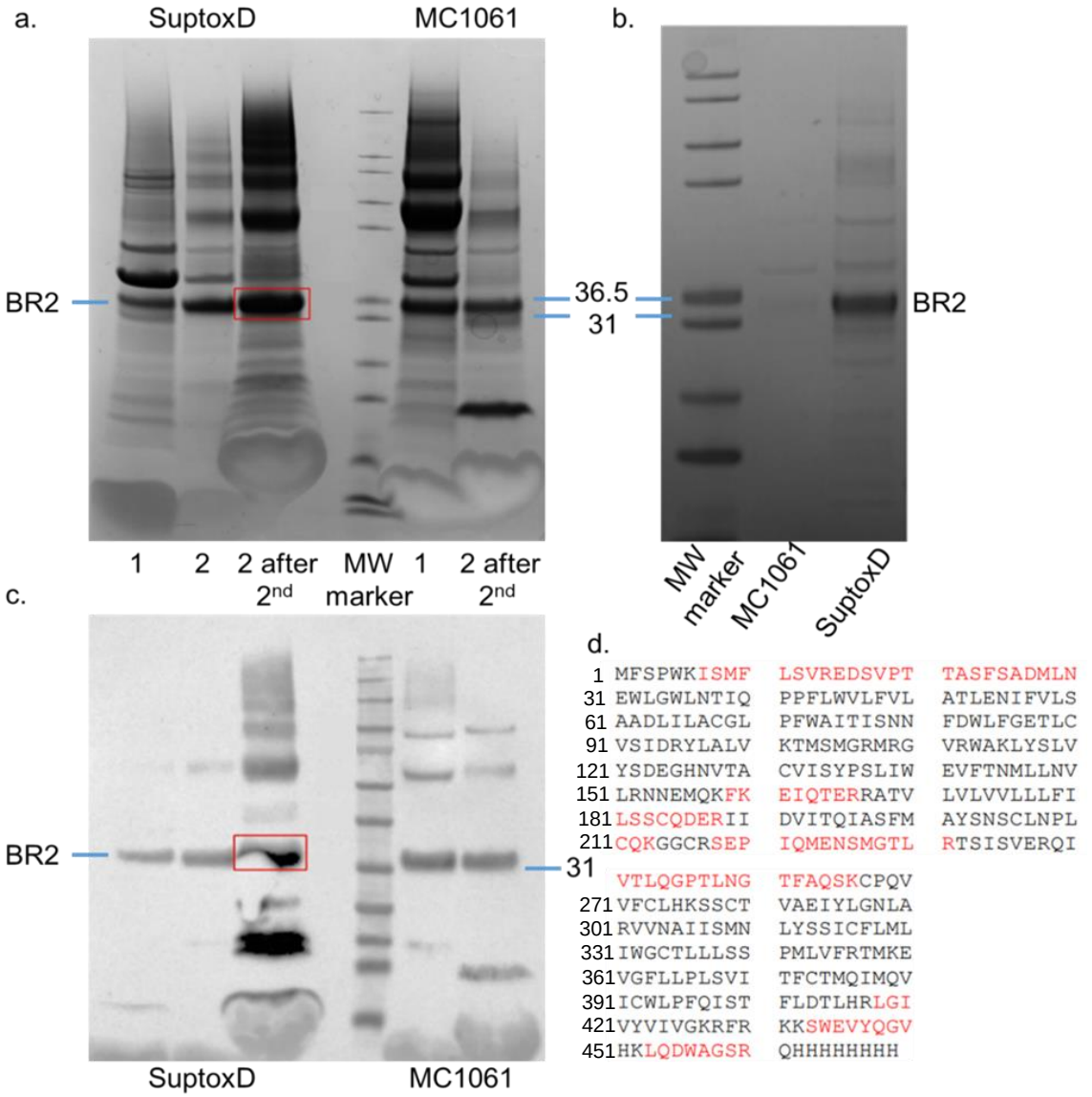

Fig. 5. 4: a. SDS – PAGE gel of samples (from both SuptoxD and MC1061 cells) from all peaks of SEC profiles. Samples 1 and 2 denote protein from peaks 1 and 2 of the 1st SEC, while "2 after 2nd" denotes the single (technically, the 2nd) peak of the 2nd SEC round. Numbers denote the MW as shown by the marker. The samples were highly concentrated beforehand, so that all possible impurities can be seen, even if present at low quantities. **b.** SDS – PAGE gel of the two samples (from SuptoxD and MC1061 cells) from the 2nd SEC, presented for easier direct comparison between the two. **c.** Western blot of the same samples presented in panel **a**. **d.** Mass – spectrometry result of the main BR2 band from SuptoxD cells (highlighted in the red rectangle in panel **a**). Positively identified regions are highlighted in red. Figure adapted from Michou, M. *et al*, *ACS Synth. Biol.,* 2019.

5. 3. Discussion and conclusions

The two engineered *E. coli* strains, SuptoxR and SuptoxD, which take advantage of the co – expression of the cell – toxicity – suppressing regulatory proteins RraA and DjlA, respectively, are able to enhance the production of recombinant membrane proteins significantly in large – scale preparations. Compared to the null MC1061 *E. coli* strain cells, there was a 10 – fold increase in the overexpression yield of TbMscL in SuptoxR cells, and a 14 – fold increase in the protein yield of BR2 in SuptoxD cells. However, quantity is only one side of the coin of protein overexpression and, as mentioned before, the greatest challenge is coupling quantity with quality, i. e. the production of relatively high amounts of a properly – folded membrane protein that will be functional, allowing for the proper and correct investigation of its structure and function.

Regarding TbMscL, the extraction and purification procedure of which had already been optimized, as shown in Chapters 3 and 4, the purity of the end product was very high. The size – exclusion chromatography profiles displayed single, monodisperse peaks and the SDS – PAGE gel electrophoresis verified the high purity of the end product, as expected and as previously seen for TbMscL overexpressed in BL21(DE3) *E. coli* cells. In addition, but possibly even more importantly, PELDOR measurements on the TbMscL F88R1 mutant produced from SuptoxR cells revealed that, at least on a structural level, the protein produced seems to be of high quality. The experimental distance distribution obtained agrees very well both with the one modelled from the closed crystal structure of TbMscL, and, by deduction, with the experimental distance distributions obtained from TbMscL F88R1 produced in BL21(DE3) cells. Hence, the protein produced in SuptoxR strain cells seems to be properly folded and functional.

Regarding the G – protein coupled receptor BR2, the end product was not totally pure, but its purity was high enough to allow for the initial investigation and characterization of the protein. The reduced purity of the product is a result of the purification procedure not being optimized and most probably does not have anything to do with the overexpression strain used. A very significant point is that when BR2 was expressed in SuptoxD cells, the yield of protein produced was so high that it allowed the addition of extra purification steps that greatly increased its purity, while keeping the amount of protein at more than adequately high levels. Western blotting and mass – spectrometry experiments verified that, even if the protein purity was not ideal, BR2 was by a very large margin the predominant protein species in the end – product of the purification procedure. The importance of this fact can be underlined by keeping in mind that human BR2 is very challenging

protein to overexpress recombinantly, not only in prokaryotic host cells[233], but in human cell cultures as well[234]. Future research on the matter should focus on the assessment of the functionality of BR2 when recombinantly expressed in these two strains.

In conclusion, the data presented here clearly demonstrate that the engineered *E. coli* strains SuptoxR and SuptoxD are capable of carrying the burden of the recombinant overexpression of both prokaryotic and eukaryotic membrane proteins in large amounts and of very high structural and functional quality. This is a very promising result that strongly implies that these strains can be utilized from now on in the research of challenging membrane proteins that had so far been proven to be quite hard to work with, and which can be used as drug targets for pharmacological purposes. Finally, identification of other proteins, apart from DjlA and RraA, that could act similarly as membrane protein chaperones could potentially lead to the generation of further *E. coli* strains with even more enhanced capability for membrane protein overexpression. The same could be achieved even with the identification of more potent DjlA and RraA orthologues from different organisms.

CHAPTER 7: SYNOPSIS AND OVERALL DISCUSSION

7. 1: Overview and goals

7. 1. 1: The evolutionary importance of protein – lipid interactions: a brief overview

Proteins and lipids are two of the four traditionally accepted major classes of biomolecules, the other two being ribonucleic acids and sugars. Their roles in living cells, from simple single – cell (e. g. bacteria and archaea) to complex higher (plants, animals and humans) organisms have been crucial and indispensable since the very emergence of life on Earth as we know it[256, 257]. They have even been postulated to be the primary (if not the only) building blocks of prebiotic proto – cells, which are hypothesized to constitute the stepping stone – forms that led to the first, primordial living cells, and which balance between the abiotic and the biotic world[256, 258-260]. Each of the two classes of biomolecules (proteins and lipids) has been described to have played clearly defined and very important roles in the emergence of the first cellular forms of life, roles that they have retained to this day. Importantly, it has been demonstrated that, in the case of both classes of these organic biomolecules, their building blocks (i. e. fatty acids for lipids and amino acids for proteins) can be spontaneously generated from very simple inorganic substances under reaction conditions that, extreme as they may seem, were common during the early stages of the formation of Earth, which is consistent with the most prevalent and probable hypothesis of an abiogenetic origin of life (meaning that life originated from the inorganic substances that were abundantly found during the early stages of Earth's formation, under the harsh conditions that were common during that era, e. g. very high temperature, extreme UV irradiation and lightning etc)[256, 258, 261, 262].

The first step towards the formation of both the marginally biotic proto – cells and the first, primordial actually living cells is the segregation of their insides from their environment, which is the first step of compartmentalization[257]. In all known forms of life this is achieved through the assembly of lipids (or, in their simplest forms, fatty acids) in bilayers, a process that takes place spontaneously in an aqueous environment. The formation of a single (e. g. in proto – cells and primordial cells) and multiple (e. g. in eukaryotes) compartments is of the utmost importance for: (a) the protection and confinement of the biologically important compounds, (b) the spatial co – localization and confinement of biochemically and metabolically associated compounds (thus making metabolism more efficient and controlled), and (c) the most basic form of energy generation, through the creation of different gradients (e. g. pH gradients) between the two sides of the lipid bilayer[256-258]. However, at least during the early steps that led to the emergence of life on Earth,

the generation of lipids (or, at the very least, surfactants) capable of forming stable bilayers by themselves must have been fairly difficult[256, 259]. Hence, small amphipathic peptides and simple proteins are suggested to have aided in the formation of the very early forms of compartmentalization, while at the same time the primordial membrane proteins that co – existed inside the bilayer could have been able to take part in the first manifestations of simple metabolic reactions and pathways[256, 259]. This is not unheard of, as proteins are now known to be the building blocks of compartmentalization in extant prokaryotic cells as well[263, 264]. Apart from this primordial function peptides and proteins are also known to be the primary metabolic machinery of the cell while, during the steps preceding the emergence of the first living cells, they are also hypothesized to have played important roles in pre – nucleic acid self – replication, as in the case of autocatalysis[256, 265].

7. 1. 2: Mechanosensation from a physical point of view and the overall goal of the present studies

Proteins and lipids individually, as well as their cooperation and interactions, are of the utmost importance for cells, from times before the emergence of life as we know it up until the present day. Membrane proteins (and, initially, their predecessor simple amphiphilic membrane peptides) have always been integral and crucial elements of organisms since the formation of the first abiotic proto – cells. Through millions of years of evolution they have themselves evolved and diversified, and can today be found in all living cells and organisms, playing a large variety of very important and fundamental roles. One of the most fundamental and the most evolutionary primal roles of some integral membrane proteins, the mechanosensitive ion channels, is mechanosensation. This is the ability to sense and respond to mechanical stimuli that come from the cell environment, which are mediated through the lateral tension and deformations of the surrounding lipid bilayer[56, 65, 266, 267]. Due to the great importance of mechanosensation, mechanosensitive ion channels can be found in cells from all kingdoms of life and, in eukaryotic cells of higher organisms (e. g. humans and other mammals), they play crucial roles in processes that range from the most fundamental to some of the most complex and advanced, including (but not limited to) cardiovascular architecture and cardiac rhythm, hearing, sensing pressure and temperature and their changes, and nociception (the ability to sense pain)[57-68].

However, despite the high importance of mechanosensation and the widespread abundance of mechanosensitive ion channels, most of the molecular details of this integral cell process and the mechanism behind these channels' response to external mechanical stimuli, their activation and their gating, remain elusive to date. This may have much to do with the nature of mechanosensation, as it differs significantly from most other biomolecular processes and responses.

Mechanotransduction is purely based on physics and has to do with molecular mechanics, while the mode of action of most proteins is mainly chemical. Thus, while, for example, in the case of enzymes, it is the chemical properties (e. g. hydrophilicity, electrophilicity and charge) of the important amino acids in the active site that, through their chemical interactions with the enzyme's substrate and other regions of the protein itself, characterize and determine the activation and mode of action of the enzyme whereas, in the case of mechanosensitive ion channels it is the physical and / or "mechanical" properties (e. g. length, volume and side – chain flexibility) of the sensitive amino acid residues that play the most important role. Hence, the projects of the thesis were, some directly and others indirectly, dedicated to this (wide) goal: the investigation and elucidation molecular details and facets of mechanosensation, by viewing mechanosensitive ion channels not only as biochemical, but as physical entities as well, and by exploring the physical aspects of their structure and architecture that may have implications on their function.

7. 1. 3: TbMscL as the ideal model for investigating mechanosensation and EPR as the ideal collective of techniques

The mechanosensitive ion channel of large conductance, MscL, is the perfect model through which to study mechanosensation, from both a biological and an experimental point of view. Regarding its biological and physiological properties, it is, to date, the only channel known to be solely mechanosensitive (which means that its activation through mechanical tension and, hence, its mechanosensitivity can be investigated independently, without other modes of action interfering in the process). It is also the mechanosensitive channel with the highest pressure activation threshold known[99, 104-108] (which means that if attempts to open it through its ability to mechanosense are successful, its highly possible that the trigger identified could work on other mechanosensitive channels as well, since they require lower lateral tension to be activated). Finally, while it is abundantly found in bacteria and archaea, it is absent from eukaryotic cells (meaning that, if the manipulation of its activation is achieved, it could be utilized as a novel, wide range antibiotic without affecting or harming human and animal cells). From a methodological and experimental point of view, MscL is a prokaryotic membrane protein (and it is, thus, probably easier to recombinantly express and subsequently purify and characterize than eukaryotic proteins), some aspects of its structure and function have been characterized (in particular for two of its orthologues, the *Mycobacterium tuberculosis* and *Escherichia coli*), and in the case of TbMscL, its closed crystal structure is known (which means that mutations can be designed and inter – residue distances can be modelled with high accuracy, without relying on computationally – derived models based on amino acid sequence similarity coupled to known structures of orthologues). It is those

characteristics of MscL, and TbMscL in particular, that led to the choice of this protein for the purpose of the investigation of mechanosensation. Furthermore, the activation and gating mechanism of MscL has never been elucidated and it would be an important advancement.

Electron Paramagnetic Resonance spectroscopy, EPR, is an ensemble of physical techniques that is perfectly suited for the structural characterization of membrane proteins[151, 155, 156, 268, 269]. For the purposes of the studies presented here, PELDOR is the most important of these techniques, as it is very sensitive, allowing for the measurement of intra – molecular distances with very high accuracy. In addition, the optimal distance measurement window of PELDOR, roughly between 15 Å and 70 Å, is very relevant for proteins (and especially TbMscL, a relatively small protein). Furthermore, other EPR techniques are suitable for the assessment of the attached spin label's environment, which is especially important in the case of membrane proteins, where the environment surrounding different regions of the proteins changes between highly polar and sterically unhindered (the aqueous solution phase close to the hydrophilic parts of the protein), and highly hydrophobic and / or sterically crowded (the detergent micelle or lipid bilayer that enshrouds the transmembrane part of the protein, as well as regions at the interface between α – helices in very close proximity). ESEEM is the ideal technique for probing the exposure of spin labelled residues to the aqueous buffer, while CW – EPR allows the assessment of the mobility of the spin label, which is a measure of how crowded its immediate environment is.

7. 2. Overall conclusions and future work

All of the projects shown in this thesis, through the investigation of MscL with EPR spectroscopy, have a common goal: the spherical, in – depth investigation of the concept and mechanism of mechanosensitivity at its core (as described in chapters 3, 4 and 6), and attempts to make this investigation easier and more efficient, by seeking to develop new tools for it or to optimize existing ones (as described in chapters 4, 5 and 6). In the following sections, the most important findings will be briefly presented in an attempt to summarize them, and potential next steps and future work will be discussed.

7. 2. 1. Chapter 3: The nano – pockets are the primary pressure – sensitive region of TbMscL

Hydrophobic crevices, or nano – pockets, had been identified on the structure of most mechanosensitive ion channels and this had given birth to the “Lipid moves first” principle, according to which mechanosensitive channels remain closed as long as these nano – pockets are occupied by acyl chains, while removal of the acyl chains from them forces the channels to open[128, 146]. This principle explains the mode of action of mechanosensation very well and in detail, but it had not been tested experimentally and, thus, that was the purpose of the experiments presented in chapter 3. By combining site – directed spin – labelling, EPR spectroscopy and single – molecule electrophysiology, it was demonstrated that these nano – pockets are indeed the primary pressure – sensitive region on the transmembrane surface of TbMscL, as hindering acyl chain penetration in them through obstruction of their entrance with a bulky and flexible moiety (the side chain of either a R1 or a tryptophan) causes the channel to adopt an expanded conformation which is also consistently more prone to gating, i. e. activated at lower pressure thresholds[177]. Hence, at least regarding TbMscL, the “Lipid moves first” principle has been verified to be true.

These findings are very important for the study of mechanosensitive ion channels in general and MscL in particular: it is the first time that molecular details regarding mechanosensation have been unveiled and the first time any conclusive piece of evidence and information regarding MscL’s physiological response to membrane tension and its gating mechanism have been elucidated. However, albeit decisive, this is only the first step and these findings leave a lot to be desired. The universal application of this mode of action and the “Lipid moves first” principle need to be tested on other mechanosensitive ion channels too. Since it has been verified in the case of the hardest to open and solely mechanosensitive MscL, it would be of very high interest to investigate whether this approach works equally well on other, easier to open channels, as well as multimodal channels that simultaneously respond to multiple stimuli, lateral bilayer tension being one of them. The case of multimodal channels should be expected to be more complicated, since it is highly possible that all gating – triggering stimuli must be present in order for full channel opening to occur or significant activation – sensitivity increase to be observed. Furthermore, there is much more to be learned regarding the gating mechanism of TbMscL in particular. The expanded state presented here is probably just one of a number of consecutive steps that eventually lead to the channel’s full opening. Thus, further research is needed in order to fully elucidate TbMscL’s gating mechanism in detail. The *de novo* synthesis of novel methanethiosulfonate reagents specifically designed to efficiently obstruct the entrance of the nano – pockets could potentially lead to greater stabilization of the observed expanded state, or of states that are even closer to the fully open one. However, it is important to bear in mind that it is quite possible that the fully open state might only be achieved and / or be stable under the

application of external negative pressure, even when modifications significantly reduce its pressure-activation threshold, as is the case of this project.

Full elucidation of the process of mechanosensation and taming of mechanosensitive ion channels could potentially lead to significant advancements in pharmacology, as such proteins are already implicated in a large variety of physiological and pathological responses (e .g. arrhythmias[75] and obesity – related development of systemic insulin resistance[76]). Regarding MscL, and bearing in mind that this protein family is found in all bacteria but not in eukaryotic cells, the full and detailed elucidation of its activation and gating mechanism could lead to the development of novel drugs with antibiotic actions, aiding in the fight against the ever – growing hazard of antibiotic – resistant bacteria. Finally, as long as its opening could be manipulated and triggered at will, MscL, with its very large full pore opening, could prove to be very useful in nanotechnological applications, such as the targeted controlled transfer and release of substances (e. g. drugs) encapsulated in hollow nanoparticles (e. g. nanocages or liposomes)[163, 165, 270].

7. 2. 2: Chapter 4: Towards fine – tuning co – expression of mutant and WT monomers for the production of an adjustable molecular ruler

7. 2. 3: Chapter 5: Engineered *E. coli* strains allow for the enhanced production of TbMscL and BR2

Membrane proteins are abundant in cells coming from all kingdoms of life[41], playing some very important pathological and physiological roles[222]. This makes them a very prominent and common target during the development of novel pharmaceutical substances[223]. However, in order for it to be properly studied, the target – membrane protein needs to be isolated in high purity and large quantity. This is very often hard to achieve[44, 224], especially in the case of membrane proteins that are demanding and hard to work with, e. g. eukaryotic ones[226-229]. Recently, two new *E. coli* strains, SuptoxD and SuptoxR, co – expressing two proteins (DjlA and RraA respectively) which have the ability to reduce the membrane protein overexpression – induced toxicity in *E.* coli cells, were developed and shown to indeed be able to enhance small – scale membrane protein production[173]. Hence, the goal of the project was to investigate whether these two strains can enhance membrane protein overexpression under large – scale conditions too. To this end, two different membrane proteins were chosen, a prokaryotic (TbMscL) and a eukaryotic (BR2) one.

In the case of both TbMscL (Fig. 5. 1) and BR2 (Fig. 5. 3 and Fig. 5. 4), overexpressed in strains SuptoxR and SuptoxD respectively, it was clearly demonstrated that the engineered strains are capable of greatly enhancing the protein production compared to the null *E. coli* MC1061 strain cells. In the case of TbMscL a 10 – fold increase in protein yield was observed, while for BR2 the increase was even larger, almost 14 – fold. Furthermore, regarding TbMscL, the purity of the sample was very high as well (Fig. 5. 1). As for BR2, the purity was adequate (Fig. 5. 4), but could certainly be optimized further. However, this is probably a matter of optimizing the purification conditions rather than the overexpression itself, as the latter seemed to work very well. Finally, PELDOR measurements were performed on TbMscL F88R1, and the resulting distance

distributions revealed that the proteins is well – folded and, thus, appropriate for structural studies. Hence, it was demonstrated that the two engineered *E. coli* strains SuptoxD and SuptoxR are capable of significantly increasing the production of well – folded and pure membrane proteins, regardless of whether they are prokaryotic or eukaryotic. This means that they could be used in cases where the overexpression of recombinant membrane proteins has proven to be challenging and problematic.

7. 2. 4: Chapter 6: Structural alignment and differences in the nano – pockets region between TbMscL and EcMscL

BIBLIOGRAPHY

1. Lim, G. H.; Singhal, R.; Kachroo, A.; Kachroo, P., Fatty Acid- and Lipid-Mediated Signaling in Plant Defense. *Annu Rev Phytopathol* **2017,** *55*, 505-536.
2. Nielson, J. R.; Rutter, J. P., Lipid-mediated signals that regulate mitochondrial biology. *J Biol Chem* **2018,** *293* (20), 7517-7521.
3. Welte, M. A.; Gould, A. P., Lipid droplet functions beyond energy storage. *Biochim Biophys Acta Mol Cell Biol Lipids* **2017,** *1862* (10 Pt B), 1260-1272.
4. van Meer, G.; Voelker, D. R.; Feigenson, G. W., Membrane lipids: where they are and how they behave. *Nat Rev Mol Cell Biol* **2008,** *9* (2), 112-24.
5. Ricciotti, E.; FitzGerald, G. A., Prostaglandins and inflammation. *Arterioscler Thromb Vasc Biol* **2011,** *31* (5), 986-1000.
6. Funk, C. D., Prostaglandins and leukotrienes: advances in eicosanoid biology. *Science* **2001,** *294* (5548), 1871-5.
7. Morgan, A. E.; Mooney, K. M.; Wilkinson, S. J.; Pickles, N. A.; Mc Auley, M. T., Cholesterol metabolism: A review of how ageing disrupts the biological mechanisms responsible for its regulation. *Ageing Res Rev* **2016,** *27*, 108-124.
8. Contreras, F. X.; Sanchez-Magraner, L.; Alonso, A.; Goni, F. M., Transbilayer (flip-flop) lipid motion and lipid scrambling in membranes. *FEBS Lett* **2010,** *584* (9), 1779-86.
9. Metzler, R.; Jeon, J. H.; Cherstvy, A. G., Non-Brownian diffusion in lipid membranes: Experiments and simulations. *Biochim Biophys Acta* **2016,** *1858* (10), 2451-2467.
10. Fahy, E.; Subramaniam, S.; Brown, H. A.; Glass, C. K.; Merrill, A. H., Jr.; Murphy, R. C.; Raetz, C. R.; Russell, D. W.; Seyama, Y.; Shaw, W.; Shimizu, T.; Spener, F.; van Meer, G.; VanNieuwenhze, M. S.; White, S. H.; Witztum, J. L.; Dennis, E. A., A comprehensive classification system for lipids. *J Lipid Res* **2005,** *46* (5), 839-61.
11. Wu, Z.; Palmquist, D. L., Synthesis and biohydrogenation of fatty acids by ruminal microorganisms in vitro. *J Dairy Sci* **1991,** *74* (9), 3035-46.
12. Jenkins, B. J.; Seyssel, K.; Chiu, S.; Pan, P.-H.; Lin, S.-Y.; Stanley, E.; Ament, Z.; West, J. A.; Summerhill, K.; Griffin, J. L.; Vetter, W.; Autio, K. J.; Hiltunen, K.; Hazebrouck, S.; Stepankova, R.; Chen, C.-J.; Alligier, M.; Laville, M.; Moore, M.; Kraft, G.; Cherrington, A.; King, S.; Krauss, R. M.; Schryver, E. d.; Veldhoven, P. P. V.; Ronis, M.; Koulman, A., Odd Chain Fatty Acids; New Insights of the Relationship Between the Gut Microbiota, Dietary Intake, Biosynthesis and Glucose Intolerance. *Scientific Reports* **2017,** *7*, 44845.
13. Keweloh, H.; Heipieper, H. J., Trans unsaturated fatty acids in bacteria. *Lipids* **1996,** *31* (2), 129-37.
14. Berg, J. M.; Tymoczko, J. L.; Stryer, L., Section 12.3 There Are Three Common Types of Membrane Lipids. In *Biochemistry (5th edition)*, W H Freeman: 2002.

15. Simons, K.; Ehehalt, R., Cholesterol, lipid rafts, and disease. *J Clin Invest* **2002,** *110* (5), 597-603.
16. Yang, S. T.; Kreutzberger, A. J. B.; Lee, J.; Kiessling, V.; Tamm, L. K., The Role of Cholesterol in Membrane Fusion. *Chem Phys Lipids* **2016,** *199*, 136-43.
17. Huang, Z.; London, E., Cholesterol lipids and cholesterol-containing lipid rafts in bacteria. *Chem Phys Lipids* **2016,** *199*, 11-6.
18. Saenz, J. P.; Grosser, D.; Bradley, A. S.; Lagny, T. J.; Lavrynenko, O.; Broda, M.; Simons, K., Hopanoids as functional analogues of cholesterol in bacterial membranes. *Proc Natl Acad Sci U S A* **2015,** *112* (38), 11971-6.
19. Alberts, B.; Johnson, A.; Lewis, J.; Raff, M.; Roberts, K.; Walter, P., The Lipid Bilayer. In *Molecular biology of the cell (4th edition)*, Garland Science: 2002.
20. Jain, S.; Caforio, A.; Driessen, A. J. M., Biosynthesis of archaeal membrane ether lipids. *Front Microbiol* **2014,** *5*.
21. Dean, J. M.; Lodhi, I. J., Structural and functional roles of ether lipids. In *Protein Cell*, 2018; Vol. 9, pp 196-206.
22. Demopoulos, C. A.; Pinckard, R. N.; Hanahan, D. J., Platelet-activating factor. Evidence for 1-O-alkyl-2-acetyl-sn-glyceryl-3-phosphorylcholine as the active component (a new class of lipid chemical mediators). *J Biol Chem* **1979,** *254* (19), 9355-8.
23. Kamal, M. M.; Mills, D.; Grzybek, M.; Howard, J., Measurement of the membrane curvature preference of phospholipids reveals only weak coupling between lipid shape and leaflet curvature. *Proc Natl Acad Sci U S A* **2009,** *106* (52), 22245-50.
24. Vamparys, L.; Gautier, R.; Vanni, S.; Bennett, W. F.; Tieleman, D. P.; Antonny, B.; Etchebest, C.; Fuchs, P. F., Conical lipids in flat bilayers induce packing defects similar to that induced by positive curvature. *Biophys J* **2013,** *104* (3), 585-93.
25. Kumar, V. V., Complementary molecular shapes and additivity of the packing parameter of lipids. *Proc Natl Acad Sci U S A* **1991,** *88* (2), 444-8.
26. Cooke, I. R.; Deserno, M., Coupling between Lipid Shape and Membrane Curvature. In *Biophys J*, 2006; Vol. 91, pp 487-95.
27. Drin, G.; Casella, J. F.; Gautier, R.; Boehmer, T.; Schwartz, T. U.; Antonny, B., A general amphipathic alpha-helical motif for sensing membrane curvature. *Nat Struct Mol Biol* **2007,** *14* (2), 138-46.
28. Vanni, S.; Vamparys, L.; Gautier, R.; Drin, G.; Etchebest, C.; Fuchs, P. F.; Antonny, B., Amphipathic lipid packing sensor motifs: probing bilayer defects with hydrophobic residues. *Biophys J* **2013,** *104* (3), 575-84.
29. Hatzakis, N. S.; Bhatia, V. K.; Larsen, J.; Madsen, K. L.; Bolinger, P. Y.; Kunding, A. H.; Castillo, J.; Gether, U.; Hedegard, P.; Stamou, D., How curved membranes recruit amphipathic helices and protein anchoring motifs. *Nat Chem Biol* **2009,** *5* (11), 835-41.
30. Vanni, S.; Hirose, H.; Barelli, H.; Antonny, B.; Gautier, R., A sub-nanometre view of how membrane curvature and composition modulate lipid packing and protein recruitment. *Nature Communications* **2014,** *5* (1), 1-10.

31. Poyry, S.; Vattulainen, I., Role of charged lipids in membrane structures - Insight given by simulations. *Biochim Biophys Acta* **2016,** *1858* (10), 2322-2333.
32. Kalli, A.; Devaney, I.; Sansom, M. S. P., Interactions of Phosphatase and Tensin Homologue (PTEN) Proteins with Phosphatidylinositol Phosphates: Insights from Molecular Dynamics Simulations of PTEN and Voltage Sensitive Phosphatase. *Biochemistry* **2014,** *53* (11), 1724-32.
33. Kalli, A. C.; Morgan, G.; Sansom, M. S., Interactions of the auxilin-1 PTEN-like domain with model membranes result in nanoclustering of phosphatidyl inositol phosphates. *Biophys J* **2013,** *105* (1), 137-45.
34. Powl, A. M.; East, J. M.; Lee, A. G., Heterogeneity in the binding of lipid molecules to the surface of a membrane protein: hot spots for anionic lipids on the mechanosensitive channel of large conductance MscL and effects on conformation. *Biochemistry* **2005,** *44* (15), 5873-83.
35. Almén, M. S.; Nordström, K. J.; Fredriksson, R.; Schiöth, H. B., Mapping the human membrane proteome: a majority of the human membrane proteins can be classified according to function and evolutionary origin. In *BMC Biol*, 2009; Vol. 7, p 50.
36. Berg, J. M.; Tymoczko, J. L.; Stryer, L., Membrane Channels and Pumps. In *Biochemistry (5th edition)*, 5th ed.; W H Freeman: 2002; Vol. 1, pp 385-416.
37. Klein, P.; Kanehisa, M.; DeLisi, C., The detection and classification of membrane-spanning proteins. *Biochim Biophys Acta* **1985,** *815* (3), 468-76.
38. Berg, J. M.; Tymoczko, J. L.; Stryer, L., Protein Structure and Function. In *Biochemistry (5th edition)*, W H Freeman: New York, 2002; Vol. 1, pp 45-82.
39. Lodish, H.; Berk, A.; Zipursky, S. L.; Matsudaira, P.; Baltimore, D.; Darnell, J., Membrane Proteins. In *Molecular cell biology (4th edition)*, W. H. Freeman: 2000.
40. Wallin, E.; von Heijne, G., Genome-wide analysis of integral membrane proteins from eubacterial, archaean, and eukaryotic organisms. *Protein Sci* **1998,** *7* (4), 1029-38.
41. Krogh, A.; Larsson, B.; von Heijne, G.; Sonnhammer, E. L., Predicting transmembrane protein topology with a hidden Markov model: application to complete genomes. *J Mol Biol* **2001,** *305* (3), 567-80.
42. Daley, D. O.; Rapp, M.; Granseth, E.; Melen, K.; Drew, D.; von Heijne, G., Global topology analysis of the Escherichia coli inner membrane proteome. *Science* **2005,** *308* (5726), 1321-3.
43. Schlegel, S.; Hjelm, A.; Baumgarten, T.; Vikstrom, D.; de Gier, J. W., Bacterial-based membrane protein production. *Biochim Biophys Acta* **2014,** *1843* (8), 1739-49.
44. Drew, D.; Froderberg, L.; Baars, L.; de Gier, J. W., Assembly and overexpression of membrane proteins in Escherichia coli. *Biochim Biophys Acta* **2003,** *1610* (1), 3-10.
45. Mathieu, K.; Javed, W.; Vallet, S.; Lesterlin, C.; Candusso, M. P.; Ding, F.; Xu, X. N.; Ebel, C.; Jault, J. M.; Orelle, C., Functionality of membrane proteins overexpressed and purified from E. coli is highly dependent upon the strain. *Sci Rep* **2019,** *9* (1), 2654.

46. Schneider, B.; Junge, F.; Shirokov, V. A.; Durst, F.; Schwarz, D.; Dotsch, V.; Bernhard, F., Membrane protein expression in cell-free systems. *Methods Mol Biol* **2010,** *601*, 165-86.
47. Reckel, S.; Sobhanifar, S.; Durst, F.; Lohr, F.; Shirokov, V. A.; Dotsch, V.; Bernhard, F., Strategies for the cell-free expression of membrane proteins. *Methods Mol Biol* **2010,** *607*, 187-212.
48. Berrier, C.; Park, K. H.; Abes, S.; Bibonne, A.; Betton, J. M.; Ghazi, A., Cell-free synthesis of a functional ion channel in the absence of a membrane and in the presence of detergent. *Biochemistry* **2004,** *43* (39), 12585-91.
49. Kuruma, Y.; Suzuki, T.; Ueda, T., Production of multi-subunit complexes on liposome through an E. coli cell-free expression system. *Methods Mol Biol* **2010,** *607*, 161-71.
50. Zemella, A.; Thoring, L.; Hoffmeister, C.; Kubick, S., Cell-Free Protein Synthesis: Pros and Cons of Prokaryotic and Eukaryotic Systems. *Chembiochem* **2015,** *16* (17), 2420-31.
51. Arachea, B. T.; Sun, Z.; Potente, N.; Malik, R.; Isailovic, D.; Viola, R. E., Detergent selection for enhanced extraction of membrane proteins. *Protein Expr Purif* **2012,** *86* (1), 12-20.
52. Kotov, V.; Bartels, K.; Veith, K.; Josts, I.; Subhramanyam, U. K. T.; Günther, C.; Labahn, J.; Marlovits, T. C.; Moraes, I.; Tidow, H.; Löw, C.; Garcia-Alai, M. M., High-throughput stability screening for detergent-solubilized membrane proteins. *Scientific Reports* **2019,** *9* (1), 1-19.
53. Seddon, A. M.; Curnow, P.; Booth, P. J., Membrane proteins, lipids and detergents: not just a soap opera. *Biochim Biophys Acta* **2004,** *1666* (1-2), 105-17.
54. Ranade, S. S.; Syeda, R.; Patapoutian, A., Mechanically Activated Ion Channels. *Neuron* **2015,** *87* (6), 1162-1179.
55. Martinac, B.; Nomura, T.; Chi, G.; Petrov, E.; Rohde, P. R.; Battle, A. R.; Foo, A.; Constantine, M.; Rothnagel, R.; Carne, S.; Deplazes, E.; Cornell, B.; Cranfield, C. G.; Hankamer, B.; Landsberg, M. J., Bacterial mechanosensitive channels: models for studying mechanosensory transduction. *Antioxid Redox Signal* **2014,** *20* (6), 952-69.
56. Martinac, B.; Kloda, A., Evolutionary origins of mechanosensitive ion channels. *Prog Biophys Mol Biol* **2003,** *82* (1-3), 11-24.
57. Coste, B.; Mathur, J.; Schmidt, M.; Earley, T. J.; Ranade, S.; Petrus, M. J.; Dubin, A. E.; Patapoutian, A., Piezo1 and Piezo2 are essential components of distinct mechanically activated cation channels. *Science* **2010,** *330* (6000), 55-60.
58. Hao, J.; Padilla, F.; Dandonneau, M.; Lavebratt, C.; Lesage, F.; Noël, J.; Delmas, P., Kv1.1 channels act as mechanical brake in the senses of touch and pain. *Neuron* **2013,** *77* (5), 899-914.
59. Noël, J.; Zimmermann, K.; Busserolles, J.; Deval, E.; A, A.; S, D.; N, G.; M, B.; P, R.; A, E.; M, L., The Mechano-Activated K+ Channels TRAAK and TREK-1 Control Both Warm and Cold Perception. *The EMBO journal* **2009,** *28* (9), 1308-1318.
60. Wilson, M. E.; Maksaev, G.; Haswell, E. S., MscS-like mechanosensitive channels in plants and microbes. *Biochemistry* **2013,** *52* (34), 5708-22.

61. Zhou, X. L.; Stumpf, M. A.; Hoch, H. C.; Kung, C., A mechanosensitive channel in whole cells and in membrane patches of the fungus Uromyces. *Science* **1991,** *253* (5026), 1415-7.
62. Gustin, M. C.; Zhou, X. L.; Martinac, B.; Kung, C., A mechanosensitive ion channel in the yeast plasma membrane. *Science* **1988,** *242* (4879), 762-5.
63. Levina, N.; Tötemeyer, S.; Stokes, N. R.; Louis, P.; Jones, M. A.; Booth, I. R., Protection of Escherichia coli cells against extreme turgor by activation of MscS and MscL mechanosensitive channels: identification of genes required for MscS activity. *EMBO J* **1999,** *18* (7), 1730-7.
64. Sukharev, S. I.; Blount, P.; Martinac, B.; Blattner, F. R.; Kung, C., A large-conductance mechanosensitive channel in E. coli encoded by mscL alone. *Nature* **1994,** *368* (6468), 265-8.
65. Martinac, B., Mechanosensitive channels in prokaryotes. *Cell Physiol Biochem* **2001,** *11* (2), 61-76.
66. Kloda, A.; Martinac, B., Mechanosensitive channel of Thermoplasma, the cell wall-less archaea: cloning and molecular characterization. *Cell Biochem Biophys* **2001,** *34* (3), 321-47.
67. Kloda, A.; Martinac, B., Molecular identification of a mechanosensitive channel in archaea. *Biophys J* **2001,** *80* (1), 229-40.
68. Le Dain, A. C.; Saint, N.; Kloda, A.; Ghazi, A.; Martinac, B., Mechanosensitive ion channels of the archaeon Haloferax volcanii. *J Biol Chem* **1998,** *273* (20), 12116-9.
69. Suzuki, M.; Mizuno, A.; Kodaira, K.; Imai, M., Impaired pressure sensation in mice lacking TRPV4. *J Biol Chem* **2003,** *278* (25), 22664-8.
70. Corey, D. P., New TRP channels in hearing and mechanosensation. *Neuron* **2003,** *39* (4), 585-8.
71. Corey, D., Sensory transduction in the ear. **2003**.
72. Askwith, C. C.; Benson, C. J.; Welsh, M. J.; Snyder, P. M., DEG/ENaC ion channels involved in sensory transduction are modulated by cold temperature. In *Proc Natl Acad Sci U S A*, 2001; Vol. 98, pp 6459-63.
73. Teng, J.; Loukin, S.; Kung, C., Mechanosensitive Ion Channels in Cardiovascular Physiology. *Exp Clin Cardiol* **2014,** *20* (10), 6550-60.
74. Zhang, H.; Walcott, G. P.; Rogers, J. M., Effects of gadolinium on cardiac mechanosensitivity in whole isolated swine hearts. *Scientific Reports* **2018,** *8* (1), 1-7.
75. Peyronnet, R.; Nerbonne, J. M.; Kohl, P., Cardiac Mechano-Gated Ion Channels and Arrhythmias. *Circ Res* **2016,** *118* (2), 311-29.
76. Zhao, C.; Sun, Q.; Tang, L.; Cao, Y.; Nourse, J. L.; Pathak, M. M.; Lu, X.; Yang, Q., Mechanosensitive Ion Channel Piezo1 Regulates Diet-Induced Adipose Inflammation and Systemic Insulin Resistance. *Front Endocrinol (Lausanne)* **2019,** *10*, 373.
77. Corey, D. P.; García-A&noveros, J., Mechanosensation and the DEG/ENaC Ion Channels. **1996**.
78. Wemmie, J. A.; Taugher, R. J.; Kreple, C. J., Acid-sensing ion channels in pain and disease. *Nat Rev Neurosci* **2013,** *14* (7), 461-71.

79. Goodman, M. B.; Ernstrom, G. G.; Chelur, D. S.; O'Hagan, R.; Yao, C. A.; Chalfie, M., MEC-2 regulates C. elegans DEG/ENaC channels needed for mechanosensation. *Nature* **2002,** *415* (6875), 1039-42.
80. Tavernarakis, N.; Shreffler, W.; Wang, S.; Driscoll, M., unc-8, a DEG/ENaC family member, encodes a subunit of a candidate mechanically gated channel that modulates C. elegans locomotion. *Neuron* **1997,** *18* (1), 107-19.
81. Venkatachalam, K.; Montell, C., TRP Channels. *Annu Rev Biochem* **2007,** *76*, 387-417.
82. Gu, Y.; Gu, C., Physiological and pathological functions of mechanosensitive ion channels. *Mol Neurobiol* **2014,** *50* (2), 339-47.
83. Yang, F.; Xiao, X.; Cheng, W.; Yang, W.; Yu, P.; Song, Z.; Yarov-Yarovoy, V.; Zheng, J., Structural mechanism underlying capsaicin binding and activation of the TRPV1 ion channel. *Nat Chem Biol* **2015,** *11* (7), 518-524.
84. Goldstein, S. A.; Bayliss, D. A.; Kim, D.; Lesage, F.; Plant, L. D.; Rajan, S., International Union of Pharmacology. LV. Nomenclature and molecular relationships of two-P potassium channels. *Pharmacol Rev* **2005,** *57* (4), 527-40.
85. Zúñiga, L.; Zúñiga, R., Understanding the Cap Structure in K2P Channels. *Front Physiol* **2016,** *7*.
86. Goldstein, S. A.; Bockenhauer, D.; O'Kelly, I.; Zilberberg, N., Potassium leak channels and the KCNK family of two-P-domain subunits. *Nat Rev Neurosci* **2001,** *2* (3), 175-84.
87. Hughes, S.; Foster, R. G.; Peirson, S. N.; Hankins, M. W., Expression and localisation of two-pore domain (K2P) background leak potassium ion channels in the mouse retina. *Scientific Reports* **2017,** *7*, 46085.
88. Berrier, C.; Pozza, A.; de Lacroix de Lavalette, A.; Chardonnet, S.; Mesneau, A.; Jaxel, C.; le Maire, M.; Ghazi, A., The purified mechanosensitive channel TREK-1 is directly sensitive to membrane tension. *J Biol Chem* **2013,** *288* (38), 27307-14.
89. Coste, B.; Xiao, B.; Santos, J. S.; Syeda, R.; Grandl, J.; Spencer, K. S.; Kim, S. E.; Schmidt, M.; Mathur, J.; Dubin, A. E.; Montal, M.; Patapoutian, A., Piezos are pore-forming subunits of mechanically activated channels. *Nature* **2012,** *483* (7388), 176-81.
90. Li, J.; Hou, B.; Tumova, S.; Muraki, K.; Bruns, A.; Ludlow, M. J.; Sedo, A.; Hyman, A. J.; McKeown, L.; Young, R. S.; Yuldasheva, N. Y.; Majeed, Y.; Wilson, L. A.; Rode, B.; Bailey, M. A.; Kim, H. R.; Fu, Z.; Carter, D. A.; Bilton, J.; Imrie, H.; Ajuh, P.; Dear, T. N.; Cubbon, R. M.; Kearney, M. T.; Prasad, R. K.; Evans, P. C.; Ainscough, J. F.; Beech, D. J., Piezo1 integration of vascular architecture with physiological force. *Nature* **2014,** *515* (7526), 279-282.
91. Burke, S. D.; Jordan, J.; Harrison, D. G.; Karumanchi, S. A., Solving Baroreceptor Mystery: Role of PIEZO Ion Channels. *J Am Soc Nephrol* **2019,** *30* (6), 911-913.
92. Zeng, W.-Z.; Marshall, K. L.; Min, S.; Daou, I.; Chapleau, M. W.; Abboud, F. M.; Liberles, S. D.; Patapoutian, A., PIEZOs mediate neuronal sensing of blood pressure and the baroreceptor reflex. **2018**.

93. Eisenhoffer, G. T.; Loftus, P. D.; Yoshigi, M.; Otsuna, H.; Chien, C. B.; Morcos, P. A.; Rosenblatt, J., Crowding induces live cell extrusion to maintain homeostatic cell numbers in epithelia. *Nature* **2012,** *484* (7395), 546-9.
94. Pivetti, C. D.; Yen, M. R.; Miller, S.; Busch, W.; Tseng, Y. H.; Booth, I. R.; Saier, M. H., Jr., Two families of mechanosensitive channel proteins. *Microbiol Mol Biol Rev* **2003,** *67* (1), 66-85, table of contents.
95. Martinac, B.; Buechner, M.; Delcour, A. H.; Adler, J.; Kung, C., Pressure-sensitive ion channel in Escherichia coli. *Proc Natl Acad Sci U S A* **1987,** *84* (8), 2297-301.
96. Booth, I. R.; Blount, P., The MscS and MscL families of mechanosensitive channels act as microbial emergency release valves. *J Bacteriol* **2012,** *194* (18), 4802-9.
97. McLaggan, D.; Jones, M. A.; Gouesbet, G.; Levina, N.; Lindey, S.; Epstein, W.; Booth, I. R., Analysis of the kefA2 mutation suggests that KefA is a cation-specific channel involved in osmotic adaptation in Escherichia coli. *Mol Microbiol* **2002,** *43* (2), 521-36.
98. Li, Y.; Moe, P. C.; Chandrasekaran, S.; Booth, I. R.; Blount, P., Ionic regulation of MscK, a mechanosensitive channel from Escherichia coli. *EMBO J* **2002,** *21* (20), 5323-30.
99. Schumann, U.; Edwards, M. D.; Rasmussen, T.; Bartlett, W.; van West, P.; Booth, I. R., YbdG in Escherichia coli is a threshold-setting mechanosensitive channel with MscM activity. *Proc Natl Acad Sci U S A* **2010,** *107* (28), 12664-9.
100. Edwards, M. D.; Black, S.; Rasmussen, T.; Rasmussen, A.; Stokes, N. R.; Stephen, T. L.; Miller, S.; Booth, I. R., Characterization of three novel mechanosensitive channel activities in Escherichia coli. *Channels (Austin)* **2012,** *6* (4), 272-81.
101. Cruickshank, C. C.; Minchin, R. F.; Le Dain, A. C.; Martinac, B., Estimation of the pore size of the large-conductance mechanosensitive ion channel of Escherichia coli. *Biophys J* **1997,** *73* (4), 1925-31.
102. Iscla, I.; Blount, P., Sensing and responding to membrane tension: the bacterial MscL channel as a model system. *Biophys J* **2012,** *103* (2), 169-74.
103. Walton, T. A.; Idigo, C. A.; Herrera, N.; Rees, D. C., MscL: channeling membrane tension. *Pflugers Arch* **2015,** *467* (1), 15-25.
104. Berrier, C.; Besnard, M.; Ajouz, B.; Coulombe, A.; Ghazi, A., Multiple mechanosensitive ion channels from Escherichia coli, activated at different thresholds of applied pressure. *J Membr Biol* **1996,** *151* (2), 175-87.
105. Brohawn, S. G.; Su, Z.; MacKinnon, R., Mechanosensitivity is mediated directly by the lipid membrane in TRAAK and TREK1 K+ channels. *Proc Natl Acad Sci U S A* **2014,** *111* (9), 3614-9.
106. Nomura, T.; Cranfield, C. G.; Deplazes, E.; Owen, D. M.; Macmillan, A.; Battle, A. R.; Constantine, M.; Sokabe, M.; Martinac, B., Differential effects of lipids and lyso-lipids on the mechanosensitivity of the mechanosensitive channels MscL and MscS. *Proc Natl Acad Sci U S A* **2012,** *109* (22), 8770-5.
107. Cox, C. D.; Bae, C.; Ziegler, L.; Hartley, S.; Nikolova-Krstevski, V.; Rohde, P. R.; Ng, C. A.; Sachs, F.; Gottlieb, P. A.; Martinac, B., Removal of the

mechanoprotective influence of the cytoskeleton reveals PIEZO1 is gated by bilayer tension. *Nat Commun* **2016,** *7*, 10366.
108. Mukherjee, N.; Jose, M. D.; Birkner, J. P.; Walko, M.; Ingólfsson, H. I.; Dimitrova, A.; Arnarez, C.; Marrink, S. J.; Koçer, A., The activation mode of the mechanosensitive ion channel, MscL, by lysophosphatidylcholine differs from tension-induced gating. *FASEB J* **2014,** *28* (10), 4292-302.
109. Chang, G.; Spencer, R. H.; Lee, A. T.; Barclay, M. T.; Rees, D. C., Structure of the MscL homolog from Mycobacterium tuberculosis: a gated mechanosensitive ion channel. *Science* **1998,** *282* (5397), 2220-6.
110. Blount, P.; Sukharev, S. I.; Moe, P. C.; Schroeder, M. J.; Guy, H. R.; Kung, C., Membrane topology and multimeric structure of a mechanosensitive channel protein of Escherichia coli. *EMBO J* **1996,** *15* (18), 4798-805.
111. Saint, N.; Lacapère, J. J.; Gu, L. Q.; Ghazi, A.; Martinac, B.; Rigaud, J. L., A hexameric transmembrane pore revealed by two-dimensional crystallization of the large mechanosensitive ion channel (MscL) of Escherichia coli. *J Biol Chem* **1998,** *273* (24), 14667-70.
112. Liu, Z.; Gandhi, C. S.; Rees, D. C., Structure of a tetrameric MscL in an expanded intermediate state. *Nature* **2009,** *461* (7260), 120-4.
113. Dorwart, M. R.; Wray, R.; Brautigam, C. A.; Jiang, Y.; Blount, P., S. aureus MscL is a pentamer in vivo but of variable stoichiometries in vitro: implications for detergent-solubilized membrane proteins. *PLoS Biol* **2010,** *8* (12), e1000555.
114. Ando, C.; Liu, N.; Yoshimura, K., A cytoplasmic helix is required for pentamer formation of the Escherichia coli MscL mechanosensitive channel. *J Biochem* **2015,** *158* (2), 109-14.
115. Reading, E.; Walton, T. A.; Liko, I.; Marty, M. T.; Laganowsky, A.; Rees, D. C.; Robinson, C. V., The Effect of Detergent, Temperature, and Lipid on the Oligomeric State of MscL Constructs: Insights from Mass Spectrometry. *Chem Biol* **2015,** *22* (5), 593-603.
116. Iscla, I.; Wray, R.; Blount, P., The oligomeric state of the truncated mechanosensitive channel of large conductance shows no variance in vivo. *Protein Sci* **2011,** *20* (9), 1638-42.
117. Li, J.; Guo, J.; Ou, X.; Zhang, M.; Li, Y.; Liu, Z., Mechanical coupling of the multiple structural elements of the large-conductance mechanosensitive channel during expansion. *Proc Natl Acad Sci U S A* **2015,** *112* (34), 10726-31.
118. Newby, Z. E. R.; O'Connel, J. D.; Gruswitz, F.; Hays, F. A.; Harries, W. E. C.; Harwood, I. M.; Ho, J. D.; Lee, J. K.; Savage, D. F.; Miercke, L. J. W.; Stroud, R., A general protocol for the crystallization of membrane proteins for X-ray structural investigation. *Nat Protoc* **2009,** *4* (5), 619-37.
119. Ostermeier, C.; Michel, H., Crystallization of membrane proteins. *Curr Opin Struct Biol* **1997,** *7* (5), 697-701.
120. Anishkin, A.; Chiang, C. S.; Sukharev, S., Gain-of-function mutations reveal expanded intermediate states and a sequential action of two gates in MscL. *J Gen Physiol* **2005,** *125* (2), 155-70.

121. Yoshimura, K.; Batiza, A.; Schroeder, M.; Blount, P.; Kung, C., Hydrophilicity of a single residue within MscL correlates with increased channel mechanosensitivity. *Biophys J* **1999,** *77* (4), 1960-72.
122. Iscla, I.; Wray, R.; Eaton, C.; Blount, P., Scanning MscL Channels with Targeted Post-Translational Modifications for Functional Alterations. *PLoS One* **2015,** *10* (9), e0137994.
123. Phillips, R.; Ursell, T.; Wiggins, P.; Sens, P., Emerging roles for lipids in shaping membrane-protein function. *Nature* **2009,** *459* (7245), 379-85.
124. Moe, P. C.; Blount, P.; Kung, C., Functional and structural conservation in the mechanosensitive channel MscL implicates elements crucial for mechanosensation. *Mol Microbiol* **1998,** *28* (3), 583-92.
125. Balleza, D.; Gómez-Lagunas, F., Conserved motifs in mechanosensitive channels MscL and MscS. *Eur Biophys J* **2009,** *38* (7), 1013-27.
126. Ou, X.; Blount, P.; Hoffman, R. J.; Kung, C., One face of a transmembrane helix is crucial in mechanosensitive channel gating. *Proc Natl Acad Sci U S A* **1998,** *95* (19), 11471-5.
127. Yoshimura, K.; Usukura, J.; Sokabe, M., Gating-associated conformational changes in the mechanosensitive channel MscL. *Proc Natl Acad Sci U S A* **2008,** *105* (10), 4033-8.
128. Pliotas, C.; Dahl, A. C.; Rasmussen, T.; Mahendran, K. R.; Smith, T. K.; Marius, P.; Gault, J.; Banda, T.; Rasmussen, A.; Miller, S.; Robinson, C. V.; Bayley, H.; Sansom, M. S.; Booth, I. R.; Naismith, J. H., The role of lipids in mechanosensation. *Nat Struct Mol Biol* **2015,** *22* (12), 991-8.
129. Marsh, D., Lateral pressure profile, spontaneous curvature frustration, and the incorporation and conformation of proteins in membranes. *Biophys J* **2007,** *93* (11), 3884-99.
130. Sukharev, S. I.; Sigurdson, W. J.; Kung, C.; Sachs, F., Energetic and spatial parameters for gating of the bacterial large conductance mechanosensitive channel, MscL. *J Gen Physiol* **1999,** *113* (4), 525-40.
131. Markin, V. S.; Sachs, F., Thermodynamics of mechanosensitivity. *Phys Biol* **2004,** *1* (1-2), 110-24.
132. Moe, P.; Blount, P., Assessment of potential stimuli for mechano-dependent gating of MscL: effects of pressure, tension, and lipid headgroups. *Biochemistry* **2005,** *44* (36), 12239-44.
133. Perozo, E.; Kloda, A.; Cortes, D. M.; Martinac, B., Physical principles underlying the transduction of bilayer deformation forces during mechanosensitive channel gating. *Nat Struct Biol* **2002,** *9* (9), 696-703.
134. Wang, Y.; Liu, Y.; Deberg, H. A.; Nomura, T.; Hoffman, M. T.; Rohde, P. R.; Schulten, K.; Martinac, B.; Selvin, P. R., Single molecule FRET reveals pore size and opening mechanism of a mechano-sensitive ion channel. *Elife* **2014,** *3*, e01834.
135. Perozo, E.; Cortes, D. M.; Sompornpisut, P.; Kloda, A.; Martinac, B., Open channel structure of MscL and the gating mechanism of mechanosensitive channels. *Nature* **2002,** *418* (6901), 942-8.

136. Zhong, D.; Blount, P., Phosphatidylinositol is crucial for the mechanosensitivity of Mycobacterium tuberculosis MscL. *Biochemistry* **2013,** *52* (32), 5415-20.
137. Foo, A.; Battle, A. R.; Chi, G.; Hankamer, B.; Landsberg, M. J.; Martinac, B., Inducible release of particulates from liposomes using the mechanosensitive channel of large conductance and L-α-lysophosphatidylcholine. *Eur Biophys J* **2015,** *44* (7), 521-30.
138. Teng, J.; Loukin, S.; Anishkin, A.; Kung, C., The force-from-lipid (FFL) principle of mechanosensitivity, at large and in elements. *Pflugers Arch* **2015,** *467* (1), 27-37.
139. Martinac, B.; Bavi, N.; Ridone, P.; Nikolaev, Y. A.; Martinac, A. D.; Nakayama, Y.; Rohde, P. R.; Bavi, O., Tuning ion channel mechanosensitivity by asymmetry of the transbilayer pressure profile. *Biophys Rev* **2018,** *10* (5), 1377-84.
140. Cox, C. D.; Bavi, N.; Martinac, B., Origin of the Force: The Force-From-Lipids Principle Applied to Piezo Channels. *Curr Top Membr* **2017,** *79*, 59-96.
141. Cox, C. D.; Bavi, N.; Martinac, B., Biophysical Principles of Ion-Channel-Mediated Mechanosensory Transduction. *Cell Rep* **2019,** *29* (1), 1-12.
142. Wang, W.; Black, S. S.; Edwards, M. D.; Miller, S.; Morrison, E. L.; Bartlett, W.; Dong, C.; Naismith, J. H.; Booth, I. R., The structure of an open form of an E. coli mechanosensitive channel at 3.45 A resolution. *Science* **2008,** *321* (5893), 1179-83.
143. Bass, R. B.; Strop, P.; Barclay, M.; Rees, D. C., Crystal structure of Escherichia coli MscS, a voltage-modulated and mechanosensitive channel. *Science* **2002,** *298* (5598), 1582-7.
144. Liao, M.; Cao, E.; Julius, D.; Cheng, Y., Structure of the TRPV1 ion channel determined by electron cryo-microscopy. *Nature* **2013,** *504* (7478), 107-12.
145. Brohawn, S. G.; Campbell, E. B.; MacKinnon, R., Physical mechanism for gating and mechanosensitivity of the human TRAAK K+ channel. *Nature* **2014,** *516* (7529), 126-30.
146. Pliotas, C.; Naismith, J. H., Spectator no more, the role of the membrane in regulating ion channel function. *Curr Opin Struct Biol* **2016,** *45*, 59-66.
147. Cao, E.; Liao, M.; Cheng, Y.; Julius, D., TRPV1 structures in distinct conformations reveal activation mechanisms. *Nature* **2013,** *504* (7478), 113-8.
148. Dong, Y. Y.; Pike, A. C.; Mackenzie, A.; McClenaghan, C.; Aryal, P.; Dong, L.; Quigley, A.; Grieben, M.; Goubin, S.; Mukhopadhyay, S.; Ruda, G. F.; Clausen, M. V.; Cao, L.; Brennan, P. E.; Burgess-Brown, N. A.; Sansom, M. S.; Tucker, S. J.; Carpenter, E. P., K2P channel gating mechanisms revealed by structures of TREK-2 and a complex with Prozac. *Science* **2015,** *347* (6227), 1256-9.
149. Reddy, B.; Bavi, N.; Lu, A.; Park, Y.; Perozo, E., Molecular basis of force-from-lipids gating in the mechanosensitive channel MscS. *Elife* **2019,** *8*.
150. Todd, A. P.; Cong, J.; Levinthal, F.; Levinthal, C.; Hubbell, W. L., Site-directed mutagenesis of colicin E1 provides specific attachment sites for spin labels whose spectra are sensitive to local conformation. *Proteins* **1989,** *6* (3), 294-305.
151. Pliotas, C.; Ward, R.; Branigan, E.; Rasmussen, A.; Hagelueken, G.; Huang, H.; Black, S. S.; Booth, I. R.; Schiemann, O.; Naismith, J. H.,

Conformational state of the MscS mechanosensitive channel in solution revealed by pulsed electron-electron double resonance (PELDOR) spectroscopy. *Proc Natl Acad Sci U S A* **2012,** *109* (40), E2675-82.
152. Pannier, M., Veit, S., Godt, A., Jeschke, G. & Spiess, H. W., Dead-Time Free Measurement of Dipole–Dipole Interactions between Electron Spins. *J of Magn Res* **2000,** *142* (2), 331-340.
153. Weil, J. A. B., J. R., *Electron Paramagnetic Resonance: Elementary Theory and Practical Applications*. 2nd ed.; John Wiley & Sons, Inc.: Hoboken, New Jersey, United States, 2006; Vol. 1, p 688.
154. Kerry, P. S.; Turkington, H. L.; Ackermann, K.; Jameison, S. A.; Bode, B. E., Analysis of influenza A virus NS1 dimer interfaces in solution by pulse EPR distance measurements. *J Phys Chem B* **2014,** *118* (37), 10882-8.
155. Endeward, B.; Butterwick, J. A.; MacKinnon, R.; Prisner, T. F., Pulsed electron-electron double-resonance determination of spin-label distances and orientations on the tetrameric potassium ion channel KcsA. *J Am Chem Soc* **2009,** *131* (42), 15246-50.
156. Hagelueken, G.; Ingledew, W. J.; Huang, H.; Petrovic-Stojanovska, B.; Whitfield, C.; ElMkami, H.; Schiemann, O.; Naismith, J. H., PELDOR spectroscopy distance fingerprinting of the octameric outer-membrane protein Wza from Escherichia coli. *Angew Chem Int Ed Engl* **2009,** *48* (16), 2904-6.
157. Glaenzer, J.; Peter, M. F.; Thomas, G. H.; Hagelueken, G., PELDOR Spectroscopy Reveals Two Defined States of a Sialic Acid TRAP Transporter SBP in Solution. *Biophys J* **2017,** *112* (1), 109-20.
158. Noll, A.; Thomas, C.; Herbring, V.; Zollmann, T.; Barth, K.; Mehdipour, A. R.; Tomasiak, T. M.; Bruchert, S.; Joseph, B.; Abele, R.; Olieric, V.; Wang, M.; Diederichs, K.; Hummer, G.; Stroud, R. M.; Pos, K. M.; Tampe, R., Crystal structure and mechanistic basis of a functional homolog of the antigen transporter TAP. *Proc Natl Acad Sci U S A* **2017,** *114* (4), E438-e447.
159. Bountra, K.; Hagelueken, G.; Choudhury, H. G.; Corradi, V.; El Omari, K.; Wagner, A.; Mathavan, I.; Zirah, S.; Yuan Wahlgren, W.; Tieleman, D. P.; Schiemann, O.; Rebuffat, S.; Beis, K., Structural basis for antibacterial peptide self-immunity by the bacterial ABC transporter McjD. *Embo j* **2017**.
160. Schmidt, T.; Walti, M. A.; Baber, J. L.; Hustedt, E. J.; Clore, G. M., Long Distance Measurements up to 160 A in the GroEL Tetradecamer Using Q-Band DEER EPR Spectroscopy. *Angew Chem Int Ed Engl* **2016,** *55* (51), 15905-15909.
161. Giannoulis, A.; Ward, R.; Branigan, E.; Naismith, J. H.; Bode, B. E., PELDOR in rotationally symmetric homo-oligomers. *Mol Phys* **2013,** *111* (18-19), 2845-2854.
162. Deligiannakis, Y.; Rutherford, A. W., Electron spin echo envelope modulation spectroscopy in photosystem I. *Biochim Biophys Acta* **2001,** *1507* (1-3), 226-46.
163. Koçer, A.; Walko, M.; Meijberg, W.; Feringa, B. L., A light-actuated nanovalve derived from a channel protein. *Science* **2005,** *309* (5735), 755-8.
164. Koçer, A.; Walko, M.; Feringa, B. L., Synthesis and utilization of reversible and irreversible light-activated nanovalves derived from the channel protein MscL. *Nat Protoc* **2007,** *2* (6), 1426-37.

165. Koçer, A., Functional liposomal membranes for triggered release. *Methods Mol Biol* **2010,** *605*, 243-55.
166. Iscla, I.; Eaton, C.; Parker, J.; Wray, R.; Kovács, Z.; Blount, P., Improving the Design of a MscL-Based Triggered Nanovalve. *Biosensors (Basel)* **2013,** *3* (1), 171-84.
167. Doerner, J. F.; Febvay, S.; Clapham, D. E., Controlled delivery of bioactive molecules into live cells using the bacterial mechanosensitive channel MscL. *Nat Commun* **2012,** *3*, 990.
168. Iscla, I.; Wray, R.; Blount, P.; Larkins-Ford, J.; Conery, A. L.; Ausubel, F. M.; Ramu, S.; Kavanagh, A.; Huang, J. X.; Blaskovich, M. A.; Cooper, M. A.; Obregon-Henao, A.; Orme, I.; Tjandra, E. S.; Stroeher, U. H.; Brown, M. H.; Macardle, C.; van Holst, N.; Ling Tong, C.; Slattery, A. D.; Gibson, C. T.; Raston, C. L.; Boulos, R. A., A new antibiotic with potent activity targets MscL. *J Antibiot (Tokyo)* **2015,** *68* (7), 453-62.
169. Wray, R.; Herrera, N.; Iscla, I.; Wang, J.; Blount, P., An agonist of the MscL channel affects multiple bacterial species and increases membrane permeability and potency of common antibiotics. *Mol Microbiol* **2019,** *112* (3), 896-905.
170. Wray, R.; Iscla, I.; Gao, Y.; Li, H.; Wang, J.; Blount, P., Dihydrostreptomycin Directly Binds to, Modulates, and Passes through the MscL Channel Pore. *PLoS Biol* **2016,** *14* (6), e1002473.
171. Iscla, I.; Wray, R.; Wei, S.; Posner, B.; Blount, P., Streptomycin potency is dependent on MscL channel expression. *Nat Commun* **2014,** *5*, 4891.
172. Kouwen, T. R.; Trip, E. N.; Denham, E. L.; Sibbald, M. J.; Dubois, J. Y.; van Dijl, J. M., The large mechanosensitive channel MscL determines bacterial susceptibility to the bacteriocin sublancin 168. *Antimicrob Agents Chemother* **2009,** *53* (11), 4702-11.
173. Gialama, D.; Kostelidou, K.; Michou, M.; Delivoria, D. C.; Kolisis, F. N.; Skretas, G., Development of Escherichia coli Strains That Withstand Membrane Protein-Induced Toxicity and Achieve High-Level Recombinant Membrane Protein Production. *ACS Synth Biol* **2017,** *6* (2), 284-300.
174. Michou, M.; Kapsalis, C.; Pliotas, C.; Skretas, G., Optimization of Recombinant Membrane Protein Production in the Engineered Escherichia coli Strains SuptoxD and SuptoxR. *ACS Synth Biol* **2019,** *8* (7), 1631-1641.
175. Skerra, A., Use of the tetracycline promoter for the tightly regulated production of a murine antibody fragment in Escherichia coli. *Gene* **1994,** *151* (1-2), 131-5.
176. Liu, H.; Naismith, J. H., An efficient one-step site-directed deletion, insertion, single and multiple-site plasmid mutagenesis protocol. *BMC Biotechnol* **2008,** *8*, 91.
177. Kapsalis, C.; Wang, B.; Mkami, H. E.; Pitt, S. J.; Schnell, J. R.; Smith, T. K.; Lippiat, J. D.; Bode, B. E.; Pliotas, C., Allosteric activation of an ion channel triggered by modification of mechanosensitive nano-pockets. *Nature Communications* **2019,** *10* (1), 1-14.
178. Denisov, I. G.; Grinkova, Y. V.; Lazarides, A. A.; Sligar, S. G., Directed self-assembly of monodisperse phospholipid bilayer Nanodiscs with controlled size. *J Am Chem Soc* **2004,** *126* (11), 3477-87.

179. Bayburt, T. H.; Sligar, S. G., Self-assembly of single integral membrane proteins into soluble nanoscale phospholipid bilayers. In *Protein Sci*, 2003; Vol. 12, pp 2476-81.
180. Matulef, K.; Valiyaveetil, F. I., Patch-clamp recordings of the KcsA K+ channel in unilamellar blisters. In *Methods in Molecular Biology*, Humana Press Inc.: 2018; Vol. 1684, pp 181-191.
181. Hagelueken, G.; Ward, R.; Naismith, J. H.; Schiemann, O., MtsslWizard: In Silico Spin-Labeling and Generation of Distance Distributions in PyMOL. *Appl Magn Reson* **2012,** *42* (3), 377-391.
182. Polyhach, Y.; Bordignon, E.; Jeschke, G., Rotamer libraries of spin labelled cysteines for protein studies. *Phys Chem Chem Phys* **2011,** *13* (6), 2356-66.
183. Martin, R. E.; Pannier, M.; Diederich, F.; Gramlich, V.; Hubrich, M.; Spiess, H. W., Determination of End-to-End Distances in a Series of TEMPO Diradicals of up to 2.8 nm Length with a New Four-Pulse Double Electron Electron Resonance Experiment. *Angew Chem Int Ed Engl* **1998,** *37* (20), 2833-2837.
184. Jeschke, G., Chechik, V., Ionita, P., Godt, A., Zimmermann, H., Banham, J., Timmel, C. R., Hilger, D. & Jung, H., DeerAnalysis2006—a comprehensive software package for analyzing pulsed ELDOR data | SpringerLink. *Applied Magnetic Resonance* **2006,** *30* (3 - 4), 473 - 498.
185. Chiang, Y. W.; Borbat, P. P.; Freed, J. H., The determination of pair distance distributions by pulsed ESR using Tikhonov regularization. *J Magn Reson* **2005,** *172* (2), 279-95.
186. Ackermann, K.; Pliotas, C.; Valera, S.; Naismith, J. H.; Bode, B. E., Sparse Labeling PELDOR Spectroscopy on Multimeric Mechanosensitive Membrane Channels. *Biophys J* **2017,** *113* (9), 1968-1978.
187. Martinac, B.; Rohde, P. R.; Cranfield, C. G.; Nomura, T., Patch clamp electrophysiology for the study of bacterial ion channels in giant spheroplasts of E. coli. *Methods Mol Biol* **2013,** *966*, 367-80.
188. Herrera, N.; Maksaev, G.; Haswell, E. S.; Rees, D. C., Elucidating a role for the cytoplasmic domain in the Mycobacterium tuberculosis mechanosensitive channel of large conductance. *Scientific Reports* **2018,** *8* (1), 14566.
189. Iscla, I.; Levin, G.; Wray, R.; Reynolds, R.; Blount, P., Defining the physical gate of a mechanosensitive channel, MscL, by engineering metal-binding sites. *Biophys J* **2004,** *87* (5), 3172-80.
190. Kocer, A.; Walko, M.; Bulten, E.; Halza, E.; Feringa, B. L.; Meijberg, W., Rationally designed chemical modulators convert a bacterial channel protein into a pH-sensory valve. *Angew Chem Int Ed Engl* **2006,** *45* (19), 3126-30.
191. Laganowsky, A.; Reading, E.; Allison, T. M.; Ulmschneider, M. B.; Degiacomi, M. T.; Baldwin, A. J.; Robinson, C. V., Membrane proteins bind lipids selectively to modulate their structure and function. *Nature* **2014,** *510* (7503), 172-175.
192. Powl, A. M.; East, J. M.; Lee, A. G., Anionic phospholipids affect the rate and extent of flux through the mechanosensitive channel of large conductance MscL. *Biochemistry* **2008,** *47* (14), 4317-28.

193. Powl, A. M.; East, J. M.; Lee, A. G., Different effects of lipid chain length on the two sides of a membrane and the lipid annulus of MscL. *Biophys J* **2007,** *93* (1), 113-22.
194. Bavi, O.; Cox, C. D.; Vossoughi, M.; Naghdabadi, R.; Jamali, Y.; Martinac, B., Influence of Global and Local Membrane Curvature on Mechanosensitive Ion Channels: A Finite Element Approach. *Membranes (Basel)* **2016,** *6* (1).
195. Moe, P. C.; Levin, G.; Blount, P., Correlating a protein structure with function of a bacterial mechanosensitive channel. *J Biol Chem* **2000,** *275* (40), 31121-7.
196. Pliotas, C., Ion Channel Conformation and Oligomerization Assessment by Site-Directed Spin Labeling and Pulsed-EPR. *Methods Enzymol* **2017,** *594*, 203-242.
197. Branigan, E.; Pliotas, C.; Hagelueken, G.; Naismith, J. H., Quantification of free cysteines in membrane and soluble proteins using a fluorescent dye and thermal unfolding. *Nat Protoc* **2013,** *8* (11), 2090-7.
198. Dowhan, W., Molecular basis for membrane phospholipid diversity: why are there so many lipids? *Annu Rev Biochem* **1997,** *66*, 199-232.
199. Buechner, M.; Delcour, A. H.; Martinac, B.; Adler, J.; Kung, C., Ion channel activities in the Escherichia coli outer membrane. *Biochim Biophys Acta* **1990,** *1024* (1), 111-21.
200. Sukharev, S.; Betanzos, M.; Chiang, C.-S.; Guy, H. R., The gating mechanism of the large mechanosensitive channel MscL. *Nature* **2001,** *409* (6821), 720.
201. Mbaye, M. N.; Hou, Q.; Basu, S.; Teheux, F.; Pucci, F.; Rooman, M., A comprehensive computational study of amino acid interactions in membrane proteins. *Sci Rep* **2019,** *9* (1), 12043.
202. Yonkunas, M.; Kurnikova, M., The Hydrophobic Effect Contributes to the Closed State of a Simplified Ion Channel through a Conserved Hydrophobic Patch at the Pore-Helix Crossing. *Front Pharmacol* **2015,** *6*.
203. Malcolm, H. R.; Blount, P.; Maurer, J. A., The mechanosensitive channel of small conductance (MscS) functions as a Jack-in-the box. *Biochim Biophys Acta* **2015,** *1848* (1 Pt A), 159-66.
204. Lai, J. Y.; Poon, Y. S.; Kaiser, J. T.; Rees, D. C., Open and shut: crystal structures of the dodecylmaltoside solubilized mechanosensitive channel of small conductance from Escherichia coli and Helicobacter pylori at 4.4 Å and 4.1 Å resolutions. *Protein Sci* **2013,** *22* (4), 502-9.
205. Rasmussen, T.; Flegler, V. J.; Rasmussen, A.; Bottcher, B., Structure of the Mechanosensitive Channel MscS Embedded in the Membrane Bilayer. *J Mol Biol* **2019,** *431* (17), 3081-3090.
206. Aryal, P.; Jarerattanachat, V.; Clausen, M. V.; Schewe, M.; McClenaghan, C.; Argent, L.; Conrad, L. J.; Dong, Y. Y.; Pike, A. C.; Carpenter, E. P.; Baukrowitz, T.; Sansom, M. S.; Tucker, S. J., Bilayer-Mediated Structural Transitions Control Mechanosensitivity of the TREK-2 K2P Channel. In *Structure*, 2017; Vol. 25, pp 708-718 e2.
207. Situ, A. J.; Ulmer, T. S., Universal principles of membrane protein assembly, composition and evolution. *PLoS One* **2019,** *14* (8), e0221372.

208. White, S. H.; von Heijne, G., The machinery of membrane protein assembly. *Curr Opin Struct Biol* **2004,** *14* (4), 397-404.
209. Von Heijne, G., Membrane protein assembly in vivo. *Adv Protein Chem* **2003,** *63*, 1-18.
210. Dalbey, R. E.; Wang, P.; Kuhn, A., Assembly of bacterial inner membrane proteins. *Annu Rev Biochem* **2011,** *80*, 161-87.
211. Dyka, F. M.; Molday, R. S., Coexpression and interaction of wild-type and missense RS1 mutants associated with X-linked retinoschisis: its relevance to gene therapy. *Invest Ophthalmol Vis Sci* **2007,** *48* (6), 2491-7.
212. Houck, S. A.; Clark, J. I., Dynamic Subunit Exchange and the Regulation of Microtubule Assembly by the Stress Response Protein Human αB Crystallin. *PLoS One* **2010,** *5* (7).
213. Aquilina, J. A.; Benesch, J. L.; Ding, L. L.; Yaron, O.; Horwitz, J.; Robinson, C. V., Subunit exchange of polydisperse proteins: mass spectrometry reveals consequences of alphaA-crystallin truncation. *J Biol Chem* **2005,** *280* (15), 14485-91.
214. Aquilina, J. A.; Shrestha, S.; Morris, A. M.; Ecroyd, H., Structural and Functional Aspects of Hetero-oligomers Formed by the Small Heat Shock Proteins αB-Crystallin and HSP27*. *J Biol Chem* **2013,** *288* (19), 13602-9.
215. Jeschke, G.; Sajid, M.; Schulte, M.; Godt, A., Three-spin correlations in double electron-electron resonance. *Phys Chem Chem Phys* **2009,** *11* (31), 6580-91.
216. Simons, K.; Toomre, D., Lipid rafts and signal transduction. *Nat Rev Mol Cell Biol* **2000,** *1* (1), 31-9.
217. Lingwood, D.; Simons, K., Lipid rafts as a membrane-organizing principle. *Science* **2010,** *327* (5961), 46-50.
218. Bieberich, E., Sphingolipids and lipid rafts: Novel concepts and methods of analysis. *Chem Phys Lipids* **2018,** *216*, 114-131.
219. Sezgin, E.; Levental, I.; Mayor, S.; Eggeling, C., The mystery of membrane organization: composition, regulation and roles of lipid rafts. *Nat Rev Mol Cell Biol* **2017,** *18* (6), 361-374.
220. Levental, I.; Veatch, S., The Continuing Mystery of Lipid Rafts. *J Mol Biol* **2016,** *428* (24 Pt A), 4749-4764.
221. Niemelä, P. S.; Ollila, S.; Hyvönen, M. T.; Karttunen, M.; Vattulainen, I., Assessing the Nature of Lipid Raft Membranes. In *PLoS Comput Biol*, 2007; Vol. 3.
222. von Heijne, G., The membrane protein universe: what's out there and why bother? *J Intern Med* **2007,** *261* (6), 543-57.
223. Yildirim, M. A.; Goh, K. I.; Cusick, M. E.; Barabasi, A. L.; Vidal, M., Drug-target network. *Nat Biotechnol* **2007,** *25* (10), 1119-26.
224. Wagner, S.; Bader, M. L.; Drew, D.; de Gier, J. W., Rationalizing membrane protein overexpression. *Trends Biotechnol* **2006,** *24* (8), 364-71.
225. Makino, T.; Skretas, G.; Georgiou, G., Strain engineering for improved expression of recombinant proteins in bacteria. *Microb Cell Fact* **2011,** *10*, 32.
226. Wagner, S.; Baars, L.; Ytterberg, A. J.; Klussmeier, A.; Wagner, C. S.; Nord, O.; Nygren, P. A.; van Wijk, K. J.; de Gier, J. W., Consequences of membrane

protein overexpression in Escherichia coli. *Mol Cell Proteomics* **2007,** *6* (9), 1527-50.
227. Klepsch, M. M.; Persson, J. O.; de Gier, J. W., Consequences of the overexpression of a eukaryotic membrane protein, the human KDEL receptor, in Escherichia coli. *J Mol Biol* **2011,** *407* (4), 532-42.
228. Gubellini, F.; Verdon, G.; Karpowich, N. K.; Luff, J. D.; Boel, G.; Gauthier, N.; Handelman, S. K.; Ades, S. E.; Hunt, J. F., Physiological response to membrane protein overexpression in E. coli. *Mol Cell Proteomics* **2011,** *10* (10), M111.007930.
229. Miroux, B.; Walker, J. E., Over-production of proteins in Escherichia coli: mutant hosts that allow synthesis of some membrane proteins and globular proteins at high levels. *J Mol Biol* **1996,** *260* (3), 289-98.
230. Lee, K.; Zhan, X.; Gao, J.; Qiu, J.; Feng, Y.; Meganathan, R.; Cohen, S. N.; Georgiou, G., RraA. a protein inhibitor of RNase E activity that globally modulates RNA abundance in E. coli. *Cell* **2003,** *114* (5), 623-34.
231. Clarke, D. J.; Jacq, A.; Holland, I. B., A novel DnaJ-like protein in Escherichia coli inserts into the cytoplasmic membrane with a type III topology. *Mol Microbiol* **1996,** *20* (6), 1273-86.
232. Gialama, D.; Delivoria, D. C.; Michou, M.; Giannakopoulou, A.; Skretas, G., Functional Requirements for DjlA- and RraA-Mediated Enhancement of Recombinant Membrane Protein Production in the Engineered Escherichia coli Strains SuptoxD and SuptoxR. *J Mol Biol* **2017,** *429* (12), 1800-1816.
233. Link, A. J.; Skretas, G.; Strauch, E. M.; Chari, N. S.; Georgiou, G., Efficient production of membrane-integrated and detergent-soluble G protein-coupled receptors in Escherichia coli. *Protein Sci* **2008,** *17* (10), 1857-63.
234. Camponova, P.; Baud, S.; Mattras, H.; Duroux-Richard, I.; Bonnafous, J. C.; Marie, J., High-level expression and purification of the human bradykinin B(2) receptor in a tetracycline-inducible stable HEK293S cell line. *Protein Expr Purif* **2007,** *55* (2), 300-11.
235. Tenaillon, O.; Skurnik, D.; Picard, B.; Denamur, E., The population genetics of commensal Escherichia coli. *Nat Rev Microbiol* **2010,** *8* (3), 207-17.
236. Beloin, C.; Roux, A.; Ghigo, J. M., Escherichia coli biofilms. *Curr Top Microbiol Immunol* **2008,** *322*, 249-89.
237. Lagier, J. C.; Edouard, S.; Pagnier, I.; Mediannikov, O.; Drancourt, M.; Raoult, D., Current and past strategies for bacterial culture in clinical microbiology. *Clin Microbiol Rev* **2015,** *28* (1), 208-36.
238. Reichlen, M. J.; Leistikow, R. L.; Scobey, M. S.; Born, S. E. M.; Voskuil, M. I., Anaerobic Mycobacterium tuberculosis Cell Death Stems from Intracellular Acidification Mitigated by the DosR Regulon. *J Bacteriol* **2017,** *199* (23).
239. Sohlenkamp, C.; Geiger, O., Bacterial membrane lipids: diversity in structures and pathways. *FEMS Microbiology Reviews* **2020,** *40* (1), 133-159.
240. Lee, R. E.; Brennan, P. J.; Besra, G. S., Mycobacterium tuberculosis cell envelope. *Curr Top Microbiol Immunol* **1996,** *215*, 1-27.
241. Berg, S.; Kaur, D.; Jackson, M.; Brennan, P. J., The glycosyltransferases of Mycobacterium tuberculosis - roles in the synthesis of arabinogalactan, lipoarabinomannan, and other glycoconjugates. *Glycobiology* **2007,** *17* (6), 35-56r.

242. Kalscheuer, R.; Palacios, A.; Anso, I.; Cifuente, J.; Anguita, J.; Jacobs, W. R., Jr.; Guerin, M. E.; Prados-Rosales, R., The Mycobacterium tuberculosis capsule: a cell structure with key implications in pathogenesis. *Biochem J* **2019,** *476* (14), 1995-2016.
243. Jackson, M.; Crick, D. C.; Brennan, P. J., Phosphatidylinositol is an essential phospholipid of mycobacteria. *J Biol Chem* **2000,** *275* (39), 30092-9.
244. Laneelle, M. A.; Prome, D.; Laneelle, G.; Prome, J. C., Ornithine lipid of Mycobacterium tuberculosis: its distribution in some slow- and fast-growing mycobacteria. *J Gen Microbiol* **1990,** *136* (4), 773-8.
245. Jankute, M.; Cox, J. A.; Harrison, J.; Besra, G. S., Assembly of the Mycobacterial Cell Wall. *Annu Rev Microbiol* **2015,** *69*, 405-23.
246. Niederweis, M.; Danilchanka, O.; Huff, J.; Hoffmann, C.; Engelhardt, H., Mycobacterial outer membranes: in search of proteins. *Trends Microbiol* **2010,** *18* (3), 109-16.
247. Bhamidi, S.; Scherman, M. S.; Rithner, C. D.; Prenni, J. E.; Chatterjee, D.; Khoo, K. H.; McNeil, M. R., The identification and location of succinyl residues and the characterization of the interior arabinan region allow for a model of the complete primary structure of Mycobacterium tuberculosis mycolyl arabinogalactan. *J Biol Chem* **2008,** *283* (19), 12992-3000.
248. Perozo, E.; Kloda, A.; Cortes, D. M.; Martinac, B., Site-directed spin-labeling analysis of reconstituted Mscl in the closed state. *J Gen Physiol* **2001,** *118* (2), 193-206.
249. Powl, A. M.; East, J. M.; Lee, A. G., Lipid-protein interactions studied by introduction of a tryptophan residue: the mechanosensitive channel MscL. *Biochemistry* **2003,** *42* (48), 14306-17.
250. Maurer, J. A.; Elmore, D. E.; Lester, H. A.; Dougherty, D. A., Comparing and contrasting Escherichia coli and Mycobacterium tuberculosis mechanosensitive channels (MscL). New gain of function mutations in the loop region. *J Biol Chem* **2000,** *275* (29), 22238-44.
251. Betanzos, M.; Chiang, C. S.; Guy, H. R.; Sukharev, S., A large iris-like expansion of a mechanosensitive channel protein induced by membrane tension. *Nat Struct Biol* **2002,** *9* (9), 704-10.
252. Bavi, N.; Cortes, D. M.; Cox, C. D.; Rohde, P. R.; Liu, W.; Deitmer, J. W.; Bavi, O.; Strop, P.; Hill, A. P.; Rees, D.; Corry, B.; Perozo, E.; Martinac, B., The role of MscL amphipathic N terminus indicates a blueprint for bilayer-mediated gating of mechanosensitive channels. *Nat Commun* **2016,** *7*, 11984.
253. Corry, B.; Hurst, A. C.; Pal, P.; Nomura, T.; Rigby, P.; Martinac, B., An improved open-channel structure of MscL determined from FRET confocal microscopy and simulation. *J Gen Physiol* **2010,** *136* (4), 483-94.
254. Konijnenberg, A.; Yilmaz, D.; Ingólfsson, H. I.; Dimitrova, A.; Marrink, S. J.; Li, Z.; Vénien-Bryan, C.; Sobott, F.; Koçer, A., Global structural changes of an ion channel during its gating are followed by ion mobility mass spectrometry. *Proc Natl Acad Sci U S A* **2014,** *111* (48), 17170-5.

255. Folgering, J. H.; Moe, P. C.; Schuurman-Wolters, G. K.; Blount, P.; Poolman, B., Lactococcus lactis uses MscL as its principal mechanosensitive channel. *J Biol Chem* **2005,** *280* (10), 8784-92.
256. Ruiz-Mirazo, K.; Briones, C.; Escosura, A. d. l., Prebiotic Systems Chemistry: New Perspectives for the Origins of Life. *Chem. Rev.* **2014,** *114* (1), 285-366.
257. Monnard, P.-A.; Walde, P., Current Ideas about Prebiological Compartmentalization. *Life* **2015,** *5* (2), 1239-1263.
258. Lopez, A.; Fiore, M., Investigating Prebiotic Protocells for a Comprehensive Understanding of the Origins of Life: A Prebiotic Systems Chemistry Perspective. *Life* **2019,** *9* (2), 49.
259. Schreiber, A.; Huber, M. C.; Schiller, S. M., Prebiotic Protocell Model Based on Dynamic Protein Membranes Accommodating Anabolic Reactions. *Langmuir* **2019,** *29* (35), 9593-9610.
260. Szostak, J. W.; Bartel, D. P.; Luisi, P. L., Synthesizing life. *Nature* **2020,** *409* (6818), 387-390.
261. Miller, S. L., A Production of Amino Acids Under Possible Primitive Earth Conditions. *Science* **1953,** *117* (3046), 528-529.
262. Johnson, A. P.; Cleaves, H. J.; Dworkin, J. P.; Glavin, D. P.; Lazcano, A.; Bada, J. L., The Miller Volcanic Spark Discharge Experiment. *Science* **2008,** *322* (5900), 404.
263. Cornejo, E.; Abreu, N.; Komeili, A., Compartmentalization and Organelle Formation in Bacteria. *Current opinion in cell biology* **2014,** *26*, 132-138.
264. Murat, D.; Byrne, M.; Komeili, A., Cell Biology of Prokaryotic Organelles. *Cold Spring Harbor perspectives in biology* **2010,** *2* (10).
265. Kauffman, S. A., Approaches to the Origin of Life on Earth. *Life* **2011,** *1* (1), 34-48.
266. Kloda, A.; Martinac, B., Common evolutionary origins of mechanosensitive ion channels in Archaea, Bacteria and cell-walled Eukarya. *Archaea* **2002,** *1* (1), 35-44.
267. Martinac, B., Mechanosensitive ion channels: molecules of mechanotransduction. *J Cell Sci* **2004,** *117* (Pt 12), 2449-60.
268. Hellmich, U. A.; Lyubenova, S.; Kaltenborn, E.; Doshi, R.; van Veen, H. W.; Prisner, T. F.; Glaubitz, C., Probing the ATP hydrolysis cycle of the ABC multidrug transporter LmrA by pulsed EPR spectroscopy. *J Am Chem Soc* **2012,** *134* (13), 5857-62.
269. Ward, R.; Pliotas, C.; Branigan, E.; Hacker, C.; Rasmussen, A.; Hagelueken, G.; Booth, I. R.; Miller, S.; Lucocq, J.; Naismith, J. H.; Schiemann, O., Probing the structure of the mechanosensitive channel of small conductance in lipid bilayers with pulsed electron-electron double resonance. *Biophys J* **2014,** *106* (4), 834-42.
270. Koçer, A., A Remote Controlled Valve in Liposomes for Triggered Liposomal Release. *Journal of liposome research* **2007,** *17* (3-4), 219-225.

APPENDIX

A) TbMscL Mutation Primer Sequences

All Primer sequences are shown as 5’ to 3’

F5C

CCA TGT TGA AAG GCT GTA AAG AAT TCC TGG C

GCC AGG AAT TCT TTA CAG CCT TTC AAC ATG G

F34C

GCT GGT GAC GAA GTG CAC CGA TTC CAT CAT CAC G

CGT GAT GAT GGA ATC GGT GCA CTT CGT CAC CAG C

L42C

CCA TCA TCA CGC CGT GCA TCA ATC GTA TCG

CGA TAC GAT TGA TGC ACG GCG TGA TGA TGG

V48C

CAA TCG TAT CGG CTG CAA CGC GCA AAG C

GCT TTG CGC GTT GCA GCC GAT ACG ATT G

N70C

CGA TTT GTG TGT CCT GCT GAG CGC

GGA CAC CAC AAA TCG ATG GTC TGA CCA CC

L72C

CGA TTT GAA TGT CTG CCT GAG CGC CGC TA

TAG CGG CGC TCA GGC AGA CAT TCA AAT CG

L73C

GTC CTG TGC AGC GCC GCT ATT AAC TTC TTT CTG ATC GC

GCG CTG CAC AGG ACA TTC AAA TCG ATG GTC TGA CCA CC

F79C

GCG CCG CTA TTA ACT GCT TTC TGA TCG C

GCG ATC AGA AAG CAG TTA ATA GCG GCG C

F84C

CTT TCT GAT CGC ATG TGC CGT CTA TTT CCT G

CAG GAA ATA GAC GGC ACA TGC GAT CAG AAA G

A85C

CTG ATC GCA TTT TGC GTC TAT TTC CTG

CAG GAA ATA GAC GCA AAA TGC GAT CAG

L89C

GTC TAT TTC TGC GTT GTG CTG CCG TAC AAC ACC C

CAC AAC GCA GAA ATA GAC GGC AAA TGC GAT CAG AAA G

R98C

CGT ACA ACA CCC TGT GCA AAA AGG GTG AGG

CCT CAC CCT TTT TGC ACA GGG TGT TGT ACG

K99C

GTA CAA CAC CCT GCG CTG CAA GGG TGA GGT C

GAC CTC ACC CTT GCA GCG CAG GGT GTT GTA C

K100C

CAC CCT GCG CAA ATG CGG TGA GGT CGA ACA G

CTG TTC GAC CTC ACC GCA TTT GCG CAG GGT G

E102C

CGC AAA AAG GGT TGC GTC GAA CAG CCA GGT

ACC TGG CTG TTC GAC GCA ACC CTT TTT GCG

R98Q

CGT ACA ACA CCC TGC AAA AAA AGG GTG AGG TC

GAC CTC ACC CTT TTT TTG CAG GGT GTT GTA CG

R98Q, K99Q, K100Q

CGT ACA ACA CCC TGC AAC AAC AGG GTG AGG TCG

CGA CCT CAC CCT GTT GTT GCA GGG TGT TGT ACG

F88W

GTC TAT TGG CTG GTT GTG CTG CCG TAC AAC AC

AAC CAG CCA ATA GAC GGC AAA TGC GAT CAG AAA G

L89W

CTA TTT CTG GGT TGT GCT GCC GTA CAA CAC C

CAC AAC CCA GAA ATA GAC GGC AAA TGC GAT CAG

L17H

GGT AAT ATT GTT GAC CAC GCG GTT GCG G

CCG CAA CCG CGT GGT CAA CAA TAT TAC C

V21H

TTG GCG GTT GCG CAT GTC ATT GGT ACC G

CGG TAC CAA TGA CAT GCG CAA CCG CCA A

B) Spheroplasts Microscope Images

Microscope photos of *E. coli* giant spheroplasts produced under different conditions. All arrows point to spheroplasts that are easy to distinguish. Green arrows point at spheroplasts of adequate size for electrophysiology experiments, while red arrows point at spheroplasts that were formed but remained too small in size for such experiments. Conditions are denoted on the top of each image group. All image dimensions are 660.16 µm x 660.16 µm.

2 h cephalexin / 20 min lysozyme

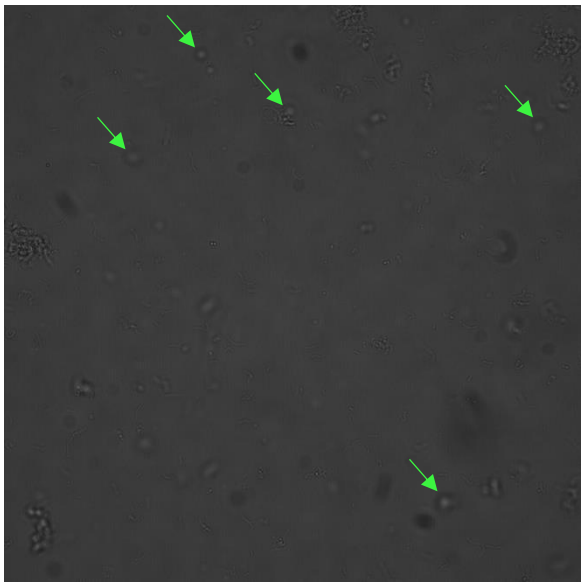

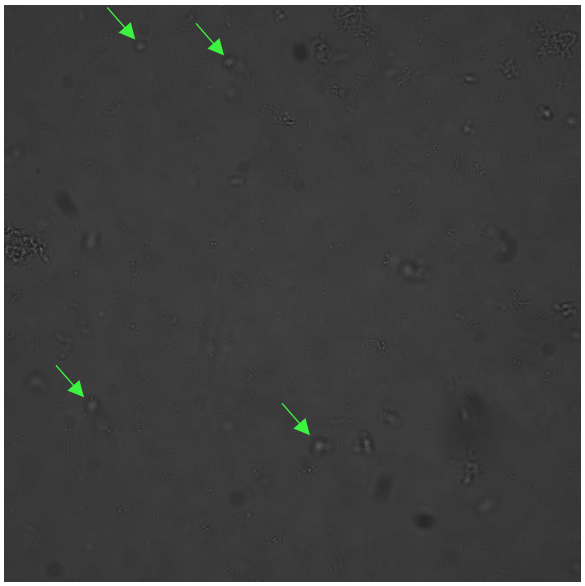

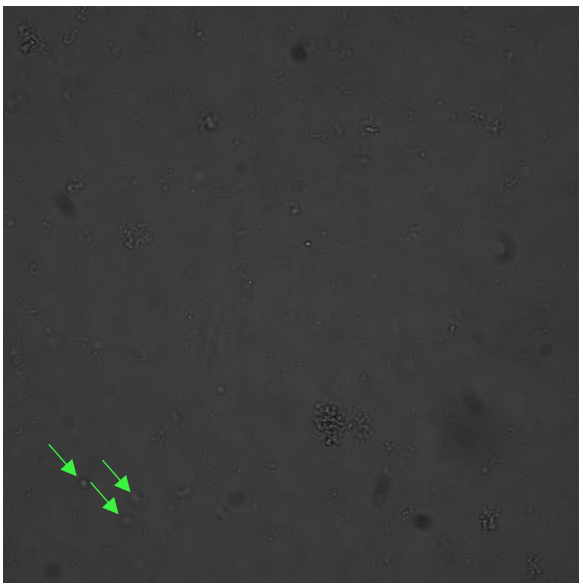

2 h cephalexin / 25 min lysozyme

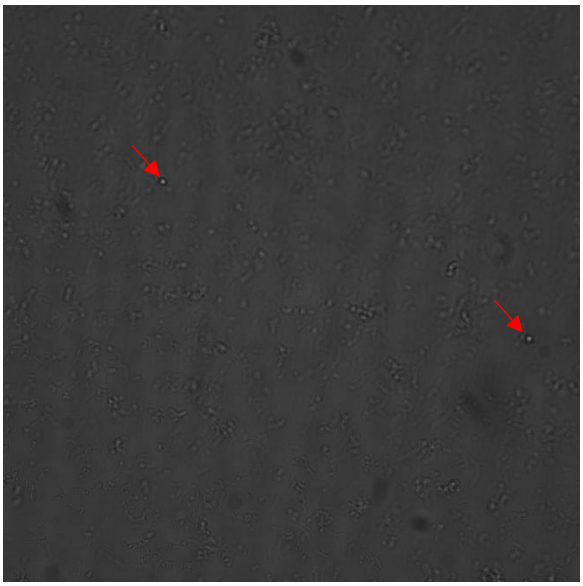

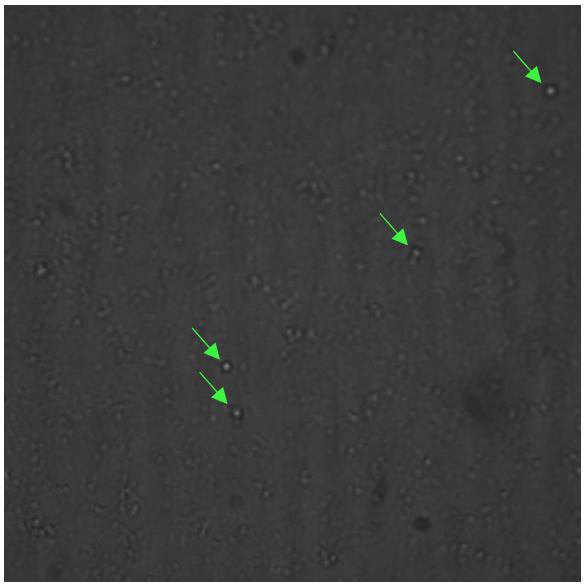

2 h cephalexin / 30 min lysozyme

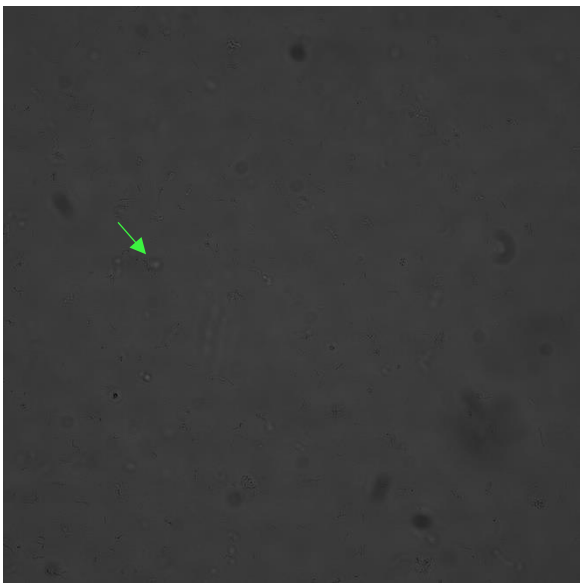

2 h cephalexin / 35 min lysozyme

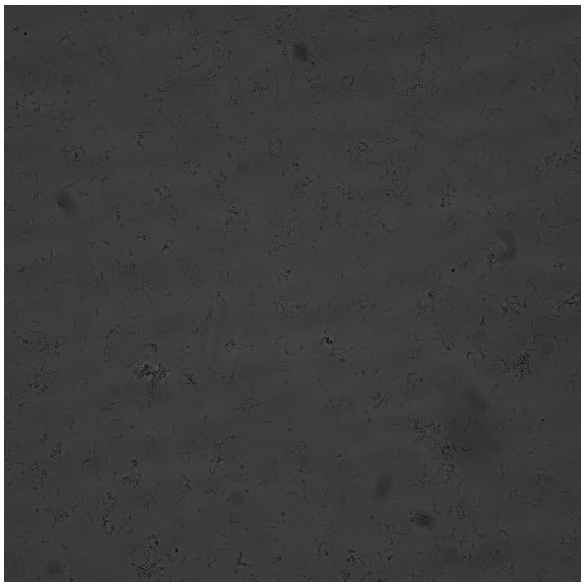

ACKNOWLEDGEMENTS

I would like to thank my primary supervisor, Christos Pliotas, for giving me the chance to work on the presented projects in St Andrews, and for his guidance and training. Also, I would like to thank my second supervisor, Juan-Carlos Penedo, for his help during the last year of my PhD. Furthermore, I would like to thank Bela Bode (Chemistry) and Hassane El Mkami (Physics) for their training and help in EPR and Sam Pitt (Medicine) for doing the same in electrophysiology.

I also want to thank my whole family, my mother, my brothers, my sister and my cousins, for all their help and support through all these years. The same stands for my friends from back home, as well as the ones I made in Scotland (that goes to you Danai, Lorenzo, Alex, Danila).

Last, but most important of all, I want to thank and dedicate this thesis to my dad, Kostas, and my friend, Katia, who I'm sure would have been very proud and happy to see me back home.

FUNDING

This work was supported by the University of St Andrews, School of Biology, the Royal Society of Edinburgh, Tenovus (T15/41) and Carnegie Trust (OS000256).